

THE UNIVERSITY OF CALGARY

QUANTIFICATION OF CONTACT INHIBITION  
IN ADC MICROCARRIER CULTURES

BY

KELLY ANNE M. HAWBOLDT

A THESIS

SUBMITTED TO THE FACULTY OF GRADUATE STUDIES  
IN PARTIAL FULFILLMENT OF THE REQUIREMENTS FOR THE  
DEGREE OF MASTER OF SCIENCE

DEPARTMENT OF CHEMICAL AND PETROLEUM ENGINEERING

CALGARY, ALBERTA

APRIL, 1993

©KELLY ANNE M. HAWBOLDT 1993



National Library  
of Canada

Acquisitions and  
Bibliographic Services Branch

395 Wellington Street  
Ottawa, Ontario  
K1A 0N4

Bibliothèque nationale  
du Canada

Direction des acquisitions et  
des services bibliographiques

395, rue Wellington  
Ottawa (Ontario)  
K1A 0N4

*Your file* *Votre référence*

*Our file* *Notre référence*

The author has granted an irrevocable non-exclusive licence allowing the National Library of Canada to reproduce, loan, distribute or sell copies of his/her thesis by any means and in any form or format, making this thesis available to interested persons.

L'auteur a accordé une licence irrévocable et non exclusive permettant à la Bibliothèque nationale du Canada de reproduire, prêter, distribuer ou vendre des copies de sa thèse de quelque manière et sous quelque forme que ce soit pour mettre des exemplaires de cette thèse à la disposition des personnes intéressées.

The author retains ownership of the copyright in his/her thesis. Neither the thesis nor substantial extracts from it may be printed or otherwise reproduced without his/her permission.

L'auteur conserve la propriété du droit d'auteur qui protège sa thèse. Ni la thèse ni des extraits substantiels de celle-ci ne doivent être imprimés ou autrement reproduits sans son autorisation.

ISBN 0-315-83190-1

Canada

Name KELLY ANNE HAWBOLDT

Dissertation Abstracts International is arranged by broad, general subject categories. Please select the one subject which most nearly describes the content of your dissertation. Enter the corresponding four-digit code in the spaces provided.

ENGINEERING - CHEMICAL

SUBJECT TERM

0542 U·M·I

SUBJECT CODE

## Subject Categories

### THE HUMANITIES AND SOCIAL SCIENCES

#### COMMUNICATIONS AND THE ARTS

Architecture ..... 0729  
 Art History ..... 0377  
 Cinema ..... 0900  
 Dance ..... 0378  
 Fine Arts ..... 0357  
 Information Science ..... 0723  
 Journalism ..... 0391  
 Library Science ..... 0399  
 Mass Communications ..... 0708  
 Music ..... 0413  
 Speech Communication ..... 0459  
 Theater ..... 0465

#### EDUCATION

General ..... 0515  
 Administration ..... 0514  
 Adult and Continuing ..... 0516  
 Agricultural ..... 0517  
 Art ..... 0273  
 Bilingual and Multicultural ..... 0282  
 Business ..... 0688  
 Community College ..... 0275  
 Curriculum and Instruction ..... 0727  
 Early Childhood ..... 0518  
 Elementary ..... 0524  
 Finance ..... 0277  
 Guidance and Counseling ..... 0519  
 Health ..... 0680  
 Higher ..... 0745  
 History of ..... 0520  
 Home Economics ..... 0278  
 Industrial ..... 0521  
 Language and Literature ..... 0279  
 Mathematics ..... 0280  
 Music ..... 0522  
 Philosophy of ..... 0998  
 Physical ..... 0523

Psychology ..... 0525  
 Reading ..... 0535  
 Religious ..... 0527  
 Sciences ..... 0714  
 Secondary ..... 0533  
 Social Sciences ..... 0534  
 Sociology of ..... 0340  
 Special ..... 0529  
 Teacher Training ..... 0530  
 Technology ..... 0710  
 Tests and Measurements ..... 0288  
 Vocational ..... 0747

#### LANGUAGE, LITERATURE AND LINGUISTICS

Language ..... 0679  
 General ..... 0289  
 Ancient ..... 0290  
 Linguistics ..... 0291  
 Modern ..... 0291  
 Literature ..... 0401  
 General ..... 0294  
 Classical ..... 0295  
 Comparative ..... 0297  
 Medieval ..... 0298  
 Modern ..... 0316  
 African ..... 0591  
 American ..... 0305  
 Asian ..... 0352  
 Canadian (English) ..... 0355  
 Canadian (French) ..... 0593  
 English ..... 0311  
 Germanic ..... 0312  
 Latin American ..... 0315  
 Middle Eastern ..... 0313  
 Romance ..... 0314  
 Slavic and East European ..... 0314

#### PHILOSOPHY, RELIGION AND THEOLOGY

Philosophy ..... 0422  
 Religion ..... 0318  
 General ..... 0321  
 Biblical Studies ..... 0319  
 Clergy ..... 0320  
 History of ..... 0322  
 Philosophy of ..... 0469  
 Theology ..... 0323

#### SOCIAL SCIENCES

American Studies ..... 0324  
 Anthropology ..... 0326  
 Archaeology ..... 0327  
 Cultural ..... 0310  
 Physical ..... 0272  
 Business Administration ..... 0770  
 General ..... 0454  
 Accounting ..... 0338  
 Banking ..... 0385  
 Management ..... 0501  
 Marketing ..... 0503  
 Canadian Studies ..... 0505  
 Finance ..... 0508  
 History ..... 0509  
 Labor ..... 0510  
 Theory ..... 0358  
 Folklore ..... 0366  
 Geography ..... 0351  
 Gerontology ..... 0578  
 History ..... 0578  
 General ..... 0578

Ancient ..... 0579  
 Medieval ..... 0581  
 Modern ..... 0582  
 Black ..... 0328  
 African ..... 0331  
 Asia, Australia and Oceania ..... 0332  
 Canadian ..... 0334  
 European ..... 0335  
 Latin American ..... 0336  
 Middle Eastern ..... 0333  
 United States ..... 0337  
 History of Science ..... 0585  
 Law ..... 0398  
 Political Science ..... 0615  
 General ..... 0616  
 International Law and Relations ..... 0617  
 Public Administration ..... 0814  
 Recreation ..... 0452  
 Social Work ..... 0626  
 General ..... 0938  
 Criminology and Penology ..... 0631  
 Demography ..... 0628  
 Ethnic and Racial Studies ..... 0629  
 Individual and Family Studies ..... 0630  
 Industrial and Labor Relations ..... 0630  
 Public and Social Welfare ..... 0700  
 Social Structure and Development ..... 0344  
 Theory and Methods ..... 0709  
 Transportation ..... 0999  
 Urban and Regional Planning ..... 0453  
 Women's Studies ..... 0453

### THE SCIENCES AND ENGINEERING

#### BIOLOGICAL SCIENCES

Agriculture ..... 0473  
 General ..... 0285  
 Agronomy ..... 0475  
 Animal Culture and Nutrition ..... 0476  
 Animal Pathology ..... 0359  
 Food Science and Technology ..... 0478  
 Forestry and Wildlife ..... 0479  
 Plant Culture ..... 0480  
 Plant Pathology ..... 0817  
 Plant Physiology ..... 0777  
 Range Management ..... 0746  
 Wood Technology ..... 0306  
 Biology ..... 0287  
 General ..... 0308  
 Anatomy ..... 0309  
 Biostatistics ..... 0379  
 Botany ..... 0329  
 Cell ..... 0353  
 Ecology ..... 0369  
 Entomology ..... 0793  
 Genetics ..... 0410  
 Limnology ..... 0307  
 Microbiology ..... 0317  
 Molecular ..... 0416  
 Neuroscience ..... 0433  
 Oceanography ..... 0821  
 Physiology ..... 0778  
 Radiation ..... 0472  
 Veterinary Science ..... 0786  
 Zoology ..... 0760  
 Biophysics ..... 0786  
 General ..... 0760  
 Medical ..... 0425  
 Biogeochemistry ..... 0996  
 Geochemistry

Geodesy ..... 0370  
 Geology ..... 0372  
 Geophysics ..... 0373  
 Hydrology ..... 0388  
 Mineralogy ..... 0411  
 Paleobotany ..... 0345  
 Paleocology ..... 0426  
 Paleontology ..... 0418  
 Paleozoology ..... 0985  
 Palynology ..... 0427  
 Physical Geography ..... 0368  
 Physical Oceanography ..... 0415

#### HEALTH AND ENVIRONMENTAL SCIENCES

Environmental Sciences ..... 0768  
 Health Sciences ..... 0566  
 General ..... 0300  
 Audiology ..... 0992  
 Chemotherapy ..... 0567  
 Dentistry ..... 0350  
 Education ..... 0769  
 Hospital Management ..... 0758  
 Human Development ..... 0982  
 Immunology ..... 0564  
 Medicine and Surgery ..... 0347  
 Mental Health ..... 0569  
 Nursing ..... 0570  
 Nutrition ..... 0380  
 Obstetrics and Gynecology ..... 0354  
 Occupational Health and Therapy ..... 0381  
 Ophthalmology ..... 0571  
 Pathology ..... 0419  
 Pharmacology ..... 0572  
 Pharmacy ..... 0382  
 Physical Therapy ..... 0573  
 Public Health ..... 0574  
 Radiology ..... 0575  
 Recreation ..... 0460  
 Speech Pathology ..... 0383  
 Toxicology ..... 0386  
 Home Economics ..... 0386

Speech Pathology ..... 0460  
 Toxicology ..... 0383  
 Home Economics ..... 0386

#### PHYSICAL SCIENCES

Pure Sciences ..... 0485  
 Chemistry ..... 0749  
 General ..... 0486  
 Agricultural ..... 0487  
 Analytical ..... 0488  
 Biochemistry ..... 0738  
 Inorganic ..... 0490  
 Nuclear ..... 0491  
 Organic ..... 0494  
 Pharmaceutical ..... 0495  
 Physical ..... 0754  
 Polymer ..... 0405  
 Radiation ..... 0605  
 Mathematics ..... 0986  
 Physics ..... 0606  
 General ..... 0608  
 Acoustics ..... 0606  
 Astronomy and Astrophysics ..... 0608  
 Atmospheric Science ..... 0748  
 Atomic ..... 0607  
 Electronics and Electricity ..... 0607  
 Elementary Particles and High Energy ..... 0798  
 Fluid and Plasma ..... 0759  
 Molecular ..... 0609  
 Nuclear ..... 0610  
 Optics ..... 0752  
 Radiation ..... 0756  
 Solid State ..... 0611  
 Statistics ..... 0463  
 Applied Sciences ..... 0346  
 Applied Mechanics ..... 0984  
 Computer Science

Engineering ..... 0537  
 General ..... 0538  
 Aerospace ..... 0539  
 Agricultural ..... 0540  
 Automotive ..... 0541  
 Biomedical ..... 0542  
 Chemical ..... 0543  
 Civil ..... 0544  
 Electronics and Electrical ..... 0348  
 Heat and Thermodynamics ..... 0545  
 Hydraulic ..... 0546  
 Industrial ..... 0547  
 Marine ..... 0794  
 Materials Science ..... 0548  
 Mechanical ..... 0743  
 Metallurgy ..... 0551  
 Mining ..... 0552  
 Nuclear ..... 0549  
 Packaging ..... 0765  
 Petroleum ..... 0554  
 Sanitary and Municipal ..... 0790  
 System Science ..... 0428  
 Geotechnology ..... 0796  
 Operations Research ..... 0795  
 Plastics Technology ..... 0994  
 Textile Technology

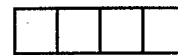
#### PSYCHOLOGY

General ..... 0621  
 Behavioral ..... 0384  
 Clinical ..... 0622  
 Developmental ..... 0620  
 Experimental ..... 0623  
 Industrial ..... 0624  
 Personality ..... 0625  
 Physiological ..... 0989  
 Psychological ..... 0349  
 Psychometrics ..... 0632  
 Social ..... 0451



Nom \_\_\_\_\_

Dissertation Abstracts International est organisé en catégories de sujets. Veuillez s.v.p. choisir le sujet qui décrit le mieux votre thèse et inscrivez le code numérique approprié dans l'espace réservé ci-dessous.



U·M·I

SUJET

CODE DE SUJET

Catégories par sujets

**HUMANITÉS ET SCIENCES SOCIALES**

**COMMUNICATIONS ET LES ARTS**

Architecture .....	0729
Beaux-arts .....	0357
Bibliothéconomie .....	0399
Cinéma .....	0900
Communication verbale .....	0459
Communications .....	0708
Danse .....	0378
Histoire de l'art .....	0377
Journalisme .....	0391
Musique .....	0413
Sciences de l'information .....	0723
Théâtre .....	0465

**ÉDUCATION**

Généralités .....	515
Administration .....	0514
Art .....	0273
Collèges communautaires .....	0275
Commerce .....	0688
Économie domestique .....	0278
Éducation permanente .....	0516
Éducation préscolaire .....	0518
Éducation sanitaire .....	0680
Enseignement agricole .....	0517
Enseignement bilingue et multiculturel .....	0282
Enseignement industriel .....	0521
Enseignement primaire .....	0524
Enseignement professionnel .....	0747
Enseignement religieux .....	0527
Enseignement secondaire .....	0533
Enseignement spécial .....	0529
Enseignement supérieur .....	0745
Évaluation .....	0288
Finances .....	0277
Formation des enseignants .....	0530
Histoire de l'éducation .....	0520
Langues et littérature .....	0279

Lecture .....	0535
Mathématiques .....	0280
Musique .....	0522
Oriantation et consultation .....	0519
Philosophie de l'éducation .....	0998
Physique .....	0523
Programmes d'études et enseignement .....	0727
Psychologie .....	0525
Sciences .....	0714
Sciences sociales .....	0534
Sociologie de l'éducation .....	0340
Technologie .....	0710

**LANGUE, LITTÉRATURE ET LINGUISTIQUE**

Langues	
Généralités .....	0679
Anciennes .....	0289
Linguistique .....	0290
Modernes .....	0291
Littérature	
Généralités .....	0401
Anciennes .....	0294
Comparée .....	0295
Médiévale .....	0297
Moderne .....	0298
Africaine .....	0316
Américaine .....	0591
Anglaise .....	0593
Asiatique .....	0305
Canadienne (Anglaise) .....	0352
Canadienne (Française) .....	0355
Germanique .....	0311
Latino-américaine .....	0312
Moyen-orientale .....	0315
Romane .....	0313
Slave et est-européenne .....	0314

**PHILOSOPHIE, RELIGION ET**

<b>THÉOLOGIE</b>	
Philosophie .....	0422
Religion	
Généralités .....	0318
Clergé .....	0319
Études bibliques .....	0321
Histoire des religions .....	0320
Philosophie de la religion .....	0322
Théologie .....	0469

**SCIENCES SOCIALES**

Anthropologie	
Archéologie .....	0324
Culturelle .....	0326
Physique .....	0327
Droit .....	0398
Économie	
Généralités .....	0501
Commerce-Affaires .....	0505
Économie agricole .....	0503
Économie du travail .....	0510
Finances .....	0508
Histoire .....	0509
Théorie .....	0511
Études américaines .....	0323
Études canadiennes .....	0385
Études féministes .....	0453
Folklore .....	0358
Géographie .....	0366
Gérontologie .....	0351
Gestion des affaires	
Généralités .....	0310
Administration .....	0454
Banques .....	0770
Comptabilité .....	0272
Marketing .....	0338
Histoire	
Histoire générale .....	0578

Ancienne .....	0579
Médiévale .....	0581
Moderne .....	0582
Histoire des noirs .....	0328
Africaine .....	0331
Canadienne .....	0334
États-Unis .....	0337
Européenne .....	0335
Moyen-orientale .....	0333
Latino-américaine .....	0336
Asie, Australie et Océanie .....	0332
Histoire des sciences .....	0585
Loisirs .....	0814
Planification urbaine et régionale .....	0999
Science politique	
Généralités .....	0615
Administration publique .....	0617
Droit et relations internationales .....	0616
Sociologie	
Généralités .....	0626
Aide et bien-être social .....	0630
Criminologie et établissements pénitentiaires .....	0627
Démographie .....	0938
Études de l'individu et de la famille .....	0628
Études des relations interethniques et des relations raciales .....	0631
Structure et développement social .....	0700
Théorie et méthodes .....	0344
Travail et relations industrielles .....	0629
Transports .....	0709
Travail social .....	0452

**SCIENCES ET INGÉNIERIE**

**SCIENCES BIOLOGIQUES**

Agriculture	
Généralités .....	0473
Agronomie .....	0285
Alimentation et technologie alimentaire .....	0359
Culture .....	0479
Élevage et alimentation .....	0475
Exploitation des péturages .....	0777
Pathologie animale .....	0476
Pathologie végétale .....	0480
Physiologie végétale .....	0817
Sylviculture et faune .....	0478
Technologie du bois .....	0746
Biologie	
Généralités .....	0306
Anatomie .....	0287
Biologie (Statistiques) .....	0308
Biologie moléculaire .....	0307
Botanique .....	0309
Cellule .....	0379
Écologie .....	0329
Entomologie .....	0353
Génétique .....	0369
Limnologie .....	0793
Microbiologie .....	0410
Neurologie .....	0317
Océanographie .....	0416
Physiologie .....	0433
Radiation .....	0821
Science vétérinaire .....	0778
Zoologie .....	0472
Biophysique	
Généralités .....	0786
Médicale .....	0760

Géologie .....	0372
Géophysique .....	0373
Hydrologie .....	0388
Minéralogie .....	0411
Océanographie physique .....	0415
Paléobotanique .....	0345
Paléocéologie .....	0426
Paléontologie .....	0418
Paléozoologie .....	0985
Palynologie .....	0427

**SCIENCES DE LA SANTÉ ET DE L'ENVIRONNEMENT**

Économie domestique .....	0386
Sciences de l'environnement .....	0768
Sciences de la santé	
Généralités .....	0566
Administration des hôpitaux .....	0769
Alimentation et nutrition .....	0570
Audiologie .....	0300
Chimiothérapie .....	0992
Dentisterie .....	0567
Développement humain .....	0758
Enseignement .....	0350
Immunologie .....	0982
Loisirs .....	0575
Médecine du travail et thérapie .....	0354
Médecine et chirurgie .....	0564
Obstétrique et gynécologie .....	0380
Ophtalmologie .....	0381
Orthophonie .....	0460
Pathologie .....	0571
Pharmacie .....	0572
Pharmacologie .....	0419
Physiothérapie .....	0382
Radiologie .....	0574
Santé mentale .....	0347
Santé publique .....	0573
Soins infirmiers .....	0569
Toxicologie .....	0383

**SCIENCES PHYSIQUES**

Sciences Pures	
Chimie	
Généralités .....	0485
Biochimie .....	487
Chimie agricole .....	0749
Chimie analytique .....	0486
Chimie minérale .....	0488
Chimie nucléaire .....	0738
Chimie organique .....	0490
Chimie pharmaceutique .....	0491
Physique .....	0494
Polymères .....	0495
Radiation .....	0754
Mathématiques .....	0405
Physique	
Généralités .....	0605
Acoustique .....	0986
Astronomie et astrophysique .....	0606
Électronique et électricité .....	0607
Fluides et plasma .....	0759
Météorologie .....	0608
Optique .....	0752
Particules (Physique nucléaire) .....	0798
Physique atomique .....	0748
Physique de l'état solide .....	0611
Physique moléculaire .....	0609
Physique nucléaire .....	0610
Radiation .....	0756
Statistiques .....	0463

Biomédicale .....	0541
Chaleur et ther modynamique .....	0348
Conditionnement (Emballage) .....	0549
Génie aérospatial .....	0538
Génie chimique .....	0542
Génie civil .....	0543
Génie électronique et électrique .....	0544
Génie industriel .....	0546
Génie mécanique .....	0548
Génie nucléaire .....	0552
Ingénierie des systèmes .....	0790
Mécanique navale .....	0547
Métallurgie .....	0743
Science des matériaux .....	0794
Technique du pétrole .....	0765
Technique minière .....	0551
Techniques sanitaires et municipales .....	0554
Technologie hydraulique .....	0545
Mécanique appliquée .....	0346
Géotechnologie .....	0428
Matières plastiques (Technologie) .....	0795
Recherche opérationnelle .....	0796
Textiles et tissus (Technologie) .....	0794

**SCIENCES DE LA TERRE**

Biogéochimie .....	0425
Géochimie .....	0996
Géodésie .....	0370
Géographie physique .....	0368

**Sciences Appliqués Et Technologie**

Informatique .....	0984
Ingénierie	
Généralités .....	0537
Agriculture .....	0539
Automobile .....	0540

**PSYCHOLOGIE**

Généralités .....	0621
Personnalité .....	0625
Psychobiologie .....	0349
Psychologie clinique .....	0622
Psychologie du comportement .....	0384
Psychologie du développement .....	0620
Psychologie expérimentale .....	0623
Psychologie industrielle .....	0624
Psychologie physiologique .....	0989
Psychologie sociale .....	0451
Psychométrie .....	0632

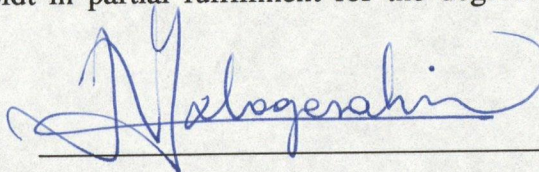


THE UNIVERSITY OF CALGARY  
FACULTY OF GRADUATE STUDIES

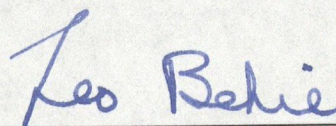
The undersigned certify that they have read, and recommend to the Faculty of Graduate Studies for acceptance a thesis entitled,

"Quantification of contact inhibition in ADC microcarrier cultures"

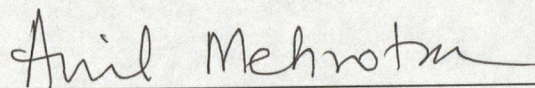
submitted by Kelly Anne Hawboldt in partial fulfillment for the degree of Master of Science.



Dr. N.E. Kalogerakis (Supervisor)  
Department of Chemical & Petroleum Engineering



Dr. L.A. Behie  
Department of Chemical & Petroleum Engineering



Dr. A.K. Mehrotra  
Department of Chemical & Petroleum Engineering



Dr. K. Riabowol  
Department of Medical Biochemistry

Date *April 26, 1993*

## ABSTRACT

Anchorage dependent cells are used extensively in the pharmaceutical industry in the production of therapeutics and diagnostics. The requirement of cell attachment onto a surface complicates the determination of growth kinetics from experimental data. Therefore, it is essential to quantify the degree of the spatial restriction to growth (contact inhibition) in the microcarrier cultures used routinely in large scale production of biopharmaceuticals.

A cellular automaton model has been developed to decouple contact inhibition from growth kinetics of microcarrier cultures. The model matches experimental data from microcarrier cultures and is capable of accounting for the unique characteristics of microcarrier cultures.

To increase our understanding of microcarrier cultures a method for the determination of the degree of contact inhibition in the cultures by flow cytometry has been developed. Flow cytometry measurements were found in agreement with the automaton model predictions. In addition, the stationary phase death rate was examined.

## ACKNOWLEDGEMENTS

There are a number of people I would like to thank for all their help, so many that my acknowledgements runs the risk of being longer than my thesis. I will try keep it short. I would first like to thank my supervisor Professor Nicolas Kalogerakis for his support, guidance and encouragement but most of all for having confidence in me and my abilities and thereby instilling that confidence in myself. I am also grateful to Professor Leo Behie for his assistance and advice throughout my graduate studies. I am indebted to Sean Forestell for taking the time and energy to teach me cell culturing and other lab skills. Without this help my experimental work would have been much longer. Thanks to Ted Linardos for his valuable contribution in the flow cytometry. I would also like to thank Richard Baker, my fellow PPRF students, secretaires and faculty for their assistance.

I would especially like to thank my parents who have always supported me and encouraged me in anything I have ever done. They continued to encourage me in my decision to go back to school and helped me through times when I doubted the choice myself. I am grateful to my brother John who lived with me through part of my graduate work (a chore in itself) and lightened things up. I thank my brother Tom who always made sure, no matter what, I never doubted myself or capabilities. Finally, I want to thank my brother Bob for advising me through the ups and downs of graduate work as only one who has been through it can. I would also like to thank my friend Maya who gave me much needed encouragement throughout my studies.

Thank You Muchly.

## TABLE OF CONTENTS

	Page
APPROVAL PAGE	ii
ABSTRACT	iii
ACKNOWLEDGEMENTS	iv
TABLE OF CONTENTS	v
LIST OF TABLES	ix
LIST OF FIGURES	x
NOMENCLATURE	xvi
I INTRODUCTION	1
I.1 ANCHORAGE DEPENDENT CELLS	1
I.2 MICROCARRIERS	2
I.3 CONTACT INHIBITION	4
I.4 CELL CYCLE DYNAMICS	5
I.5 SCOPE OF STUDY	6
II LITERATURE REVIEW	7
II.1 CELL STRAINS	7
II.2 CONTACT INHIBITION	8

III	MATERIALS AND METHODS	13
III.1	CELL HANDLING PROCEDURES	13
III.1.1	Cell Stock	13
III.1.2	Cell Freezing	13
III.1.3	Cell Thawing	14
III.1.4	Cell Propagation	15
III.2	MEDIA CONTENT AND PREPARATION	16
III.3	SPINNER FLASK EXPERIMENTS	17
III.3.1	Spinner Flask Preparation	17
III.3.2	Microcarrier Preparation	17
III.3.3	Inoculation Procedures	19
III.3.4	Media Replenishments	20
III.3.5	General Sampling	21
III.3.6	Sampling for Flow Cytometry	22
III.4	ANALYTICAL PROCEDURES	23
III.4.1	Cell Enumeration	23
III.4.2	Environmental and Nutrient Analysis	23
III.4.3	Flow Cytometry	24
IV	CELLULAR AUTOMATON MODEL	25
IV.1	OVERVIEW	25
IV.2	CELLULAR AUTOMATON MODEL	28

IV.2.1	Cellular Automaton Theory	28
IV.2.2	Model Development	28
IV.2.3	Model Assumptions	32
IV.2.4	Algorithm Considerations	33
IV.3	MODEL ATTRIBUTES	35
IV.3.1	Variation of growth curves in microcarrier cultures	36
IV.3.2	Number of neighbouring cells	40
IV.3.3	Microcarrier size distribution	42
IV.3.4	Inoculum density effect	44
IV.3.5	Inoculation distribution	46
IV.4	OVERALL EFFECT ON MICROCARRIER CULTURE	48
IV.5	SUMMARY	50
V	COMPARISON WITH EXPERIMENTAL MICROCARRIER CULTURES	52
V.1	OVERVIEW	52
V.2	COMPARISON WITH EXPERIMENTAL DATA	52
V.2.1	Experimental data versus automaton predictions	53
V.3	DECOUPLING CONTACT INHIBITION	57
V.3.1	Generalized contact inhibition curves	57
V.3.2	Combination with Monod kinetics	59

VI	CELL CYCLE DYNAMICS OF MICROCARRIER CULTURES	65
VI.1	OVERVIEW	65
VI.2	THE CELL CYCLE	66
VI.2.1	The cell cycle in microcarrier cultures	72
VI.3	PROPORTION OF CULTURE IN A GIVEN PHASE	76
VI.4	CONTACT INHIBITED REGION IN CELL CYCLE	79
VI.4.1	Determination of contact inhibited region	79
VI.4.2	Comparison of flow cytometry with automaton model predictions	81
VI.5	DEATH RATE	86
VI.6	SUMMARY	90
VIII	CONCLUSIONS AND RECOMMENDATIONS	92
VIII.1	CONCLUSIONS	92
VIII.2	RECOMMENDATIONS	94
	REFERENCES	95
	APPENDIX A	102

## LIST OF TABLES

Table	Title	Page
4.1	Example of the cellular automaton neighbour table.	31
5.1	Kinetic parameters used in ACSL program.	61
A.1	Components of DMEM/F12 cell culture medium.	103
A.2	Physical Characteristics of Cytodex 1 microcarriers.	104
A.3	Components of Ca <sup>++</sup> and Mg <sup>++</sup> free PBS.	105

## LIST OF FIGURES

Figure	Title	Page
3.1	Diagram of 250 mL Corning spinner flasks used in experiments.	18
4.1	The progression of the growth of Vero cells, growing on Cytodex 1 microcarriers, from inoculation to near confluence.	26
4.2	Portion of a neighbour table, generated by cellular automaton, superimposed on attached Vero cells on a Cytodex 1 microcarrier.	31
4.3	Variability in the cellular automaton generated growth curves at an inoculum of 1 cell/bead. The minimum and maximum curves represent the minimum and maximum doubling times required to reach confluence of the 1000 simulations run. The average curve represents the average of the 1000 simulations.	37
4.4	Variability in the cellular automaton generated growth curves at an inoculum of 5 cells/bead. The minimum and maximum curves represent the minimum and maximum doubling times required to reach confluence of the 1000 simulations run. The average curve represents the average of the 1000 simulations.	38

<b>Figure</b>	<b>Title</b>	<b>Page</b>
4.5	<p>Variability in the cellular automaton generated growth curves at an inoculum of 10 cells/bead. The minimum and maximum curves represent the minimum and maximum doubling times required to reach confluence of the 1000 simulations run. The average curve represents the average of the 1000 simulations.</p>	39
4.6	<p>Effect of varying the neighbour space, 5 neighbours/cell and 6 neighbours/cell, on the progression of the cellular automaton generated growth curves at an inoculum of 1 cell/bead.</p>	41
4.7	<p>Effect of varying the microcarrier radius, 98 <math>\mu\text{m}</math>, 90 <math>\mu\text{m}</math> and 82 <math>\mu\text{m}</math>, on the progression of the cellular automaton generated growth curves at an inoculum of 1 cell/bead. Where "r" is radius.</p>	43
4.8	<p>Comparison of the cellular automaton generated growth curve at three different inoculums, 1, 5 and 10 cells/bead.</p>	45
4.9	<p>Percentage of beads with attached cells, upon inoculation, when inoculation and attachment follows a Poisson distribution. The average inoculation (<math>\lambda</math>) is 2 cells/bead.</p>	47

<b>Figure</b>	<b>Title</b>	<b>Page</b>
4.10	Progression of growth on a population of microcarriers predicted by the cellular automaton, at three different average inoculums (1 , 2 and 5 cells/bead), when inoculation follows a Poisson distribution.	49
5.1	Comparison of experimental MRC-5 microcarrier culture growth curves, at two different average inoculums ( $\lambda=2.26$ (●) and 4.76 (■) cells/bead), with cellular automaton generated growth curves initiated at experimental inoculum.	54
5.2	Comparison of experimental Vero microcarrier culture growth curves, at two different average inoculums ( $\lambda=9.72$ (●) and 2.0 (■) cells/bead), with cellular automaton generated growth curves initiated at experimental inoculum.	55
5.3	Contact inhibition curves at three different average inoculation ( $\lambda = 1$ (—), 5 (...) and 10 (---) cells/bead). Figure corresponds to MRC-5 cells growing on Cytodex 1 microcarriers (number of neighbours=5.2 cells/cell, cell density at confluence=62 cells/bead).	58

<b>Figure</b>	<b>Title</b>	<b>Page</b>
5.4	Comparison between experimental batch reactor data, the cellular automaton coupled with Monod kinetics and the cellular automaton model alone. Both automaton models were initiated with the experimental inoculum of 2.3 cells/bead. The data is for MRC-5 cells growing on Cytodex 1 microcarriers at a loading of 5g/L.	63
6.1	Representation of a typical cell cycle. Cells enter the M phase where nuclear and cytoplasm division occurs and then enters interphase. At this point cells may enter either quiescent stage ( $G_0$ ) or continue cycling ( $G_1$ ). Biosynthesis occurs in $G_1$ (production of RNA and proteins). Cells then enter the S phase where the replication of DNA and other cellular matter occurs. Prior to re-entry to the M phase the cells enter the second gap phase ( $G_2$ ).	67
6.2	Growth curves of the two MRC-5 microcarrier cultures ( $\lambda = 2.0$ (a) and 2.2 (b) cells/bead) used in the flow cytometry experiments. The data points are represented by symbols ( $\bullet$ ) and the cellular automaton model predictions are represented as lines (—).	69

<b>Figure</b>	<b>Title</b>	<b>Page</b>
6.3	<p>Growth curves of the two Vero microcarrier cultures (<math>\lambda = 3.2</math> (a) and 5.5 (b) cells/bead) used in the flow cytometry experiments. The data points are represented by symbols (●) and the cellular automaton model predictions are represented as lines (—).</p>	70
6.4	<p>(a) DNA histogram of a sample from MRC-5 culture of figure 6.2(b), at a time of 25 hours. the different phases are differentiated by DNA content.</p> <p>(b). Dot plot of DNA (FL1) versus RNA (FL3), of same MRC-5 sample of figure 6.4(a), illustrating the different phases of the cell cycle.</p>	71
6.5	<p>Contour plots of DNA (FL1) versus RNA (FL3), of MRC-5 microcarrier culture of figure 6.2(b), illustrating the progression of culture cell cycle from inoculation to confluence. The outermost lines represent 10% of the total cell sample, the next 30%, then 50%, 70% and the innermost contour is 90%.</p>	74
6.6	<p>Contour plots of DNA (FL1) versus RNA (FL3), of Vero microcarrier culture of figure 6.3(b), illustrating the progression of culture cell cycle from inoculation to confluence. The outermost lines represent 10% of the total cell sample, the next 30%, then 50%, 70% and the innermost contour is 90%.</p>	75

<b>Figure</b>	<b>Title</b>	<b>Page</b>
6.7	Variation of the fraction of cells in each defined phase of the cell cycle, of the two MRC-5 cultures, as time progresses (G <sub>0</sub> +G <sub>1</sub> (●), S (○) and G <sub>2</sub> +M (▽)).	77
6.8	Variation of the fraction of cells in each defined phase of the cell cycle, of the two Vero cultures, as time progresses (G <sub>0</sub> +G <sub>1</sub> (●), S (▽), G <sub>2</sub> +M (▼)).	78
6.9	(a) Dot plot of DNA (FL1) versus RNA (FL3) of the attached cell sample from the Vero culture of figure 6.3 (b) at a time of 92.75 hours.  (b). Dot plot of DNA (FL1) versus RNA (FL3) of the supernatant sample from the Vero culture of figure 6.3 (b) at a time of 92.75 hours.  These two figures illustrate the technique used to define the contact inhibited region of the attached cell samples. The cycling cells are defined in the attached cell sample (a) and then the contact inhibited region is defined in the supernatant sample (b).	82
6.10	Comparison of the fraction of contact inhibited cells predicted by the cellular automaton model (—) and the flow cytometry determined from the experiments (●) for the two MRC-5 cultures ((a) $\lambda = 2.0$ cells/bead, (b) $\lambda = 2.3$ cells/bead).	83

<b>Figure</b>	<b>Title</b>	<b>Page</b>
6.11	Comparison of the fraction of contact inhibited cells predicted by the cellular automaton model (—) and the flow cytometry determined from the experiments (●) for the two Vero cultures ((a) $\lambda=3.2$ cells/bead, (b) $\lambda=5.5$ cells/bead).	84
6.12	Contour plots of DNA (FL1) versus RNA (FL3) of the stationary phase of the Vero culture from figure 6.3 (b). The plots represent samples from 275 to 444.5 hours. The outermost contour represent 2.5% of the total cell sample while the innermost represents 97.5% of the cell sample.	87

## NOMENCLATURE

FBS	Fetal Bovine Serum
$G_0$	Quiescent phase of the cell cycle
$G_1$	Gap 1 phase of the cell cycle
$G_2$	Gap 2 phase of the cell cycle
I	Inoculation density (cells/bead)
$K_s$	Saturation constant for substrate in Monod equation (mmol/L)
M	Mitosis phase of the cell cycle
$m_s$	substrate maintenance coefficient ( $\mu\text{mol}/10^5$ cells/h)
$n_b$	Number of neighbouring cells per cell
$N_{\text{max}}$	Maximum cell number per bead at confluence
$N(t)$	Number of cells per bead at any time
$P(I)$	Probability a microcarrier is inoculated with "I" cells/bead
PBS	Phosphate Buffered Saline
PDL	Population Doubling Level
$q_s$	uptake rate of substrate ( $\mu\text{mol}/10^5$ cells/h)
s	concentration of substrate (mmol/L)
S	Synthesis phase of the cell cycle
t	time (h)
$t_d$	doubling time of the cell line (h)
$t/t_d$	dimensionless doubling time

$x$	cell density (cells/mL)
$x_m$	maximum cell density at confluence
$Y_s$	substrate yield coefficient ( $10^5$ cells/ $\mu$ mol)

### Greek Letters

$\lambda$	average inoculation density (cells/bead)
$\mu$	specific growth rate ( $h^{-1}$ )
$\mu_a$	apparent specific growth rate ( $h^{-1}$ )
$\mu_{\text{auto}}$	specific growth rate predicted by the cellular automaton ( $h^{-1}$ )
$\mu_{\text{max}}$	maximum specific growth rate of cell line ( $h^{-1}$ )
$\sigma$	standard deviation for $m$ simulations (cells/bead)

## CHAPTER I

### INTRODUCTION

#### I.1 ANCHORAGE DEPENDENT CELLS

Mammalian cells are used extensively in the biotechnology industry for a variety of diagnostic and therapeutic purposes. There are a number of advantages to the use of mammalian cells. Many times it is necessary to use mammalian cells over genetically engineered prokaryotes, such as yeast and bacteria, in the production of some proteins. Currently, several biologically active proteins can only be produced by their natural producers or familiar species (Leist et al., 1990). The activity of these proteins tends to be lower when produced from prokaryotes due to the inability to exactly replicate the complicated structure of the proteins. Further, the quantity of product produced from genetically altered prokaryotes is much smaller than that produced from mammalian cells, a typical ratio being 1:10 (Nilsson, 1989). The opposition to animal testing, on both the political and economic front, are also providing the demand for mammalian cell technology. The use of animals in evaluating the toxicity of chemicals produced in the pharmaceutical, food processing and cosmetic industry is costly, time consuming and receiving increasing opposition from the public, therefore new methods are being developed in testing at the cellular rather than at the organism level (Goldberg and Frazier, 1989). Therefore, the use of mammalian cells, rather than mammals, will increase. To develop reliable test procedures for the efficient production of biological

products determination of the optimal cultivation procedures for cell cultures and the knowledge of the cell's growth kinetics is a necessity.

Anchorage dependent cells, a type of mammalian cell, are commonly used in the pharmaceutical industry to produce a variety of biological products. These products include viral vaccines, lymphokines and plasminogen activators. The characteristic distinction of anchorage dependent cells from other types of mammalian cells is as a precursor to growth the cells must first attach to a surface. The type of surface may range from a flat to spherical as long as the cells have the proper environmental conditions for growth. In the biotechnology industry the large scale cultivation of anchorage dependent cells is commonly accomplished through the use of microcarriers.

## **I.2 MICROCARRIERS**

As previously mentioned as a precondition for growth, anchorage dependent cells must first attach to a surface. In order to achieve high cell densities and therefore high volumetric productivities a number of different systems for attachment have been used (Peringer, 1988). However, the most widely used for the large scale cultivation of anchorage dependent cells is the microcarrier system (Nilsson, 1989).

Microcarriers were introduced in 1967 by van Wezel and are small beads, having a diameter between 100 and 300  $\mu\text{m}$ , which provide a surface for anchorage dependent cells to attach to and grow on. The advantages of microcarrier use over flat surface techniques (such as Nunc cell factories and roller bottles) or immobilized bed reactors are numerous. Firstly, microcarriers may be used in a standard suspension type reactor,

therefore no special reactor design is needed (as in the case of hollow filter reactors). As a result of using suspension type reactors one has control of environmental conditions and sampling ease. Secondly, microcarriers offer a high surface area to volume ratio, typically  $30 \text{ cm}^2/\text{cm}^3$  where as a T-flask ratio is approximately  $2 \text{ cm}^2/\text{cm}^3$ . A high surface area to volume ratio results in higher cell yields without the accompanying increase in equipment and methodology. Further, as compared to other monolayer culture methods, microcarriers cultures produce 2 to 4 times as many cells for a given volume of medium (Pharmacia, 1981). In addition, as large cell numbers can be cultured in small volumes (more than  $10^6$  cells/mL), fewer culture vessels and less labour is required. As an example, a 1.25 L microcarrier culture can yield as many cells as 175 T-flasks (175  $\text{cm}^2$  surface area per T-flask) or 62 roller bottles. In this case the reduced labour requirement for the microcarrier culture versus the conventional flat surface techniques (T-flasks and roller bottles) is substantial. Finally, with the decrease in labour requirements there is corresponding decrease in the number of handling procedures. In cell culture reducing the number of handling steps serves to reduce the risk of contamination.

The characteristics of microcarrier cultures coupled with the ease in reactor scale up (up to 4000 L; Griffiths, 1992) illustrate the advantage of their use in the large scale cultivation of anchorage dependent cultures. To accurately model the growth of cells on microcarriers and hence control and optimize bioreactors, the growth characteristics of anchorage dependent cells must be determined.

### I.3 CONTACT INHIBITION

The growth kinetics of anchorage dependent cells are more complex than the kinetics of nonanchorage dependent cell lines. In nonanchorage dependent cell cultures, such as hybridomas, the growth rate and other parameters are functions of the physical environment (pH and shear stress) and the nutritional limitations (substrate and inhibitor concentrations). However, in anchorage dependent cell cultures in conjunction with the nutritional and physical environment limitations, the growth is further constrained by the cells spatial environment.

The spatial restriction to growth arises from a unique growth characteristic of anchorage dependent cells. In order to divide and grow an anchorage dependent cell must first adhere to a surface. Once attached, the cell divides and after several divisions a small colony will form. As a result of division and growth the available surface area for growth decreases as time progresses. Eventually cells in the colony will become completely surrounded by neighbouring cells and therefore can no longer divide or grow, at this point the cells' growth is *contact inhibited*. As a result of contact inhibition only cells on the perimeter of a cell colony can grow and divide. Due to the decreasing surface area for growth colonies will begin to merge and it follows there will be a parallel decrease in the number of perimeter cells. With fewer cells dividing there will be a corresponding decrease in the overall growth rate of the culture. When the entire surface area is covered the culture is referred to as confluent.

The end result of contact inhibition on the cell growth kinetics is that both cell density and growth rate vary with time. This complicates the determination of kinetic

parameters necessary for an accurate growth kinetic model. In addition, contact inhibition effects may also obscure the influence of other environmental factors (such as pH, nutrient and toxin concentrations) and result in an imprecise determination of key kinetic parameters. The determination of such parameters is of fundamental importance in order to accurately model the dynamic behaviour of large scale microcarrier bioreactors.

#### **I.4 CELL CYCLE DYNAMICS**

The cell growth kinetics of microcarrier cultures may be further clarified by analysis of the cell cycle dynamics of the culture. The physiological state of the culture, whether the cell is in a growth, dividing or quiescent state, is of key importance when attempting to optimize the control and operation of a bioreactor. Further, the differentiation between the "normal" and contact inhibited stages of growth can assist in the understanding and modelling of microcarrier cultures.

The most common method for analyzing the cell cycle of a cell culture is flow cytometry. Cytometry refers to the measurement of physical and/or chemical characteristics of cells (Shapiro, 1988). When the cells pass through a measuring apparatus in a fluid stream the process is called flow cytometry. Flow cytometry applications range from cell sorting to counting. However, the most common use of flow cytometers is in the definition and quantification of heterogeneity of cell populations. For this work the flow cytometer was used to quantify the DNA and RNA content of a sample of cells. From these measurements the various stages of the cell cycle may be differentiated. Chapter III gives a more detailed explanation of the flow cytometer and

techniques.

## **I.5 SCOPE OF STUDY**

In this study the growth kinetics of anchorage dependent cells on microcarriers were examined. Two type of anchorage dependent cell lines were used, MRC-5 and Vero cells. Particular focus was given to the following topics:

- (1) The development of a contact inhibition growth model to represent the growth of anchorage dependent cells on microcarriers.
- (2) The examination of the cell cycle dynamics of microcarrier cultures.
- (3) The determination of a physiological state in the cell cycle which would correspond to contact inhibited cells.
- (4) A quantitative comparison of the degree of contact inhibition between experimental measurements and the contact inhibition model predictions.

## CHAPTER II

### LITERATURE REVIEW

#### II.1 CELL STRAINS

In the experiments in this study two types of mammalian cell lines were used, MRC-5 and Vero. MRC-5 cells are a normal diploid fibroblast derived from normal lung tissue of a 14 week-old male fetus (Jacobs, 1970). MRC-5 are used for the production of a variety of viruses including rabies (Majer et al., 1977; Kuwert et al., 1977), rubella (Michamsy et al., 1977), herpes simplex (Griffiths et al., 1982; Thorton et al., 1985), measles (Mirchamsy et al., 1977) and poliovirus Types I, II, and III (Majer et al., 1977; Kuwert et al., 1977, v. Seefried and Chun, 1981; v. Seefried et al., 1984). The basis for using MRC-5 cells is the susceptibility of the cells to both infection by these viruses and to adverse culture conditions.

Vero cells were derived from African green monkey kidney cells in 1963 by Y. Yasurumura. The advantage of using Vero cells are similar those for MRC-5 cells. Vero cells are susceptible to a wide variety of viruses such as; arboviruses (Simizu et al., 1967), Lassa fever (Buckley and Casalls, 1970), haemorrhagic fever (Johnson et al., 1977), rubella (Oker-Blom et al., 1983), measles (Makmo and Kasahara, 1964), herpes (Kieff et al., 1971) and rickettsiae (Simizu and Terasima, 1988). The susceptibility of the Vero cell line to these viruses has aided in diagnostic virology in both the identification and characteristics of the viruses. Production of human vaccines from Vero cells is not

as widespread as in the case of MRC-5 cells due to concerns on the transformed nature of the cell line and the potential of passing oncogenic material with the vaccine (Horodniceanu, 1981 and 1982; Montagnon et al., 1984). However, killed poliovirus vaccine produced by Vero cells has been approved in France since 1984 (Montagnon et al., 1984). Vero cells are also being used in the production of rabies vaccine to study the kinetics of the virus (Celer et al., 1991).

The large scale production of biopharmaceuticals from anchorage dependent cells is commonly accomplished by microcarriers. For instance, anchorage dependent cells are used to produce vaccines (Montagnon et al., 1982), interferons (Meignier et al., 1980; Smiley et al., 1989) and recombinant proteins (Griffiths, 1992b). The utilization of both MRC-5 and Vero cells in the diagnostic and therapeutic stages of pharmaceutical development illustrate the need for the accurate determination of the growth kinetics of anchorage dependent cells.

## II.2 CONTACT INHIBITION

Previous cell growth models have accounted for the nutritional/inhibitor effects to cell growth by incorporating these factors into the growth kinetics. Monod kinetics is one example of a kinetic model which accounts for nutrient limitations:

$$\mu = \frac{\mu_{\max} S}{K_s + S} \quad (2.1)$$

where  $\mu$  is the specific growth rate,  $\mu_{\max}$  is the maximum specific growth rate of the cell line,  $s$  is the limiting nutrient concentration and  $K_s$  is the limiting nutrient saturation constant. The disadvantage to these models when applied to anchorage dependent cells is the kinetics do not account for the spatial limitation in the growth rate. In order to accurately model the growth of anchorage dependent mammalian cells the spatial restriction to growth, or contact inhibition, must be accounted for. A number of researchers have addressed the effect of contact inhibition on cell growth.

Frame and Hu (1988) developed a deterministic equation to anchorage dependent cell growth where the specific growth rate varies according to the degree of cell crowding:

$$\mu = \mu_{\max} \left[ 1 - \exp\left(-C \frac{x_m - x}{x_m}\right) \right] \quad (2.2)$$

where  $x$  is the cell density and  $\mu_{\max}$  and  $\mu$  are the maximum specific growth rate and the specific growth rate respectively. The shape of the growth curves, and hence the effect of contact inhibition, is determined by  $x_m$ , the cell density at confluence,  $C$ , an adjustable parameter, and  $\mu_{\max}$ . All three of these parameters are determined by the cell type. The specific growth rate is now a function of the spatial environment and may be coupled to nutrient/toxin kinetics. However, the fundamental drawback to this equation is all cells are assumed to be equally contact inhibited. In fact, only cells in the interior of a cell colony are subject to contact inhibited growth, cells on the perimeter of the colony grow normally.

Recognizing that perimeter cells and interior cells will have different growth rates

Cherry and Papoutsakis (1989) developed a deterministic equation relating the growth rate to the spatial environment. In their model the growth rate is assumed to be proportional to the number of perimeter cells in a patch (colony). Cells at the perimeter of a patch grow at a rate  $\mu$ , while the interior cells have a zero growth rate. For growth on flat surfaces, such as T-flasks, the colonies are assumed to form circles resulting in the following equation:

$$\frac{P}{P_o} = \left(1 + \frac{\pi^{1/2} \mu t}{P_o^{1/2}}\right) \quad (2.3)$$

where  $P$  is the population of cells per patch,  $P_o$  is the initial inoculum per patch,  $\mu$  is the specific growth rate and  $t$  is the elapsed time. A similar approach was used to model contact inhibited growth on microcarriers however instead of circular colonies the shape of the colonies was assumed to be a spherical caps. Although this model overcomes the shortcomings of the model by Frame and Hu, it is limited in applicability by its assumptions. Firstly, the assumption of circular or spherical shapes of the colonies limits the colony geometry. The shape a colony takes will influence the rate of growth. The end result is an overprediction of the growth rate of small colonies. As a result a simple exponential model was used in the early phases of growth and a switch to the contact inhibited model is made in the middle and latter stages of growth. Secondly, it is assumed that the growth rate of a colony is not affected by the presence of other colonies. Obviously the merging of colonies will have a major effect on the growth rate of the cell culture.

In 1990 Lim and Davies developed a stochastic model to predict the growth rate

of contact inhibited cells on a flat surface. They concluded current models do not take into account the topology of the colonies of cells. Since cell division takes place at the perimeter of cell colonies the shape of these colonies will determine the shape of the growth curves. In the computer simulation the cells are modelled as irregular polygons. A mathematical technique was used to model cell division and growth, a Voronoi tessellation. In a Voronoi tessellation only perimeter cells may divide and grow. Division occurs over discrete time intervals. Colony merging is accounted for by restricting growth to perimeter cells with a "free" edge, that is perimeter cells which are not completely surrounded by neighbouring cells. The direction of cell division is random. Due to the randomness of cell division and the irregular shape of the cells, no assumptions are made to the shape of the colonies and therefore the drawback of the Cherry and Papoutsakis model is eliminated. However, as a consequence of the Voronoi tessellation, the number of neighbouring cells per cell in the culture follows a normal distribution with a mean neighbour size of 6 cells per cell.

Zygourakis et al. (1991) used a similar discrete time approach to characterize contact inhibited cell growth. However, in their approach a cellular automaton model was used. A detailed description of cellular automaton theory will be given later, for the present it is sufficient to describe it as a discrete time approach where cell division is determined by the cell's spatial environment. The advantage to using a cellular automaton is the ease in computational application and the analogy to contact inhibited growth. Again, as in the previous model, division is a discrete process however the direction of division is determined by the growth probability of neighbouring cell sites. The value of

a site's growth probability effectively determines the shape of a colony. Up until now the models have been restricted to flat surfaces. Zygourakis suggests their model could be altered to represent cell growth on a microcarrier by substituting a toroid for the flat surface. However, there is no attempt at the microcarrier-toroid modelling. Further, principal factors affecting growth which are unique to microcarrier cultures have not been discussed.

Very recently work in our laboratory (Forestell et al., 1992) was reported in which a cellular automaton was used to model the growth of contact inhibited cells and account for these factors. In this model the effects of inoculation density, microcarrier loading and initial cell attachment distribution could be readily accounted for. For simplicity the microcarrier was modelled as a pentagonal hexacontrahedron, a polyhedron with 60 faces each face having five sides. The faces of the polyhedron represent the number of cells on a microcarrier at confluence, ie 60 cells with each cell having 5 neighbours. Cell division occurs if one of the cell's five neighbouring sites is empty. The automaton model predictions agreed well with experimental data for MRC-5 cells growing on Cytodex 1 microcarriers. However, the model is restricted to the particular cell and microcarrier type. If a different cell line or microcarrier is used, where the number of cells at confluence is not very close to 60, the model is no longer applicable.

## CHAPTER III

### MATERIALS AND METHODS

#### III.1 CELL HANDLING PROCEDURES

##### III.1.1 Cell Stock

Both the MRC-5 and Vero cells were acquired from Connaught Laboratories, Ltd., Willowdale, Ontario. The MRC-5 cells used were from a frozen stock at an initial population doubling level (PDL) of 12. The population doubling level is simply the number of doublings the cells have been passaged. Cells with a PDL greater than 46 usually show signs of a decline in proliferation.

Vero cells are specified by the number of times they have been passaged. The original cell stock used was at a passage level of 122. Cells at a passage level greater than 140 begin to show tumorigenicity (or anchorage independence).

##### III.1.2 Cell Freezing

To maintain a stock of cells for later use cells cultured on T-flasks were frozen. In order to protect mammalian cells from genetic drift and/or contamination, cell lines are frozen in liquid nitrogen. A cryopreservant, dimethylsulfoxide (DMSO), is used to safeguard the cells from freezing effects (mechanical injury or denaturation of proteins). The freezing medium is made up of culture medium containing 15% serum and 8% DMSO. Cell freezing was a stepwise procedure detailed below:

- (i) Cells for freezing were in the exponential phase of growth. The cells were removed from the surface of one 175 cm<sup>2</sup> T-flask using standard trypsinization procedures, discussed in detail later, and resuspended in 10 % serum medium to neutralize the trypsin.
- (ii) To recover the cells from the medium the cells were pelleted by centrifugation at 125 g for approximately 10 minutes and the medium was removed.
- (iii) Cells were resuspended in 18 mL of freezing medium at 1x10<sup>6</sup> to 2x10<sup>6</sup> cells/mL and immediately transferred to 1.8 mL cryovials (Nunc, Sweden).
- (iv) The cryovials were placed into a styrofoam box with 2.5 cm walls lined with cotton and transferred to the -80°C freezer. The cells remained in the freezer overnight to allow for a slow, controlled freezing rate.
- (v) The following day the vials were transferred from the box to canes and stored in the liquid nitrogen vessel.

### **III.1.3 Cell Thawing**

The procedure of cell thawing was done as quickly as possible since sustained exposure of the cells to DMSO may result in a loss in cell viability. The cell ampoule was removed from the canes in the liquid nitrogen and the cap was loosened. This was done to vent any nitrogen which seeped into the ampoule. Once vented the cap was tightened and transferred to a 37°C water bath. After the sample had melted the ampoule was removed and the outside of the ampoule was cleaned with 70% ethanol solution. In a sterile hood the ampoule contents were transferred to one 175 cm<sup>2</sup> T-flask containing

75 mL of medium supplemented with 10% fetal bovine serum (FBS) and 1 % antibiotic supplement (content detailed in section III.2).

#### **III.1.4 Cell Propagation**

The culturing of cells from T-flask to T-flask is described below:

- (i) Thawed cells were grown to confluence on a 175 cm<sup>2</sup> in an incubator set at 37°C and 5 % CO<sub>2</sub>.
- (ii) Once confluent the medium was removed and the cells were treated with 10 mL of a 0.27 % trypsin in 0.03 M citrate buffer. After 30 seconds excess trypsin solution was poured out and the T-flask was placed in the incubator.
- (iii) After 10-15 minutes, at which point the cells should be detached from the surface, the T-flask was removed from the incubator. Cells were detached when the cells peel off the surface in a sheet. Care was be taken that the cells were not left too long in the incubator as prolonged exposure to trypsin will kill the cells.
- (iv) In a sterile hood the trypsin was neutralized by the addition of medium containing 10% serum.
- (v) The cell suspension was then repeatedly aspirated with a 10 mL pipette until a homogeneous cell suspension was attained.
- (vi) The cell suspension was then aliquoted to a new 175 cm<sup>2</sup> T-flask containing 75 mL of 10% FBS, 1% penicillin-streptomycin medium. The volume of cell suspension added to the T-flask was varied to attain a initial inoculum of 5x10<sup>4</sup> to 1x10<sup>5</sup> cells/mL.

The PDL of the MRC-5 cells used in experiments varied from 18 to 21. The passage level of the Vero cells used were between 123 and 125.

### **III.2 MEDIA CONTENT AND PREPARATION**

All media components were supplied by Gibco, BRL, Ltd. (Burlington, Ontario). The medium was Dulbecco's modified Eagle medium/F-12 (DMEM/F12) powder, catalogue number 430-2500EL. The exact ingredients in the DMEM/F-12 are available in Appendix A, Table A.1. Five liter batches were made by mixing one container of DMEM/F12 with 5 L of pyrogen free water. All water used in media preparation was softened, purified by reverse osmosis and passed through an ion exchange cartridge, organic removal cartridge and eventually through an ultrafilter (Aries model, Osmonics Inc., Minnetonka, MN).

Two batches of the 5 L media were made up. One of the 5 L batches was adjusted to a pH of 7.2 with 4 M HCl, the other was adjusted to a pH of 7.5 with 0.4 M NaOH. The medium batches were filtered into autoclaved 2 L bottles in the sterile hood. The filters were supplied by Nalgene Company (Rochester, NY) catalogue number 46509520 (0.2 $\mu$ m pore size).

Before use in cell culturing, the media was supplemented with fetal bovine serum (FBS). The FBS was supplied by Gibco BRL Ltd., catalogue number 200-614OAJ, control number 42N7125. To reduce the risk of contamination, an antibiotic supplement was also added prior to cell culturing. The antibiotic supplement, supplied again by Gibco BRL Ltd., contained; 10 units/mL of penicillin G sodium, 10  $\mu$ g/L of streptomycin and

25  $\mu\text{g/L}$  of amphotericin B as a Fungizone.

For the reactor experiments instead of FBS, adult bovine serum (ABS) supplemented with PPRF92 supplement mixture, developed by Forestell et al. (1990) was used. The ABS was supplied from a donor herd from Bocknek Ltd., Ontario.

### **III.3 SPINNER FLASK EXPERIMENTS**

#### **III.3.1 Spinner Flask Preparation**

Figure 3.1 depicts the spinner flask experiments used in the experiments. Prior to use the spinner flasks were washed, siliconized and autoclaved. This ensured the cells would not grow on the flask walls and the flasks were sterile. The working volume of the spinner flasks was 250 mL, the vessels were 70 mm in diameter and 220 mm high. Two side arms, 24 mm in diameter, allowed for sampling and media entries. To maintain a suspension a 55 mm teflon coated stirring bar was suspended approximately 10 mm above the bottom of the flask. The spinner flasks were placed on Thermodyne slow speed magnetic stirrers placed inside incubators, at 37°C and 5% CO<sub>2</sub>, and set between 40 and 60 rpm.

#### **III.3.2 Microcarrier Preparation**

In this study the microcarriers used were Cytodex 1 obtained in the dry form from Pharmacia Fine Chemicals, Upsalla, Sweden. The properties of the microcarriers are defined in Appendix A, Table A.2. Any glass vessels used with the microcarriers were siliconized with Surfasil (Pierce Chemical Co., IL.) prior to use. This prevented the microcarriers from sticking to the containers walls. The microcarrier loading was 5 g/L

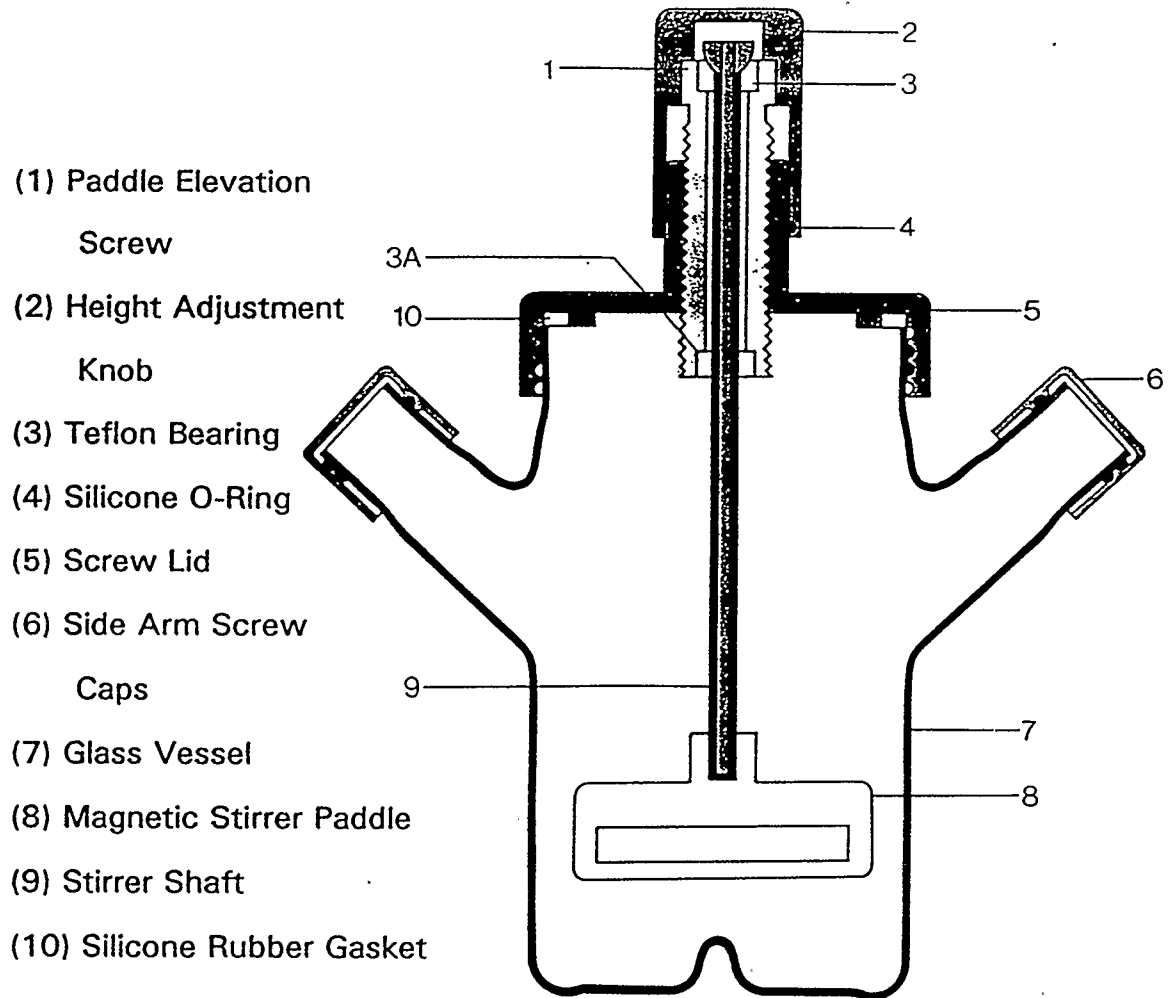


Figure 3.1. Diagram of 250 mL Corning spinner flask used in experiments.

in all experiments. A quantity of microcarriers was weighed to achieve this loading and transferred to a siliconized 125 mL erlemeyer flask. One hundred mL of  $\text{Ca}^{++}$  and  $\text{Mg}^{++}$  free phosphate buffered solution (PBS) was added to hydrate the beads. The beads were allowed to hydrate for a minimum of 3 hours, and then were washed three times with  $\text{Ca}^{++}$  and  $\text{Mg}^{++}$  free PBS (summarized in Appendix A, Table A.3) by allowing the beads to settle and decanting the microcarrier-free PBS. The flasks, containing approximately 75 mL  $\text{Ca}^{++}$  and  $\text{Mg}^{++}$  free PBS, were wrapped in aluminum foil and autoclaved using a Amsco model Eagle 3021 steam sterilizer (AMSCO Canada Inc., Woodridge, Ontario). The sterilizer was set at 120°C and the microcarriers were autoclaved for 30 minutes. Immediately after autoclaving the beads were removed from the sterilization unit and allowed to cool.

### **III.3.3 Inoculation Procedures**

T-flasks at approximately 80 to 100 % confluency were used to inoculate spinner flask cultures. The inoculation procedure developed by Forestell et al. (1992b) was used. This procedure was developed through extensive experimental work and ensures maximum cell attachment to the microcarriers. The work also differentiates between optimal inoculation and growth conditions. The procedure is as follows:

- (i) In a sterile hood the cooled, autoclaved beads were conditioned to the medium by washing three times with 100 mL of the low pH (pH = 7.2) serum free medium and then transferred to the culture vessel.
- (ii) Prior to cell inoculation, the culture vessel was supplemented with 4 % serum and 1 % antibiotic supplement to a final volume of 125 mL (ie. one

spinner flask contained 5 mL FBS, 1.25 mL antibiotic supplement and 118.75 mL medium). The rationale behind initiating the culture using a low pH, low serum medium is to facilitate the attachment and flattening of the cells to the microcarrier. Flat cells indicate complete attachment. The spinner flask was then allowed to equilibrate to culture conditions by placing it in the 5% CO<sub>2</sub>, 37°C incubator for 15 minutes to half an hour.

- (iii) Cells were removed from the surface of the T-flask using the previously mentioned trypsinization procedure. The cell suspension was added to the spinner flask.
- (iv) The spinner flask was then immediately transferred to the incubator and placed on the magnetic stirrers. The stirrer speed was set to 40 rpm.
- (v) After 3 hours cells have attached and flattened onto the microcarriers. At this point the remaining culture medium is added (125 mL). To bring the culture pH and serum levels up to optimal growth levels (ie. a pH between 7.4-7.6 and serum level of 10%) the medium added contains 20 mL of FBS, 1.25 mL antibiotic supplement and 103.75 mL of the 7.6 pH medium.

#### **III.3.4 Media Replenishments**

In order to investigate the effects of contact inhibition other external influences had to be controlled. That is, factors such as nutrient levels, toxin levels, oxygen levels and pH must be constant at optimal growth levels. To accomplish this, media replenishments were routinely performed for all spinner flask experiments.

Replenishments involved allowing the beads and cells to settle at the bottom of the

spinner flask in a sterile hood. Approximately 125 mL to 150 mL of spent medium was removed and replaced with 125 to 150 mL of fresh medium supplemented with 10 % FBS and 1 % antibiotic supplement. The initial pH of the medium was at 7.4. This was obtained from a 1:1 mixture of the high and low pH medium. The medium was warmed for approximately 15 minutes in a 37°C water bath. Care was taken in performing the media change to prevent loss of cells and contamination by venting the opposite arm of the spinner flask and pouring only the medium out (not cells and beads) when removing media. The frequency of media replenishments was determined by pH and nutrient levels. For all experiments pH, glucose, lactate and glutamine levels were maintained between; 7.0-7.5, 1.8-2.7 g/L, 0.2-1.0 g/L and 0.117-0.250 mg/L respectively. The agitation levels were initiated at 40 RPM and gradually increased to 60 RPM to ensure no limitations to oxygen transfer. These agitation levels were determined by Forestell et al. (1992) to maintain dissolved oxygen levels.

### **III.3.5 General Sampling**

In general three samples were taken from the spinner flasks; a media sample for pH and glucose/lactate measurements, a media sample for glutamine levels and a cell sample for enumeration purposes. All samples were taken in a sterile hood.

Media samples were taken by first allowing the cells and microcarriers to settle on the bottom of the spinner flask. Then a 5 mL sample of the supernatant sample was taken, pH and glucose/lactate levels were measured from this sample. A 1.5 mL sample of the supernatant was also taken for determination of glutamine measurements.

A cell sample was also taken to determine the cell density. The spinner flask was

agitated, to ensure a homogeneous suspension, then 1 to 2 mL of the cell and microcarrier suspension was transferred to a 5 mL test tube. The volume of the cell sample was varied according to the cell density.

### **III.3.6 Sampling for Flow Cytometry**

In order to analyze the cell cycle dynamics of the microcarrier culture a cell sample was necessary. The volume of the sample was varied according to cell density, as the cell density determines the quantity of staining chemicals which will be used on the cells.

Again the spinner flasks were agitated to provide a homogeneous cell sample. Immediately after the microcarriers in the sample settled the supernatant was removed and transferred to another test tube. This ensured the separation of any free cells (cells or cell debris not attached to microcarriers) from the attached cell sample. This sample was referred to as the "supernatant" sample. The microcarrier sample was then washed with 2 mL of  $\text{Ca}^{++}$  and  $\text{Mg}^{++}$  free PBS. The PBS was subsequently removed and the microcarriers were resuspended in 1 mL of 0.27 % trypsin in a 0.03 M citrate buffered solution. Once the microcarriers had settled the excess trypsin was removed. The microcarrier sample was then transferred to the incubator for 10 minutes to allow for cell detachment. The cells were subsequently resuspended in 1 mL of medium supplemented with 10% FBS, to neutralize the trypsin. To ensure the flow cytometer orifice would not be blocked by microcarriers, the beads were separated from the cells by aspirating the cell suspension through a pipette and filtering the cell/bead suspension through a fine mesh screen. This final cell suspension was referred to as the "attached cell" sample.

### **III.4 ANALYTICAL PROCEDURES**

#### **III.4.1 Cell Enumeration**

To determine the viable cell densities of cell inoculum, a portion of the inoculum was transferred to a test tube. The cell suspension was aspirated and a 50  $\mu\text{L}$  sample was transferred to a sampling well and stained with 250  $\mu\text{L}$  of trypan blue. This results in a 5x dilution of the cell sample. The stained cells were then counted with a haemocytometer.

Cell densities in microcarrier cultures were determined by treatment with 1.0 g/L of crystal violet in 0.1 M citric acid for 1 hour at 37° C. The microcarriers in the sample were first allowed to settle and the supernatant removed. A volume of crystal violet was added (the volume was varied according to cell density, typically the volume ranged between 0.5 to 2mL) and after one hour the stained nuclei were counted with a haemocytometer.

#### **III.4.2 Environmental and Nutrient Analysis**

The pH of the culture was determined by allowing the 5 mL medium sample to equilibrate at 37° C and 5 % CO<sub>2</sub> for approximately 30 minutes. The measurement was taken with a Cole Parmer microcomputer pH-vision. D-glucose and L-lactate levels were determined with a YSI 2000 Glucose/Lactate Analyzer (Yellow Springs Instruments, Yellow Springs, Ohio). The only amino acid analyzed was glutamine. Glutamine levels were determined by measuring the absorbances at 340 nm of orthophthaldialdehyde (OPA) derivatives after separation on a reverse phase HPLC column (Supelcosil LC-18, Supelco, PA.). To convert the absorbency readings (ie. area of the absorbency peaks) to

concentrations (mM) a standard curve was generated.

### **III.4.3 Flow Cytometry**

All flow cytometry analyses were performed immediately after cell sampling. A Becton Dickinson FACScan flow cytometer equipped with a Hewlet Packard work station and software supplied by Becton Dickinson. The flow cytometer was used to differentiate cells in the various phases of the cell cycle using the acridine orange method described by Darzynkiewicz et al (1975,1976). A brief description of this method follows. The cells were made permeable by 1 mL of Triton X-100 (Sigma) and stained with 2 mL of chromatographically purified acridine orange 2(Polysciences Inc., Warrington, PA.) at a final dye concentration of 13  $\mu$ M and dye to DNA molar ratio greater than 2 in the presence of 1mM Na-EDTA. At these conditions, the interaction of the dye with the DNA results in a green fluorescence at 530 nm. The content of DNA is proportional to the amount of fluorescence measured by the flow cytometer at this wavelength. Interaction of the dye with RNA gives a red fluorescence with maximal emission at 640 nm. Again RNA content is proportional to the amount of fluorescence.

## CHAPTER IV

### CELLULAR AUTOMATON MODEL

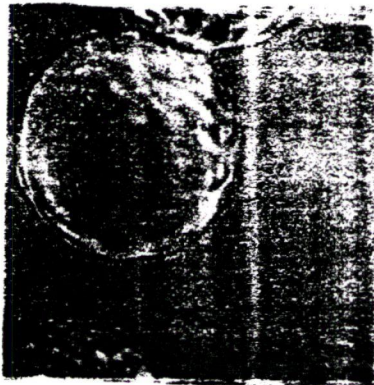
#### IV.1 OVERVIEW

For all anchorage dependent cell lines, cell attachment to a surface is necessary for growth and proliferation. This results in a phenomena called contact inhibition. Contact inhibition is the condition where normal cell growth is interrupted as a cell becomes surrounded by neighbouring cells. In a typical microcarrier culture cells first attach to the microcarrier and begin to grow and divide. As cell division and growth proceeds the surface area available for growth decreases. The decreasing surface area results in less space for new cell growth and division and therefore, the overall growth rate of the culture decreases. The growth of a cell on a microcarrier from initial attachment to confluence is pictured in Figure 4.1. The end result of contact inhibition is that both the cell density and apparent growth rate varies with time even when there are no nutritional limitations to growth.

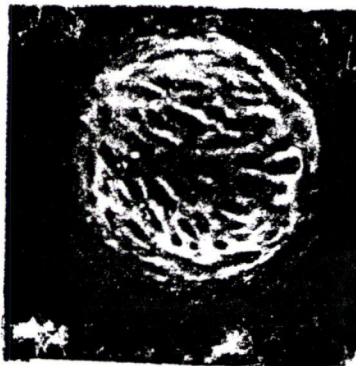
In order to properly study and analyze the cell growth kinetics it is necessary to decouple the effect of contact inhibition from the nutrient and environmental kinetics. This would allow the accurate evaluation of nutrient/toxin uptake/production rates and other environmental effects on the cell culture without the influence of contact inhibition. This is of key importance when developing cell growth models for large scale microcarrier cultures. In order to efficiently design and operate large scale bioreactors for



(a) time = 0 hours (inoculation)



(b) time = 60 hours



(c) time = 150 hours

Figure 4.1. The progression of the growth of Vero cells, growing on Cytodex 1 microcarriers, from inoculation to near confluence.

for microcarrier cultures contact inhibition must be decoupled from the growth kinetics.

In this chapter a cellular automaton model has been developed to model the growth of anchorage dependent cells on microcarriers. Previous models developed to incorporate the effects of contact inhibition, although moderately effective on flat surfaces, have failed to address the unique growth characteristics of microcarrier cultures. In both the Lim and Davies (1990) and the Zygourakis (1991a, 1991b) papers the models were limited to flat surfaces, and hence low cell densities. As the large scale cultivation of anchorage dependent cells is performed using microcarriers, the growth kinetics particular to microcarriers must be accounted for.

A microcarrier culture will have a distribution of microcarrier sizes and have a distribution of surface areas. Therefore a percentage of the microcarrier will be able to support more than the average number of cells whereas a percentage will be able to support less than the average. For instance, Cytodex 1 microcarriers have an average diameter of 180  $\mu\text{m}$  (Pharmacia, 1981), however the diameters may range from 130 to 220  $\mu\text{m}$  (see Table A.2). The end result is that there will be a distribution of the number of cells which a microcarrier can support at confluence. In microcarrier cultures the inoculation density on a microcarrier will affect the progression of cell growth. The size of the inoculation and the proximities of cells seeded on the microcarrier will be determining factors in the onset of contact inhibition. When this concept is expanded to a microcarrier culture, where there are millions of microcarriers (for a microcarrier loading of 5g/L there are about 34 million microcarriers/L) there will be a variety of seeding and growth probabilities. The cellular automaton model proposed effectively

incorporates these effects and overcomes the limitations of previous models.

The proposed model is simple to apply yet provides an accurate representation of anchorage dependent cell growth on microcarriers. The model is capable of accounting for the unique characteristics of cell growth on microcarriers such as the distribution of the number of neighbouring cells per cell, the distribution of microcarrier sizes and the distribution of the inoculum. The theory behind the cellular automaton approach, model assumptions, computer simulation methodology and the model attributes are covered in this chapter.

## **IV.2 CELLULAR AUTOMATON MODEL**

### **IV.2.1 Cellular Automaton Theory**

A cellular automaton is a mathematical description of a physical system where space and time are discrete variables (Wolfram, 1983). The space consists of a multidimensional network of computational sites. Each site may have a finite number of states and a finite number of adjacent sites, or neighbours, which may influence the sites state. In short, in the progression of a cellular automaton, the value of a site is determined by the value of its neighbouring site. In contact inhibited cell growth, the growth and division of a cell seeded on a surface is dependent upon its local population density. The definitions of a cellular automaton progression and contact inhibited cell growth illustrate the analogy between the two concepts.

### **IV.2.2 Model Development**

In the proposed model the cellular automaton "space" is defined as the surface

area of the microcarrier. The surface area is described in the form of a neighbour table. The table is simply a matrix defining a cell and its neighbouring cells. The dimensions of the matrix are determined by the number of cells the microcarrier can support at confluence and the number of neighbours a cell may have. The number of rows in the matrix is the number of cells at confluence, the number columns correspond to the number of neighbours a cell may have. For instance if a microcarrier can support 62 cells at confluence and each cell is assumed to have five neighbours the neighbour table is a 62 by 5 matrix. A sample of a neighbour table is illustrated in Table 4.1. For each cell site,  $n_i$  ( $i=1, \dots, 5$ ) represents the neighbouring cells. Each neighbouring site in the matrix represents attachment sites. Figure 4.2 depicts a portion of the neighbour table superimposed on an actual microcarrier with attached cells.

In order to construct a neighbour table which is physically representative of a confluent microcarrier a number of rules must be adhered to. First, if cell 1 has cell 2 as a neighbour, it follows cell 2 must have cell 1 as a neighbour. Second, a cell cannot have itself as a neighbour. Finally, in order for the table to be physically representative of the microcarrier, cells which are neighbours to each other must have similar neighbourhoods. The advantage to defining the surface area of the microcarrier is the mathematical ease in producing the table and the physical correlation to an actual microcarrier.

As required by the automaton theory each neighbour site in the matrix is assigned a state at the onset of the program. The site may have one of four states:

1. "Unoccupied" - the site is not populated at the current time step.

**Table 4.1:** Example of the cellular automaton neighbour table.

cell site	$n_1$	$n_2$	$n_3$	$n_4$	$n_5$
1	2	3	4	5	6
2	1	3	7	8	13
3	1	2	8	9	14
.	.	.	.	.	.
.	.	.	.	.	.
.	.	.	.	.	.
62	57	58	59	60	61

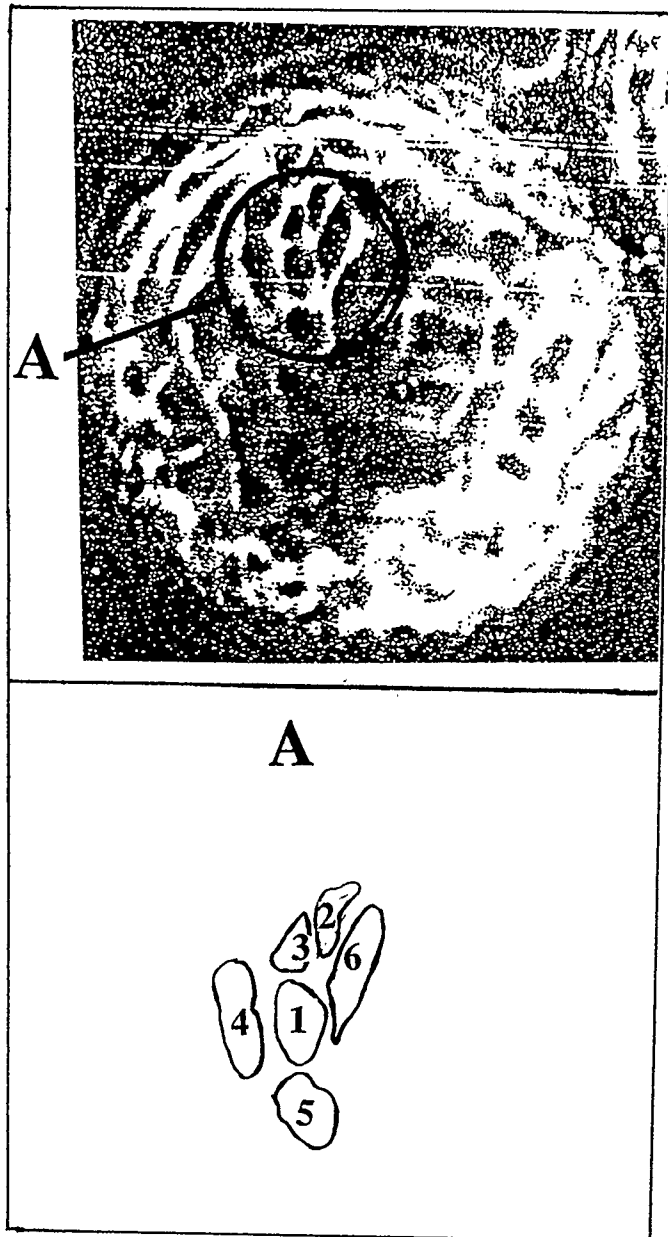


Figure 4.2. Portion of a neighbour table, generated by cellular automaton, superimposed on attached Vero cells on a Cytodex 1 microcarrier.

2. "Occupied" - the site is occupied by a cell capable of division in the current time step.
3. "Newly Occupied" - the site is occupied by a new daughter cell and therefore not capable of division in the current time step.
4. "Inhibited" - the cell is occupied by a cell which is completely surrounded by neighbouring cells and therefore cannot divide.

It is important to note that the neighbour sites in the matrix simply represent where a cell will attach. That is, at time equals 0 only inoculated cell sites are "occupied", all other sites in the neighbour table are deemed "unoccupied".

#### **IV.2.3 Model Assumptions**

Inherent in the above model description are a number of assumptions.

- Firstly it is assumed the cells form a monolayer over the entire microcarrier surface area. That is, cells do not grow on top of each other. For the two cell lines used in this thesis the monolayer assumption is valid.
- Secondly, it is also assumed the doubling time is uniform among all cells in the culture. Although there will be deviation in the doubling times of the cells in the culture the overall average doubling time of the culture will be the observed. The model could readily be modified to account for deviations in cell doubling times by applying a distribution to the observed cell doubling time which could be easily incorporated into the computer program.
- Thirdly, it is assumed we have synchronous growth of the microcarrier culture, that is cell division occurs at the same point in time for all cells

capable of division in the culture. Although, initially synchronous populations eventually become asynchronous, the number of doublings on microcarrier to confluence is characteristically low (typically 10 to 20 doublings) and the deviation in synchronicity becomes less of a factor.

- Finally, the death rate is assumed to be negligible. In Chapter 6 this assumption is validated with experimental data.

#### **IV.2.4 Algorithm Considerations**

Up to this point each cell's neighbourhood and the conditions of cell growth have been defined. The computer simulation may then be initiated. Each simulation represents the cell attachment and subsequent cell growth progression for one microcarrier. The program was written in Fortran77 and run on the departmental Apollo workstations. An algorithm of the program for a one microcarrier simulation is:

- (i) The neighbour table is set up according to the number of cells at confluence (which varies according to the cell type and microcarrier size and type) and the number of neighbouring cells per cell.
- (ii) Cell (neighbour) sites are randomly filled according to the given inoculation density.
- (iii) Each cell site is examined with respect to its state. If a cell is capable of division, a neighbour site is randomly chosen. At this point one of three things can occur:
  - (a) If the neighbour site is "unoccupied" division occurs and the new daughter cell is designated as "newly occupied".

- (b) If the neighbour site is "occupied" or "inhibited" a different neighbour is chosen.
- (c) If there are no "unoccupied" neighbour site the cell is designated "inhibited".
- (iv) After all cell sites have been inspected "newly occupied" sites are updated to "occupied" and the time step (ie. doubling time) is advanced.
- (v) Steps (ii) through to (iv) are repeated until confluence is reached.

Since the direction of division is random the shape of the cells and the cell colonies will vary from simulation to simulation. In microcarrier cultures there is no pattern to cell or cell colony shape and therefore the simulation parallels actual cell cultures.

To approximate an actual microcarrier culture, where there are millions of microcarriers present, 1000 bead simulations are performed for one set of data. The set of data includes the inoculation density, number of neighbouring sites and number of cells at confluence. In general, the average of the  $m$  simulations for a given inoculation density ( $I$ ), number of neighbouring cells ( $n_b$ ) and maximum cell number at confluence ( $N_{\max}$ ) is obtained from:

$$N(t | I, n_b, N_{\max}) = \frac{1}{m} \sum_{j=1}^m N_j(t | I, n_b, N_{\max}) \quad (4.1)$$

where  $N_j(t | I, n_b, N_{\max})$  is the number of cells per bead, for simulation  $j$ , given the  $I$ ,  $n_b$  and  $N_{\max}$ .

The choice of 1000 simulations as opposed to a higher or lower number of simulations was based on the standard deviation of the mean responses. The standard

deviation between number of cells computed by the automaton for the  $m$  simulations is given by:

$$\sigma^2 = \frac{\sum_{j=1}^m (N(t)_j - N(t))^2}{m-1} \quad (4.2)$$

where  $\sigma^2$  is the variance (standard deviation squared). As expected the standard deviation showed an increasing trend with time until the seventh time step (dimensionless doubling time) was reached. At this time the standard deviation hit a maximum and began to decrease with time. The point of maximum deviation was used to determine the optimal number of simulations which would accurately represent a microcarrier culture. For 100 simulations the  $\sigma$ , at doubling time seven, was 2.943. For 500 simulations the deviation decreased to 2.843. For 1000 and 5000 simulations the standard deviation was virtually unchanged, 2.731 and 2.730. For the 1000 simulations the program execution times are much faster than the 5000 simulations and there was no significant variability between the two cases, therefore 1000 simulations was more than sufficient to represent a microcarrier population. Further the standard error in the automaton predictions is the same as the standard error in the estimation of the sample mean, hence it is equal to  $\sigma/m^{0.5}$ . For  $m=1000$  the standard error was 0.08 which was concluded to be acceptable.

### IV.3 MODEL ATTRIBUTES

The computer program described above generates the number of cells per microcarrier at each time step (or dimensionless doubling time) for a specific inoculation, number of neighbouring cells and maximum cell number attached at confluence. The

progression of the automaton generated growth curves will be affected by each of these factors. In the following sections the effect of these three elements on the automaton will be examined.

#### **IV.3.1 Variation of growth curves in microcarrier cultures**

As previously mentioned, in a typical microcarrier culture there are millions of microcarriers and therefore a multitude of ways in which cells attach and divide on the microcarrier surface. The result is that cell attachment and the growth progression on one microcarrier will vary from another. Further, the observed experimental growth curve will be a suitable average of all the different microcarrier growth curves (as in Equation 4.1). Figures 4.3, 4.4 and 4.5 illustrate this fact.

In Figure 4.3 the variation of initial cell attachment and growth possibilities, for an inoculum of 1 cell/bead and final cell density of 60 cells/bead, is captured. A thousand simulations were run, the upper line represents the simulation which required the minimum doublings (dimensionless doubling time) to reach confluence, the lower line represents the simulation requiring the maximum doublings to reach confluence. The middle line represents the average of the 1000 simulations, calculated from Equation 4.1, and should represent the growth curve that would be experimentally obtained if all microcarrier were seeded with exactly 1 cells. As the figure illustrates the growth curves for a microcarrier, under the same inoculation density, can exhibit considerable variation. In Figure 4.4 the same growth curves were generated but at an inoculum of 5 cells/bead. The increase in the inoculum has led to a decrease in the variability between the maximum and minimum growth curves. This is not an unexpected phenomenon as a

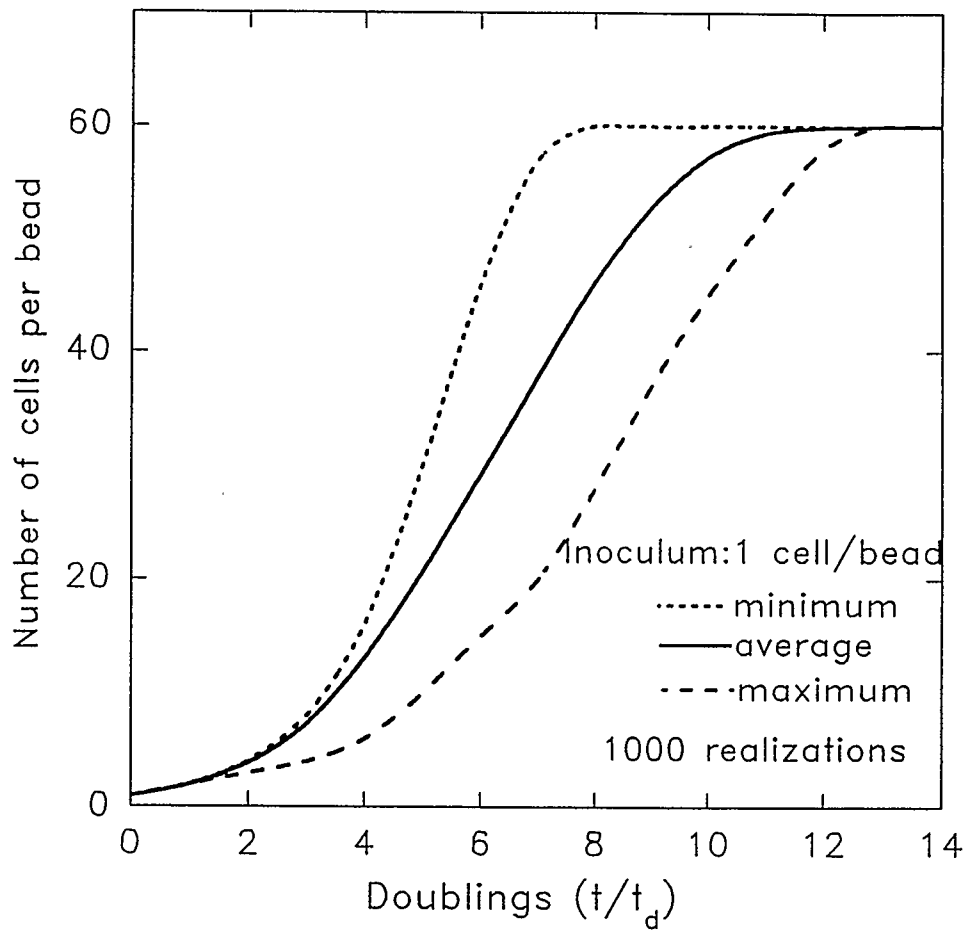


Figure 4.3. Variability in the cellular automaton generated growth curves at an inoculum of 1 cell/bead. The minimum and maximum curves represent the minimum and maximum doubling times required to reach confluence of the 1000 simulations run. The average curve represents the average of the 1000 simulations.

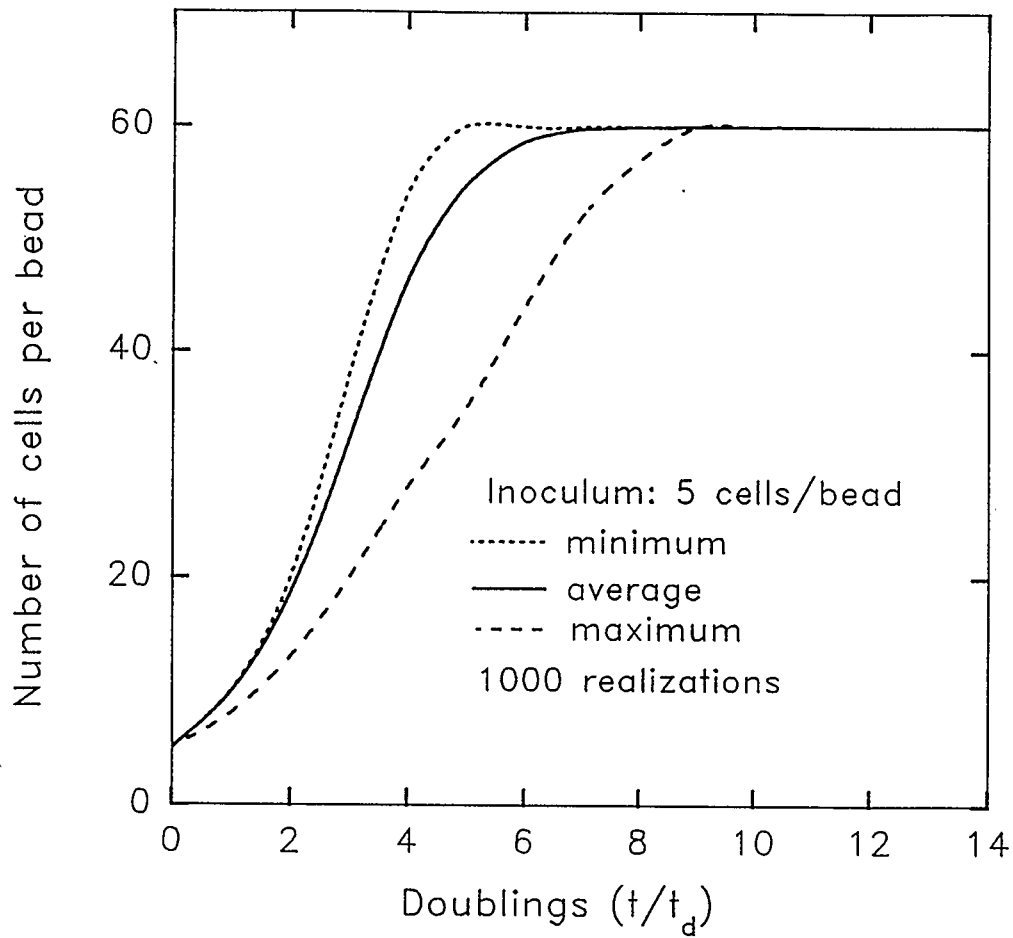


Figure 4.4. Variability in the cellular automaton generated growth curves at an inoculum of 5 cells/bead. The minimum and maximum curves represent the minimum and maximum doubling times required to reach confluence of the 1000 simulations run. The average curve represents the average of the 1000 simulations.

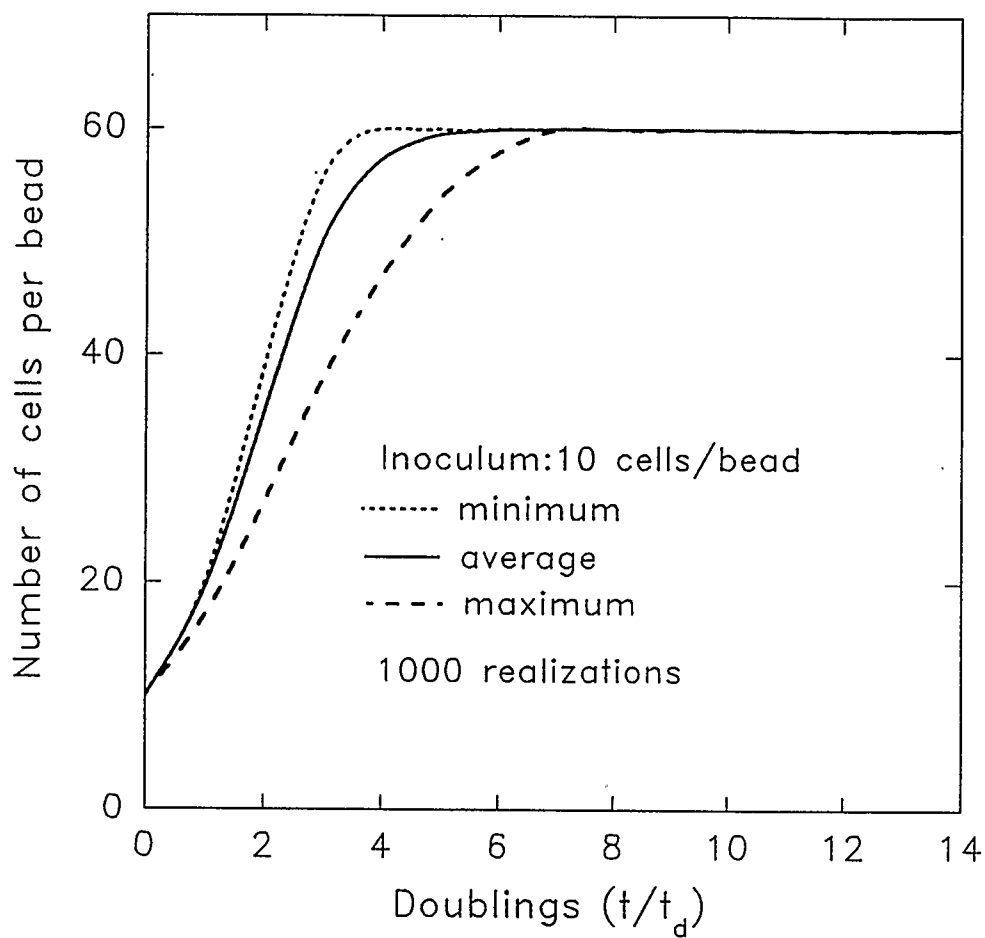


Figure 4.5. Variability in the cellular automaton generated growth curves at an inoculum of 10 cells/bead. The minimum and maximum curves represent the minimum and maximum doubling times required to reach confluence of the 1000 simulations run. The average curve represents the average of the 1000 simulations.

higher inoculum results in contact inhibition effecting the culture more rapidly. The effect of contact inhibition is a decreasing surface area and therefore decreasing growth possibilities, that is cell crowding will become a factor much earlier in the culture life. The result is a corresponding decrease in the variability of the growth curves. Figure 4.5 further validates this conclusion by showing the predictions for the case at an inoculum of 10 cells per bead.

#### **IV.3.2 Number of neighbouring cells**

The number of neighbouring cells a cell may have on a microcarrier will affect the onset of contact inhibition. Figure 4.6 depicts the average growth curves for two different neighbourhood sizes, five and six neighbouring cells/cell. The cell density per microcarrier is plotted against the number of doublings. Again both curves were generated from the average of 1000 simulations, each simulation representing the growth progression on one microcarrier. The initial inoculum for each simulation was one cell per bead and the final cell density was assumed to be 60 cells per bead. The six neighbourhood curve requires fewer doublings to reach confluence than the five neighbourhood. Further, the slope of the two curves begins to differ after approximately eight doublings. This indicates the growth rate is slightly greater, for the same doubling interval, for the larger neighbourhood than the smaller. Again this can be explained by the effects of contact inhibition. The greater the number of neighbouring sites the greater probability of a larger number of actively dividing cells. Although the surface area for growth is the same the cells have more directions in which to divide and hence the

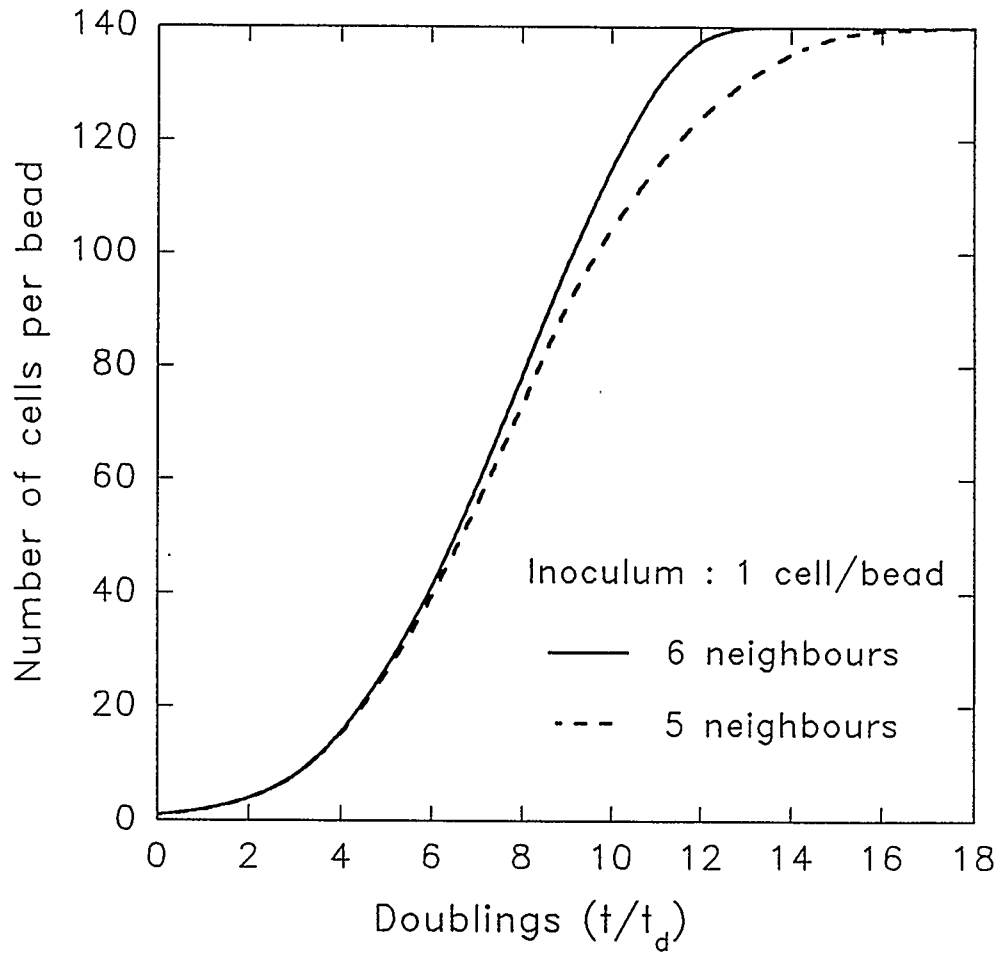


Figure 4.6. Effect of varying the neighbour space, 5 neighbours/cell and 6 neighbours/cell, on the progression of the cellular automaton generated growth curves at an inoculum of 1 cell/bead.

growth rate on the microcarrier does not decrease as quickly. The increase in the growth rate translates to a shorter time to reach confluence.

As the number of neighbours will have an effect on the growth curves it is important to account for the possibility of a distribution in the number of neighbouring cells in a microcarrier culture. The automaton can account accomplish this by generating growth curves for a variety of neighbour spaces and calculating a suitable average based on experimental observations taken under a microscope. The average over all possible neighbouring sites is given by:

$$N(t|I, N_{\max}) = \sum_r P(n_{b,r}) \times N(t|I, n_{b,r}, N_{\max}) \quad (4.3)$$

In this equation the probability of a cell having  $r$  neighbouring cells,  $P(n_{b,r})$  is obtained from the neighbour distribution. The sum of the weighted averages,  $P(n_{b,r}) \times N(t|I, n_{b,r}, N_{\max})$  is then used to calculate the number of cells per microcarrier,  $N(t|I, N_{\max})$ , as time progresses given the inoculation density and maximum cell number per bead at confluence.

### IV.3.3 Microcarrier size distribution

In a microcarrier culture there is a distribution of microcarrier radii and therefore a distribution of the size of the surface areas available for growth. It follows microcarriers on the higher end of the distribution, or larger radii, will be capable of supporting more cells than smaller microcarriers. Figure 4.7 graphically illustrates this fact. In the figure the effect of the microcarrier radii on the progression of growth on the microcarrier is depicted. The curves are an average of 1000 simulations at an inoculum of one cell per bead and a neighbour space of 5. The final cell density for the 82, 90 and

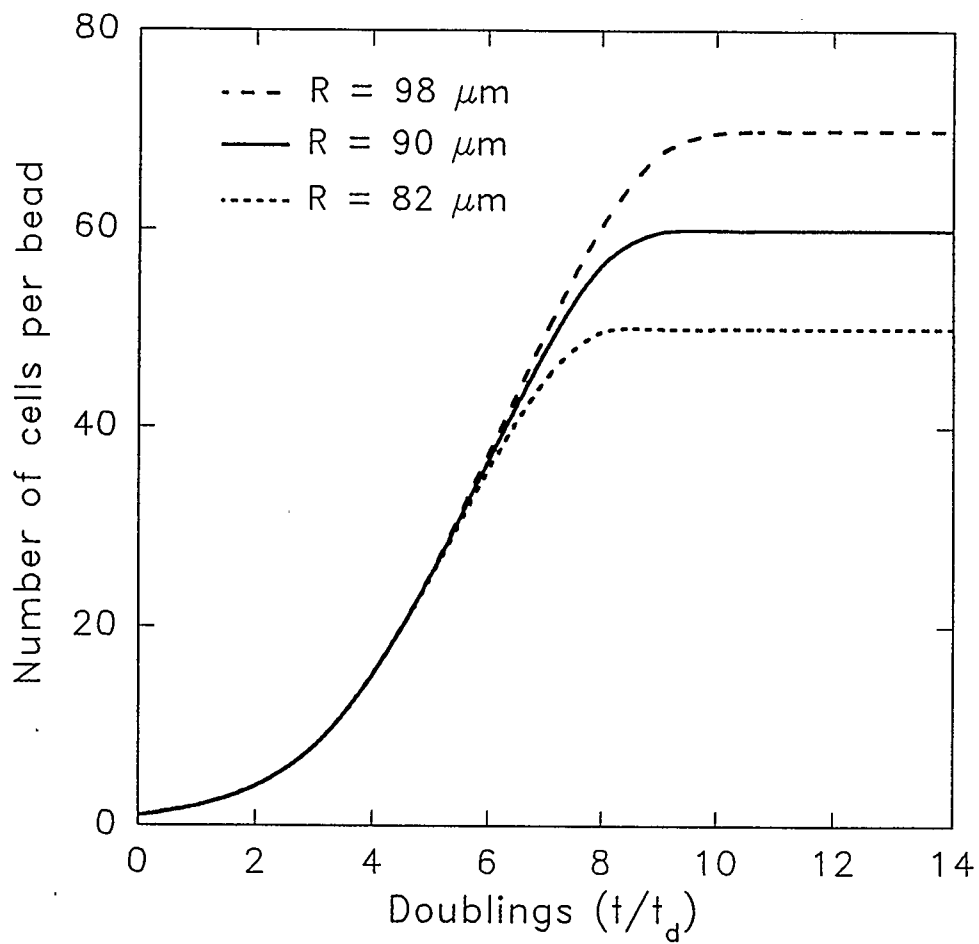


Figure 4.7. Effect of varying the microcarrier radius,  $98 \mu\text{m}$ ,  $90 \mu\text{m}$  and  $82 \mu\text{m}$ , on the progression of the cellular automaton generated growth curves at an inoculum of 1 cell/bead. Where "r" is radius.

98  $\mu\text{m}$  microcarrier radii are 50, 60 and 70 cells per bead respectively. The only parameter affected is the time to reach confluence. Since the number of cells at confluence on the microcarrier is less for smaller radii microcarriers the time to reach confluence should be correspondingly smaller.

Again the distribution of microcarrier sizes can be incorporated into the cellular automaton model through the following equation:

$$N(t|n_b, I) = \sum_{k=1}^s P(N_{\max,k}) N(t|I, n_b, N_{\max,k}) \quad (4.4)$$

The probability,  $P(N_{\max,k})$ , of a microcarrier with a certain surface area, corresponding to  $N_{\max,k}$ , is determined from the microcarrier specifications. The probability is then used as a weighting factor and multiplied by the number of cells at a given inoculation density and number of neighbouring cells,  $N(t|I, n_b, N_{\max,k})$  as a function of the maximum cell density.

#### IV.3.4 Inoculum density effect

In Figure 4.8 the effect of the size of the inoculum on cell growth on a microcarrier is shown. Again each curve is an average of 1000 simulations. The shape of the growth curve tends to become less flat as the inoculum is increased from one to ten cells per bead. This indicates that the growth rate is decreasing more rapidly with time at the higher inoculum than the lower. A higher inoculum will accelerate the onset of contact inhibition. At higher cell inoculum colony merging and seeding effects (ie. the proximity of cells seeded on the surface) will decrease the overall growth rate more rapidly. However, the higher inoculum also translates to a more rapid transition to confluence. These are important factors when cultivating microcarriers for production

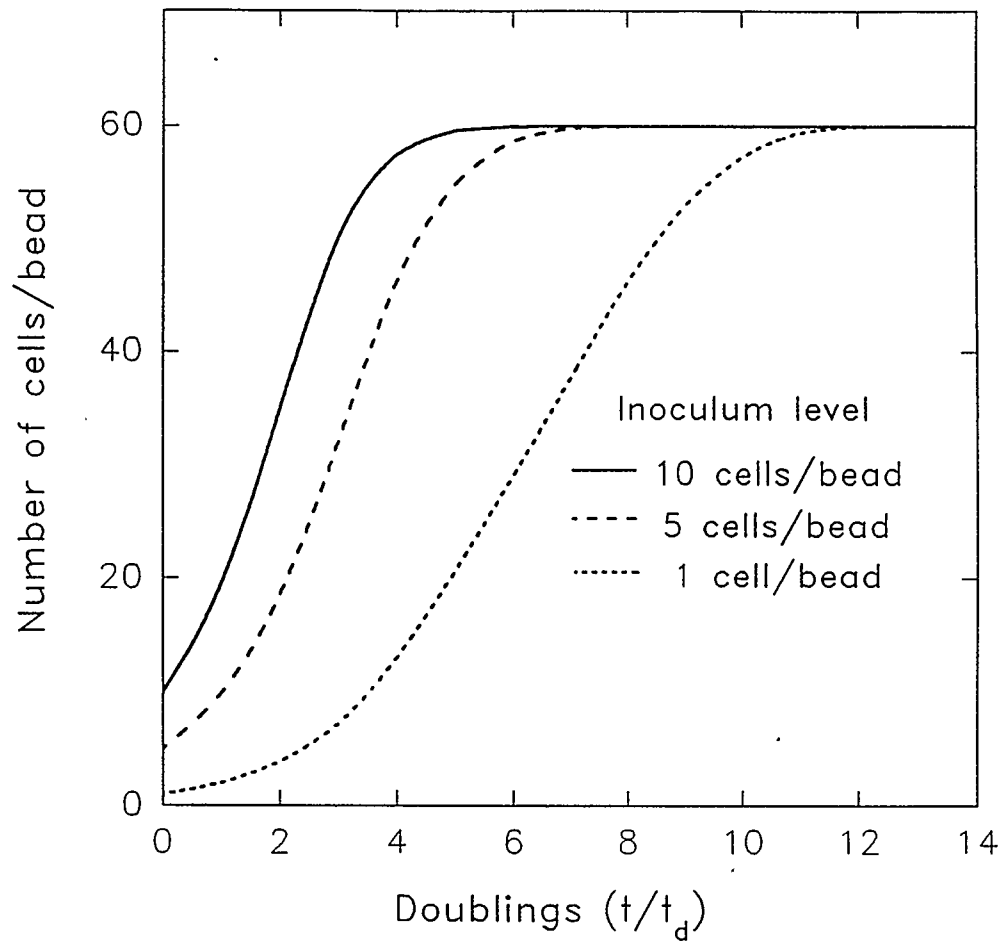


Figure 4.8. Comparison of the cellular automaton generated growth curves at three different inoculums, 1, 5 and 10 cells/bead.

purposes. If the production of the pharmaceutical is growth associated then it is desirable to maximize the growth rate by using a low inoculum. However, if the purpose is to achieve high cell densities in a short time a larger inoculum is preferred. The automaton thereby becomes a tool in determining optimal inoculum conditions.

#### IV.3.5 Inoculation distribution

It should be noted the Figure 4.8 growth curves assume each microcarrier is inoculated with exactly 1, 5, or 10 cells per bead. However, in a microcarrier culture this is not the case. It has been observed cells inoculated into a microcarrier culture follow a Poisson distribution (Forestell et al., 1992a):

$$P(I) = \frac{e^{-\lambda} \lambda^I}{I!} \quad (4.5)$$

where  $\lambda$  is the average inoculation density per bead and  $P(I)$  is the probability a bead will be inoculated with exactly  $I$  cells. The impact of the distribution becomes evident when it is considered as a result of the distribution a portion of the microcarriers will not be populated upon inoculation. Figure 4.9 illustrates this phenomena for a  $\lambda$  of 2 cells per bead. Note from the figure about 13 percent of the beads in a culture will remain vacant. Further, 27 percent of the beads have 1 and 2 cells/bead and 2.5 percent of the beads have as high as 6 cells/bead. With a percentage of beads unpopulated the microcarrier culture cannot reach maximum cell density. To accurately predict the growth of actual microcarrier cultures, the Poisson distribution must be applied to the automaton data. By generating automaton data for an inoculum of  $I$  cells per bead growth curves can be produced corresponding to actual cell cultures by combining the probabilities with the

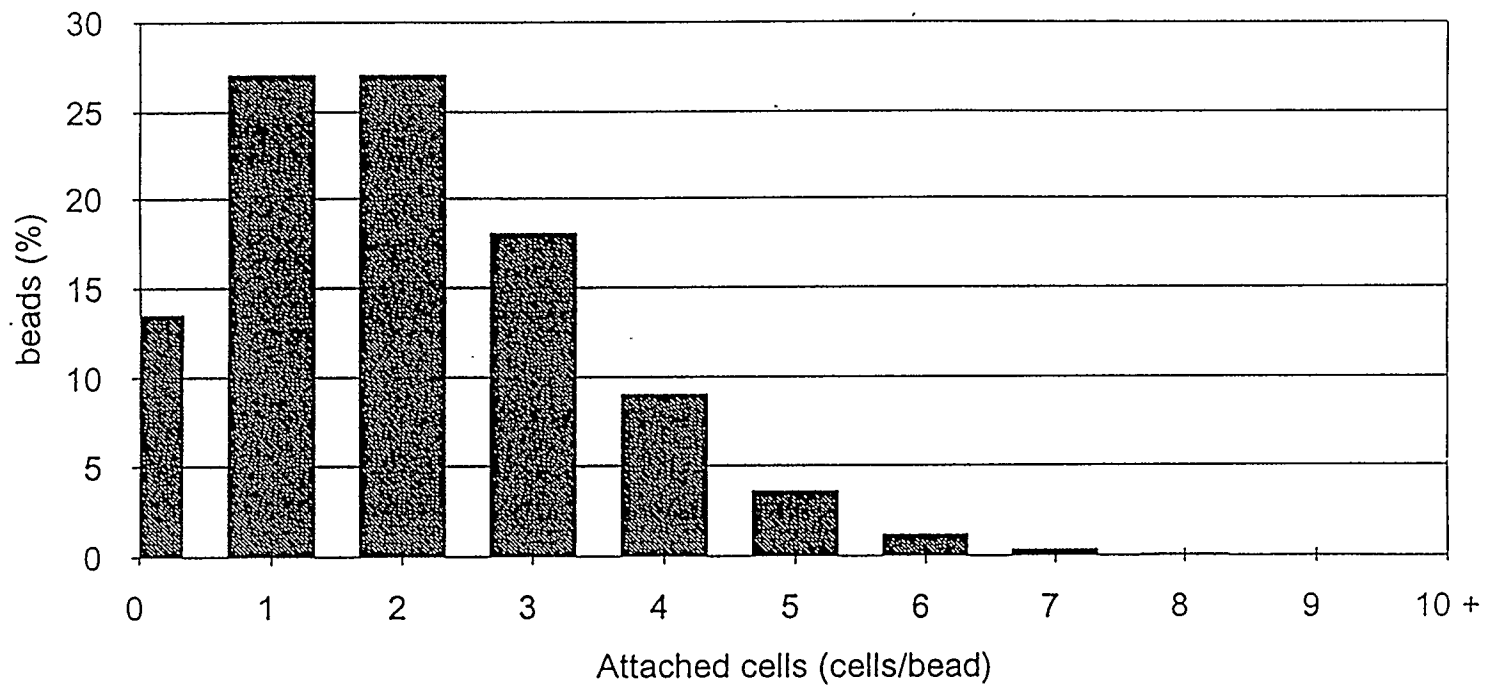


Figure 4.9. Percentage of beads with attached cells, upon inoculation, when inoculation and attachment follows a Poisson distribution. The average inoculation ( $\lambda$ ) is 2 cells/bead.

automaton data:

$$N(t|n_b, N_{\max}) = \sum_i P(I_i) N(t|I_i, n_b, N_{\max}) \quad (4.6)$$

In this equation the  $n_b$  and  $N_{\max}$  are given and the number of cells per bead is calculated as a function of the inoculation density per bead.  $N(t|I_i, n_b, N_{\max})$  is the number of cell per microcarrier at any time,  $t$ , for a microcarrier inoculated with  $I$  cells.

With this distribution the effect of the inoculum on a *population* of microcarrier may be depicted. Figure 4.10 represents the growth curves generated by the automaton with the distribution. A loading of 5 g/L of Cytodex 1 (Pharmacia, 1981) microcarriers was used to simulate the microcarrier culture. The maximum cell density was 62 cells per bead and 5 neighbours per cell. At an average inoculum ( $\lambda$ ) of 1 cell per bead the final cell density is  $12.2 \times 10^5$  cells/mL while at 10 cells per bead the final cell density is the maximum of  $21.0 \times 10^5$  cells/mL. The lower cell density at the lower inoculum reflects the larger percentage of vacant beads.

#### IV.4 OVERALL EFFECT ON MICROCARRIER CULTURE

Before the automaton model may be compared to the experimental data the distribution of the inoculation density, distribution of the number of neighbouring cells and the distribution of microcarrier sizes must be combined. The resulting equation will give the number of cells per microcarrier at any time.

$$N(t|I, N_{\max}) = \sum_r P(n_{b,r}) N(t|I, n_{b,r}, N_{\max}) \quad (4.3)$$

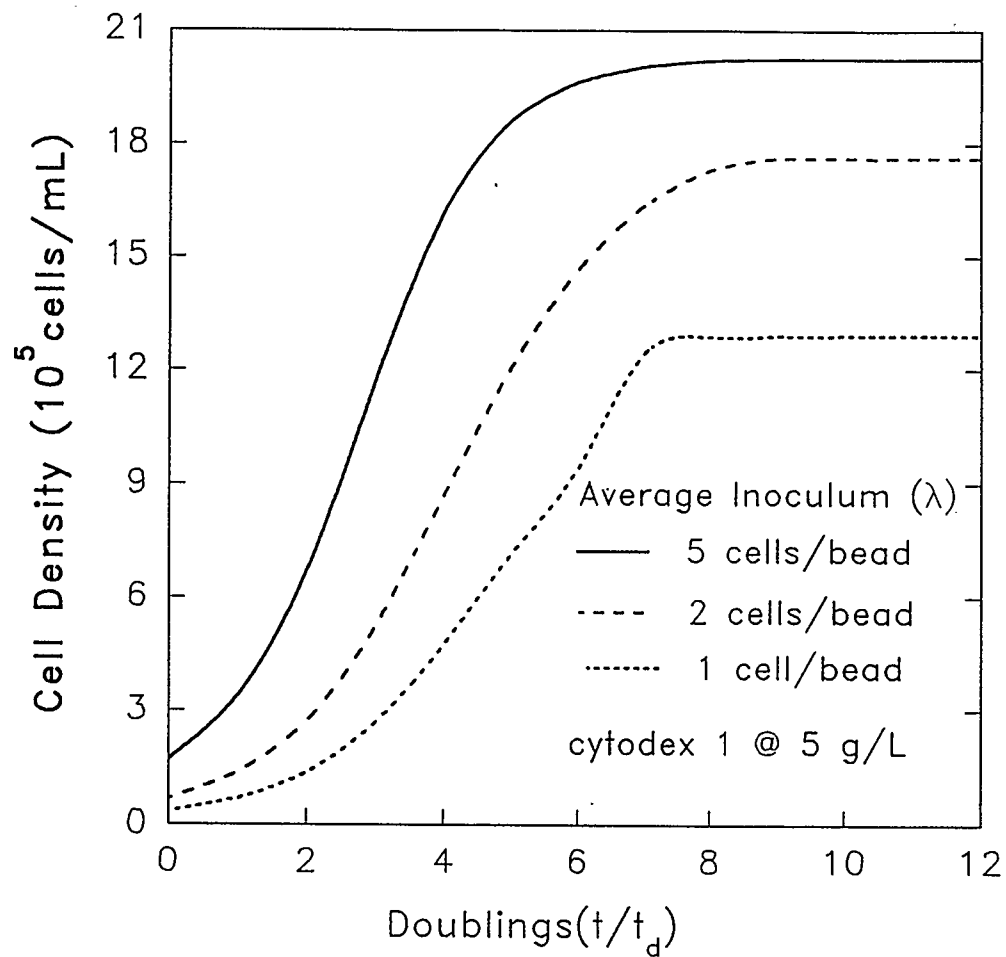


Figure 4.10. Progression of growth on a population of microcarriers predicted by the cellular automaton, at three different average inoculum levels (1, 2 and 5 cells/bead), when inoculation follows a Poisson distribution.

Equation 4.3 gives the number of cells per bead for any given value of  $I$  and  $N_{\max}$  when the distribution of neighbouring cells is incorporated. This equation is combined with the surface area distribution of microcarriers to give:

$$N(t|I) = \sum_k P(N_{\max,k}) N(t|I, N_{\max,k}) \quad (4.7)$$

$N(t|I)$  is the number of cells per bead at any time at a given inoculation density and consolidates the  $n_b$  and  $N_{\max}$  distributions. Finally the Equation 4.7 may be further combined with the distribution of the inoculum to give:

$$N(t) = \sum_i P(I_i) N(t|I_i) \quad (4.8)$$

$N(t)$  combines the distributions in  $I$ ,  $n_b$  and  $N_{\max}$ . If we substitute back into equation 4.8 we obtain:

$$N(t) = \sum_i \sum_r \sum_k w_{irk} N(t|I_i, n_{b,r}, N_{\max,k}) \quad (4.9)$$

where the weighting factors ( $w_{irk}$ ) are the suitable products of the corresponding probability distributions, namely:

$$w_{i,r,k} = P(I_i) \cdot P(n_{b,r}) \cdot P(N_{\max,k}) \quad (4.10)$$

This equation can in turn be used to approximate an actual microcarrier culture.

#### IV.5 SUMMARY

In this Chapter a description of the cellular automaton model developed has been given. The use of a cellular automaton to model the growth of anchorage dependent cells

on a surface offers a number of advantages. Firstly, the progression of a cellular automaton is related to the state of the computational sites in the automaton. This is directly analogous to contact inhibited cell growth where the growth rate is dependent upon the population density of the cells. Secondly, the ease in programming the model and computational efficiency make the cellular automaton model an applicable and functional tool.

The advantages of this model over previous models include the ability to model cell growth on microcarriers (a high cell density cultivation system) as opposed to flat surfaces and the model is not limited to one cell line or type of microcarrier. The model is also capable of accounting for a number of factors unique to microcarrier cultures; microcarrier size distribution, inoculation levels and inoculation distribution among the microcarrier population.

## CHAPTER V

### COMPARISON WITH EXPERIMENTAL MICROCARRIER CULTURES

#### V.1 OVERVIEW

The automaton developed in Chapter IV may be used to examine the characteristics of anchorage dependent cell growth on microcarriers. This examination gives a better understanding of the growth of cells on microcarriers which would be difficult to determine strictly from experimental data. In this Chapter to verify the automaton model the cellular automaton predictions are compared to experimental microcarrier culture growth curves. The model can further be used to generate growth curves which can be used to decouple the effect of contact inhibition from growth kinetics. With this decoupling the accurate determination of kinetic parameters and the effects of other environmental factors can be readily established.

#### V.2 COMPARISON WITH EXPERIMENTAL DATA

As demonstrated in a microcarrier culture the aforementioned factors (inoculation density, microcarrier distribution, neighbour space distribution) will influence the progression of growth in the culture. The cellular automaton model can account for these factors and therefore provide an accurate prediction of actual growth curves.

##### V.2.1 Experimental data versus automaton predictions

To compare the automaton predictions to actual experimental data four parameters

are obtained from the experimental data; the average cell density at confluence, the cell line doubling time, the average number of neighbouring cells and the average inoculation density. In order to simulate the actual cultures the automaton computer program was run for the different microcarrier sizes and number of neighbouring cells. The neighbour distributions and surface area were then applied to the resulting data (equations of 4.2 and 4.3). The experimental inoculation is incorporated into the automaton data by applying the Poisson distribution to the automaton data at the given inoculation density (equation 4.4). As automaton simulation results are given as number of cell per bead and the time step is the doubling time, to compare to experimental data the results must be converted to real time and cells/mL. The cell line average doubling time and microcarrier loading are used to accomplish this. The resulting automaton predictions compared to experimental data are given in Figures 5.1 (MRC-5 cultures) and 5.2 (Vero cultures).

The microcarriers used were Cytodex 1, supplied by Pharmacia. All experiments were carried out at a microcarrier loading of 5 g/L. The experiments were run in 250 mL spinner flasks. Two cell lines were used in the experimental cultures, MRC-5 cells and Vero cells. For the MRC-5 culture the data was taken from Forestell et al.(1992). The maximum cell density was  $21.0 \times 10^5$  cells/mL. This corresponds to approximately 61.8 cells per bead at the specified microcarrier loading and average microcarrier surface area (Pharmacia, 1981). For the automaton model the average cell density at confluence was taken as 62 cells per bead. Applying the distribution of sizes of the microcarriers to this number gives 32 cells per bead as the cell density the smallest microcarrier (130  $\mu\text{m}$ ) can support and 92 cells per bead as the cell density largest microcarrier (210  $\mu\text{m}$ ) can

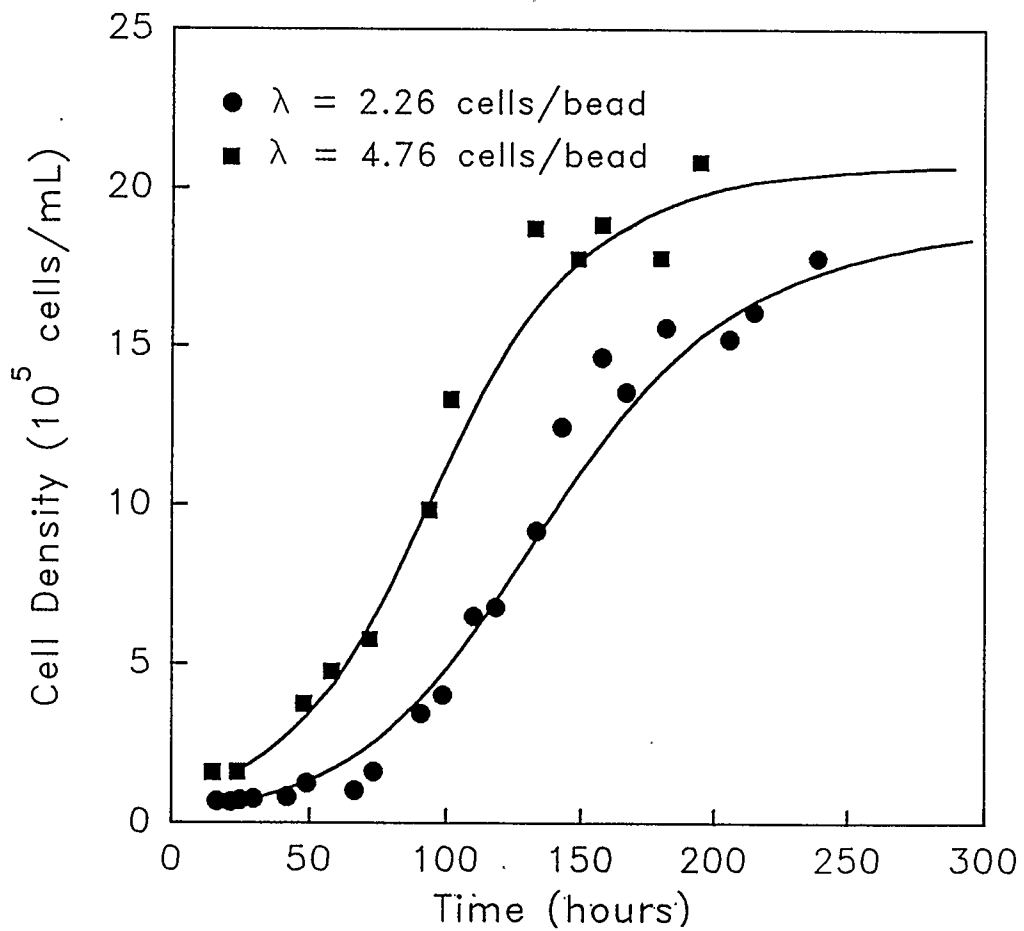


Figure 5.1. Comparison of experimental MRC-5 microcarrier culture growth curves, at two different average inoculums ( $\lambda=2.26$  (●) and  $4.76$  (■) cells/bead), with cellular automaton generated growth curves initiated at experimental inoculum.

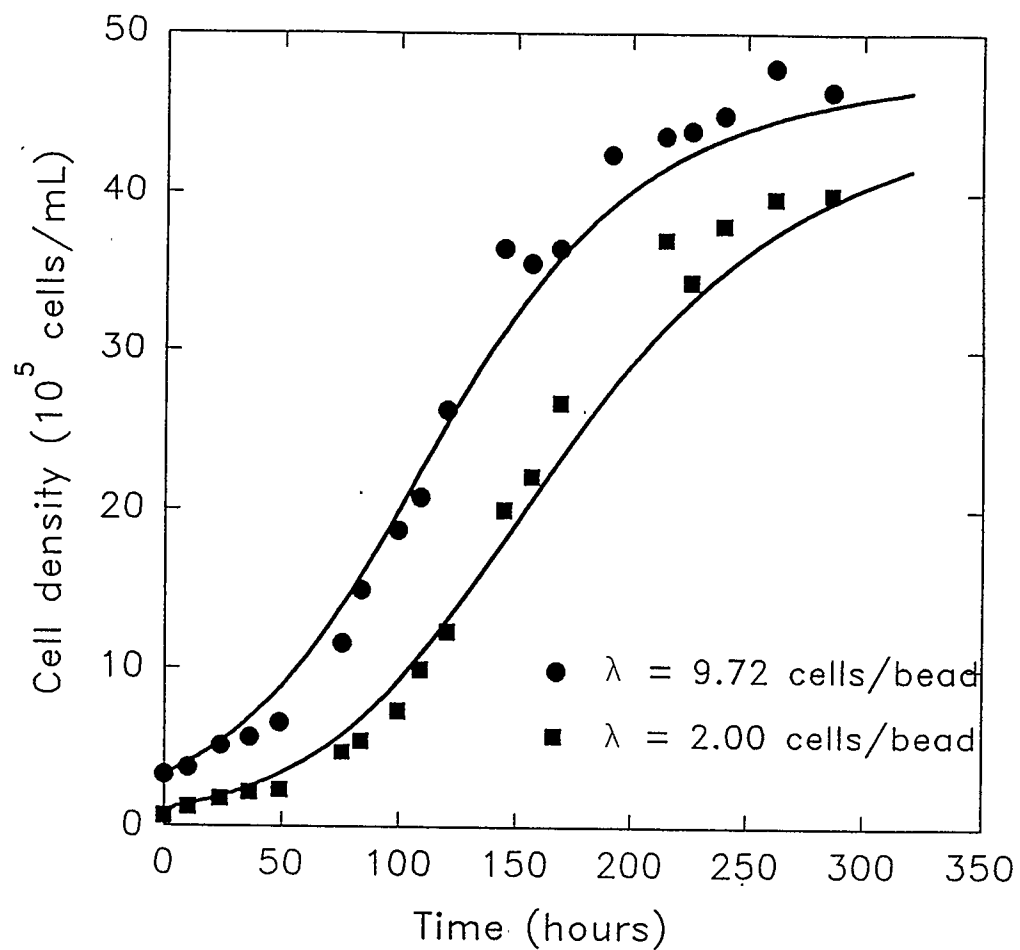


Figure 5.2. Comparison of experimental Vero microcarrier culture growth curves, at two different average inoculums ( $\lambda=9.72$  (●) and  $2.0$  (■) cells/bead), with cellular automaton generated growth curves initiated at experimental inoculum.

support. The average doubling time determined from the experimental data was 23.5 hours. Numerous past experiments have established MRC-5 cells growing on microcarriers have an average of 5.2 neighbours per cell.

For Vero cells the cell density at confluence was determined as 139 cells per bead, which for the model purposes was approximated as 74, 140 and 220 cells per bead for the smallest, average and largest microcarrier respectively. The average doubling time for this experiment was determined to be 31 hours. The experimental data on Vero cells is not as extensive as MRC-5 cells, however in these experiments the average number of neighbour cells was observed to be 5.

In both microcarrier cultures regular media changes were performed to ensure there were no nutrient or environmental limitations to growth. Further, the agitation rate of 60 rpm was chosen for optimal oxygen transfer (Forestell et al. 1992). Consequently, the only limitation to growth will be spatial and the effects of contact inhibition may be isolated from other environmental factors.

The lag portion of the experimental data has been excluded as the automaton does not predict this stage of growth. Both a high and low average inoculum was initiated for both cell lines to illustrate the effect of the Poisson distribution of the inoculum. The final cell density for the higher inoculum is larger than for the lower inoculum. In both sets of experiments, MRC-5 and Vero, the automaton gives an accurate representation of the experimental data. The automaton predictions approximate the actual cultures from inoculation, through the rapid phase of growth and confluent stages. It should be noted no parameters were used to "fit" the model to the data. Any parameters used in the model

were determined from the experimental data.

### V.3 DECOUPLING CONTACT INHIBITION

#### V.3.1 Generalized contact inhibition curves

The ultimate objective in developing the cellular automaton model was to be able to remove the influence of contact inhibition from the growth kinetics. With the effectiveness of the cellular automaton method established, by comparison with experimental data, the model can now be used to decouple the effect of contact inhibition from the growth kinetics.

Contact inhibition is a function of the number of cells growing on the microcarrier at any point in time. It is therefore logical to relate the specific growth rate of contact inhibited cells growth to the cell density and the inoculum size:

$$\frac{\mu_{auto}}{\mu_{max}} = f(x, \lambda) \quad (5.1)$$

where  $\mu_{auto}$  is the overall specific growth rate predicted with the automaton model,  $\mu_{max}$  is the maximum specific growth rate of the cell line,  $x$  is the cell density and  $\lambda$  is the average inoculation density of the microcarrier culture. From this equation growth curves have been generated and are depicted in Figure 5.3. Three average inoculum are shown 1, 5, and 10 cells per bead. The figure illustrates the decreasing overall dimensionless growth rate,  $\mu_{auto}/\mu_{max}$  with increasing cell density. Such a figure can be used in the analysis of experimental data to eliminate the effect of contact inhibition from the

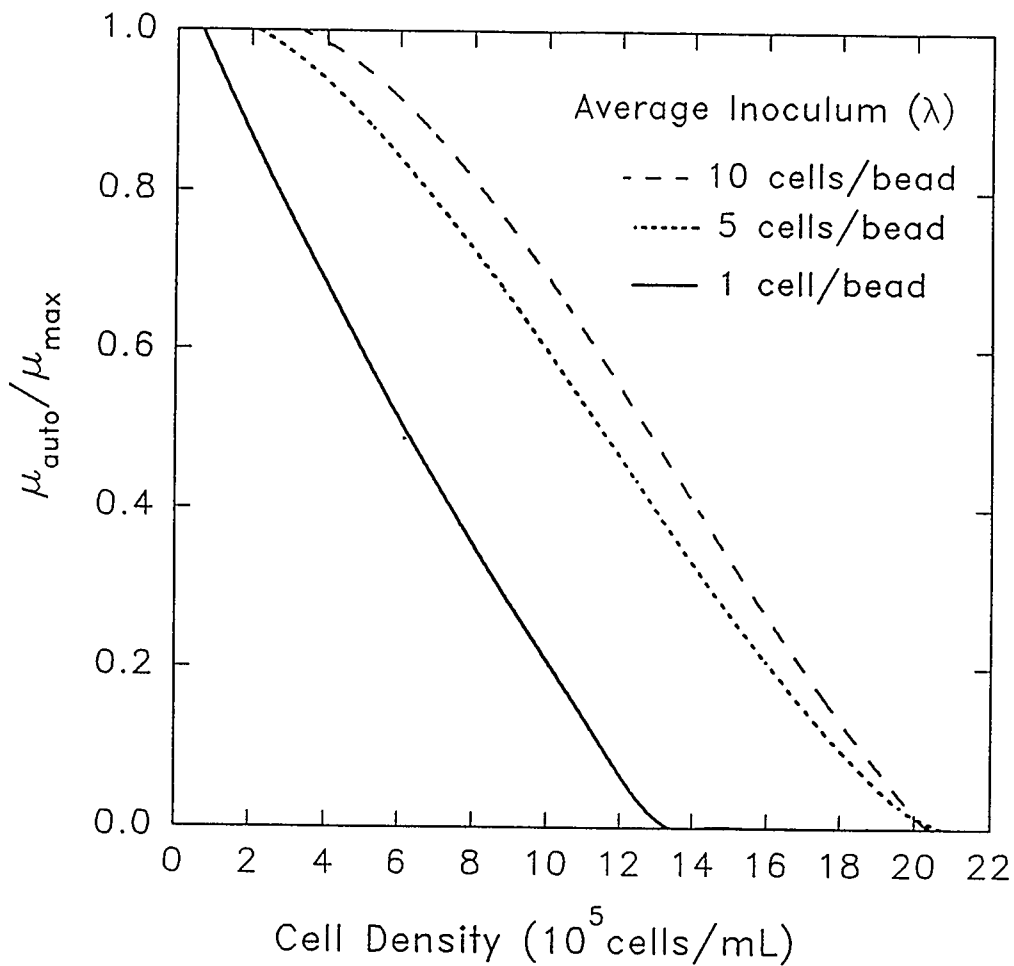


Figure 5.3. Contact inhibition curves at three different average inoculation ( $\lambda = 1$  (—), 5 (···) and 10 (---) cells/bead). Figure corresponds to MRC-5 cells growing on Cytodex 1 microcarriers (number of neighbours=5.2 cells/cell, cell density at confluence=62 cells/bead).

measured growth rates. In addition, the dimensionless growth rate can be coupled with any kinetic model where the effect of nutrient and by-product concentrations, pH and other environmental factors are included to predict the performance of the culture under any operating scenario (batch, perfusion, fed-batch etc...).

### V.3.2 Combination with Monod kinetics

In typical model development the automaton would be used to generate the growth curve and the resulting growth rate equation could be used another growth model or to develop an overall growth model. Further, with the effect of contact inhibition accounted for the determination of maintenance coefficients and nutrient uptake rates may be determined and the effects of environmental conditions can be investigated.

To demonstrate the automaton's applicability in this capacity comparison of the cellular automaton coupled with a kinetic model to an experimental batch reactor culture has been performed. The batch reactor experimental data was taken from a MRC-5 culture at a microcarrier loading of Cytodex 1 microcarrier of 5 g/L. Obviously in a batch experiment nutrient limitations will be a factor in the arrest of cell growth. For this reason the contact inhibition curve was coupled with simple Monod kinetics:

$$\mu_a = \frac{\mu_{auto} S}{K_s + S} \quad (5.2)$$

where  $\mu_a$  ( $h^{-1}$ ) is the apparent, or observed, specific growth rate of the batch culture,  $s$  is the limiting substrate concentration (mmol/L) and  $K_s$  (mmol/L) is the saturation constant. The saturation constant is that concentration of the nutrient when the specific growth rate is at half the maximum specific growth rate. The  $\mu_{auto}$  ( $h^{-1}$ ) is calculated from

the contact inhibition curves initiated at the experimental inoculum. The cell density,  $x$  ( $10^5$  cells/MI), is calculated using the simple exponential growth model:

$$\frac{dx}{dt} = \mu_a x \quad (5.3)$$

where  $t$  is the time in hours. The limiting substrate concentration is calculated by a material balance on the reactor:

$$\frac{ds}{dt} = -q_s x \quad (5.4)$$

where  $q_s$  is the specific substrate uptake rate ( $\mu\text{mol}/10^5 \text{ cell}\cdot\text{h}$ ). The uptake rate is related to the growth rate using the maintenance energy model of Pirt (1985):

$$q_s = \frac{\mu_a}{Y_s} + m_s \quad (5.5)$$

where  $Y_s$  is the cell growth yield ( $10^5$  cells/ $\mu\text{mol}$ ) for the substrate and  $m_s$  is the maintenance energy requirement for the substrate ( $\mu\text{mol}/(10^5 \text{ cells}\cdot\text{h})$ ). Both of these parameters as well as  $K_s$  were taken from Ozturk (1990). Table 5.1 gives a summary of the kinetic parameters and their values used in the computer simulation.

**Table 5.1. Kinetic parameters used in ACSL batch reactor simulation program**

Kinetic parameter	Value
$K_s$ (mmol/L)	0.20
$m_s$ ( $\mu\text{mol}/10^5 \text{ cell}\cdot\text{h}$ )	0.0056
$Y_s$ ( $10^5 \text{ cells}/\mu\text{mol}$ )	1.37
$\mu_{\max}$ ( $\text{h}^{-1}$ )	0.0291

Figure 5.4 shows the comparison of the automaton + Monod kinetic model predictions with the experimental data. The differential equation were predicted using a computer simulation language, ACSL (Advanced Computer Simulation Language). As seen, the automaton/Monod model approximates the batch reactor data throughout the growth of the culture. Included in this figure is the automaton predictions without any nutrient limitations accounted for by the Monod kinetics. It is obvious that nutrient exhaustion does limit the growth in both the experimental and model data. This further validates the effectiveness of the automaton as a tool in the analysis of data and modelling of anchorage dependent cell growth.

#### **V.4 SUMMARY**

A general cellular automaton model has been developed to model the growth of anchorage dependent cell growth on anchorage dependent cells on microcarriers. By combining the distributions; in the number of neighbouring cells, microcarrier radii and inoculation density the automaton predictions are representative of actual microcarrier cultures. Comparison with experimental data demonstrates the automaton's applicability to actual microcarrier cultures. The automaton predictions represented the experimental data throughout all phases of the culture growth. No adjustable parameters were used to conform the model to data. All required information, such as maximum cell density, doubling time, inoculum level and the number of neighbouring cells was obtained from experimental data. Generalized contact inhibition growth curves have been developed from intrinsic growth kinetics and can be used in bioreactor models. This was

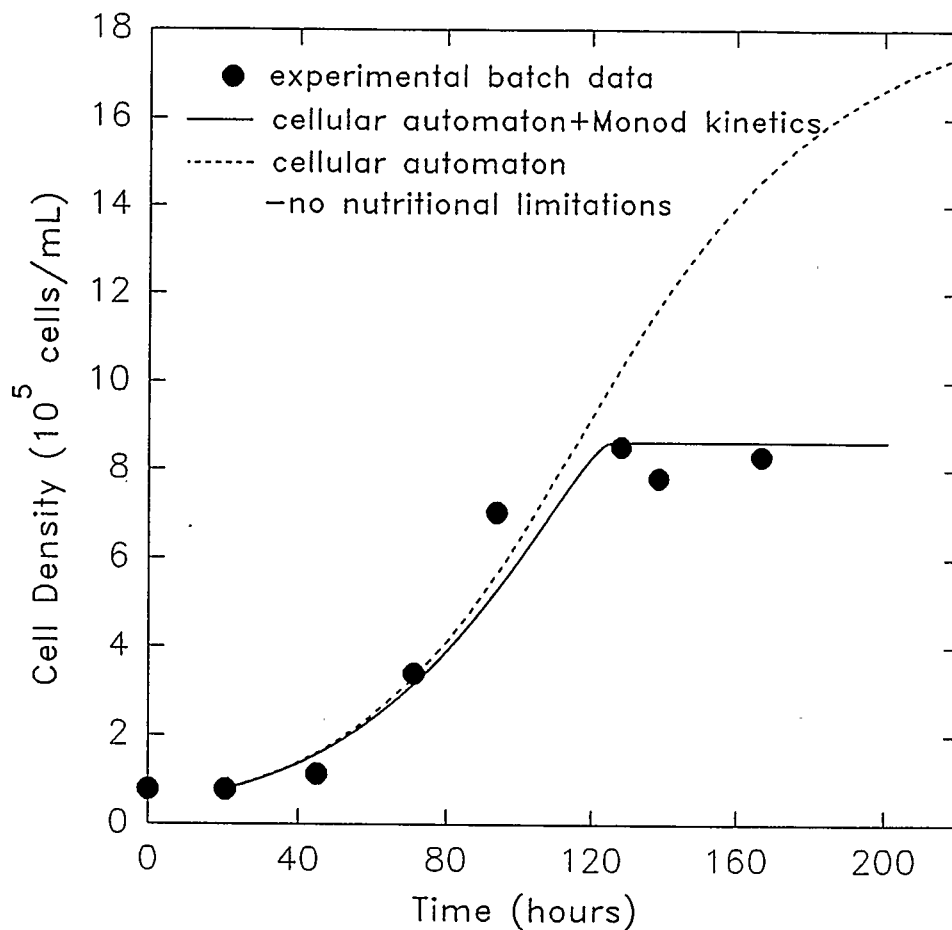


Figure 5.4. Comparison between experimental batch reactor data, cellular automaton predictions coupled with Monod kinetics and cellular automaton predictions alone. Both automaton simulations were initiated with the experimental inoculum of 2.3 cells/bead. The data is of MRC-5 cells growing on Cytodex 1 microcarriers (5g/L).

demonstrated by coupling the automaton curves with simple Monod kinetics and comparing with experimental data.

## CHAPTER VI

### CELL CYCLE DYNAMICS OF MICROCARRIER CULTURES

#### VI.1 OVERVIEW

In this Chapter the cell cycle progression of the growth and division of two types of microcarrier cultures, MRC-5 and Vero cells, were observed through the use of a flow cytometer. By differential staining of DNA and RNA the development of the various stages of the cell cycle were examined. Flow cytometry enabled the inspection of the progression of the cell cycle in a microcarrier culture from inoculation to rapid growth and the stationary phase. The flow cytometry analyses indicated that even in the stationary phase there is a small percentage of cells still growing and dividing.

Besides the knowledge of growth kinetics, to optimize anchorage dependent cultures an understanding of the physiological state of the culture is also of key importance. Whether a culture is predominantly in the growth, division or stationary stages and the proportion of cells in the various stages can facilitate the efficient operation of large scale systems. For instance, to optimize the production of monoclonal antibody from hybridoma cells many researchers have attempted to identify if there is a particular phase of the cell cycle where there is maximum antibody production.

Analysis of the cell cycle is commonly accomplished by flow cytometry (Shapiro, 1988). The advantage of using flow cytometry is that it allows the simultaneous analysis of DNA and RNA content. Little work has been done on the cell cycle dynamics of

microcarrier cultures. In this Chapter a more detailed analysis of the cell cycle progression of two types of microcarrier cultures, MRC-5 and Vero, is presented.

Further, in this Chapter a flow cytometry analysis of the supernatant, from the microcarrier culture, was combined with the attached cell to define the contact inhibited cells. An investigation into the death rate was also performed.

## VI.2 THE CELL CYCLE

Figure 6.1 is a diagram of a typical mammalian cell cycle. The processes within the cell cycle can be divided into; cell division and cell growth (interphase). The cycle can be further divided on the basis of DNA content. The synthesis phase (S) is where DNA is replicated, therefore the DNA in this phase varies from diploid levels to tetraploid (twice diploid) levels. The S phase is followed by  $G_2$ , the second of two gap phases. Mitosis, or the M phase, follows  $G_2$ . In this stage nuclear and cytoplasmic division occurs. At this point in the cycle the cell enters the first gap phase,  $G_1$ , and one of two processes may occur. The cell may continue to cycle, in which case the cell enters a functional interval where the cell increases in mass and size and a considerable part of cellular biosynthesis occurs, such as the production of ribosomal RNA and other proteins, in preparation for the S phase (Pardee, 1989). However, should the necessary factors for division and growth not be present the cell may enter an arrested state,  $G_0$  (Lanks and Kasambalides, 1980) or  $G_{1A}$  (Darzynkiewicz et al, 1980). It has been suggested that whether the cell continues to cycle or enters an arrested state is determined by the RNA content (Darzynkiewicz et al., 1980).

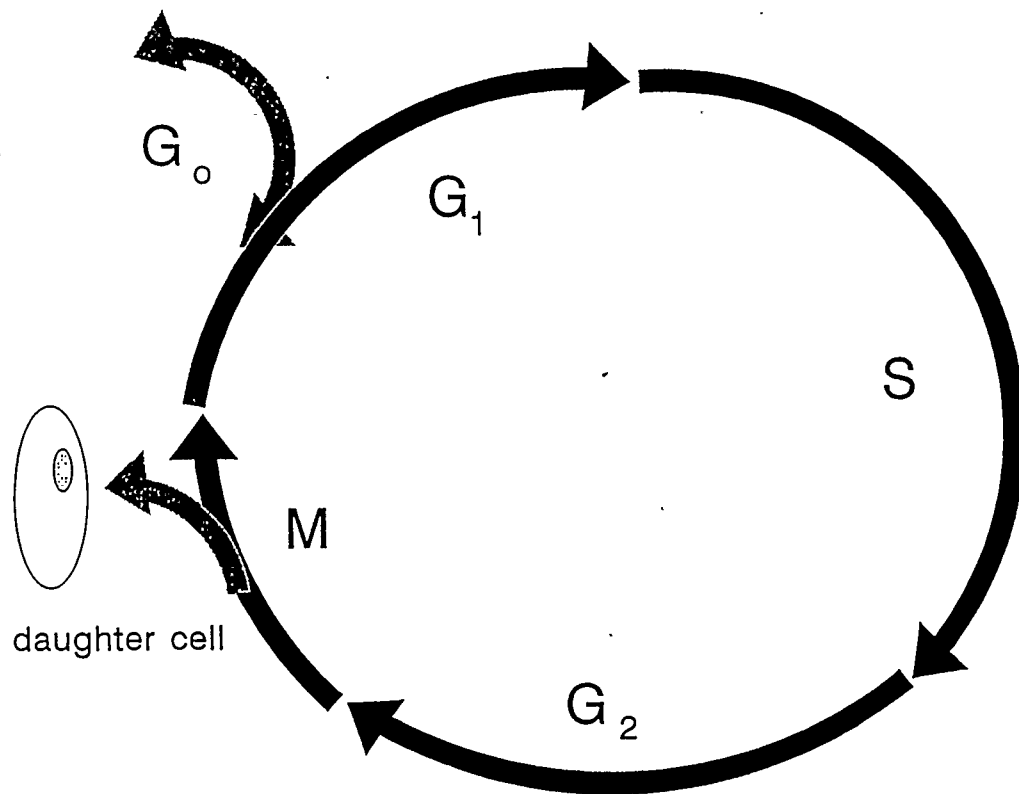


Figure 6.1. Representation of a typical cell cycle. Cells enter the M phase where nuclear and cytoplasm division occurs and then enters interphase. At this point cells may enter either quiescent stage ( $G_0$ ) or continue cycling ( $G_1$ ). Biosynthesis occurs in  $G_1$  (production of RNA and proteins). Cells then enter the S phase where the replication of DNA and other cellular matter occurs. Prior to re-entry to the M phase the cells enter the second gap phase ( $G_2$ ).

Cells in  $G_0$  have been shown to decrease in size as protein and RNA molecules are degraded, have slower macromolecule synthesis and low transport activities (Pardee, 1989). The increase in RNA content has been shown to be the most reliable way of determining if the cell will to continue cycle (Darzynkiewicz et al., 1982). As 80 % of cellular RNA is of the ribosomal species (Darzynkiewicz et al., 1979) which is responsible for protein synthesis, measurement of the rRNA paired with DNA measurements can define the various stages of the cell cycle.

Figures 6.2 and 6.3 illustrate the growth of the two sets of microcarrier cultures for the MRC-5 and Vero cells respectively. The figures illustrate the experimental and cellular automaton generated growth curves. The average doubling time, determined from experimental data, for the MRC-5 and Vero cultures are 23.5 and 24 hours respectively. To analyze the cell cycle dynamics of the culture a flow cytometry analysis of these two sets of cultures was performed.

To distinguish the various stages of the cell cycle the cellular DNA content may be used. Cells in  $G_0$  and  $G_1$  have a normal, or diploid, amount of DNA while cells in the  $G_2+M$  phases have twice the normal DNA content. The S phase is in between these phases and is therefore characterized by a linear increase in the DNA content as the cell moves from  $G_0+G_1$  to  $G_2+M$ . Figure 6.4 (a) is a histogram of DNA content, generated by the flow cytometer for a sample of the MRC-5 culture of Figure 6.2 (b) at 25 hours. The x-axis is fluorescence 1 and represents the DNA content plotted against the percentage of cells. In the histogram the first peak is the  $G_0+G_1$  phases, the second peak is the  $G_2+M$  phases and the area in between is the S phase. Obviously the exact

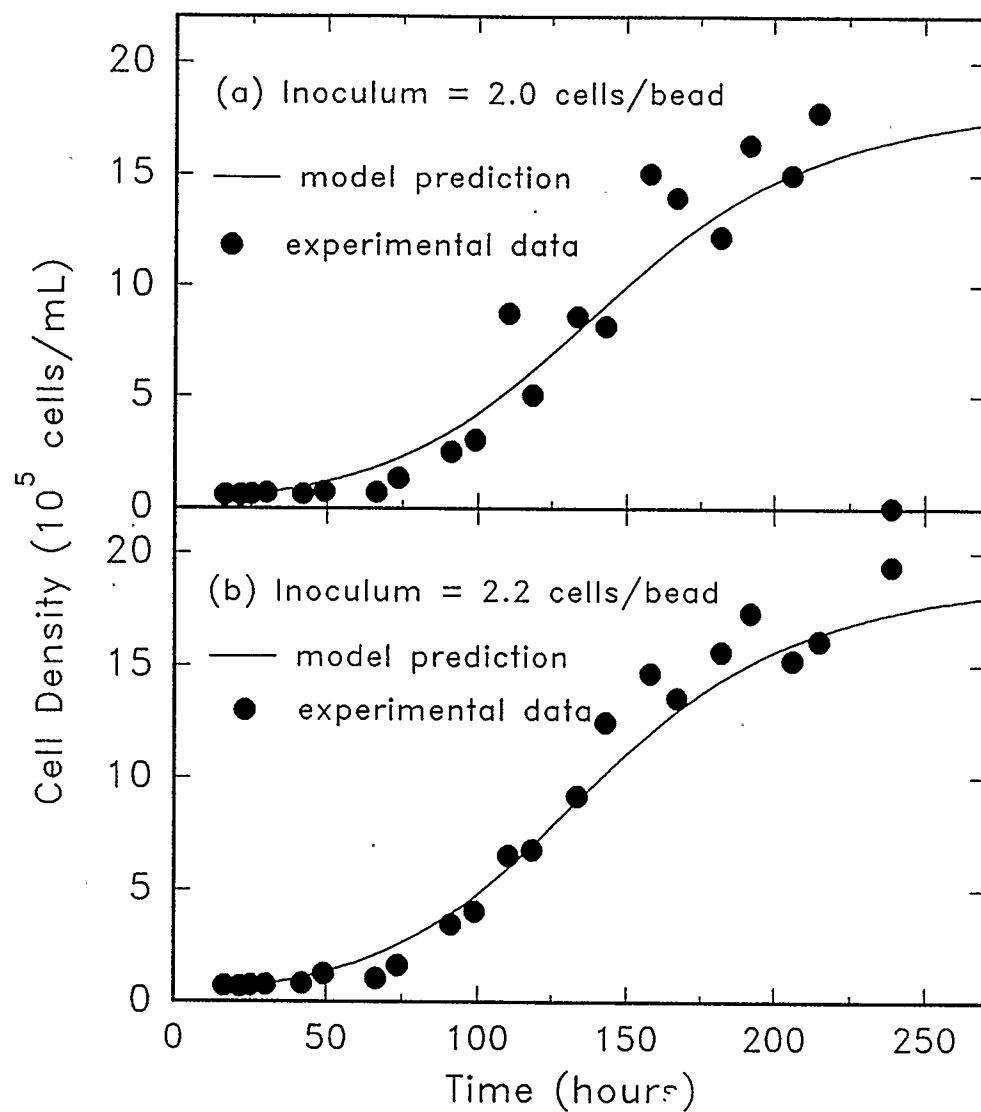


Figure 6.2. Growth curves of the two MRC-5 microcarrier cultures ( $\lambda = 2.0$  (a) and 2.2 (b) cells/bead) used in the flow cytometry experiments. The data points are represented by symbols (●) and the cellular automaton model predictions are represented as lines (—).

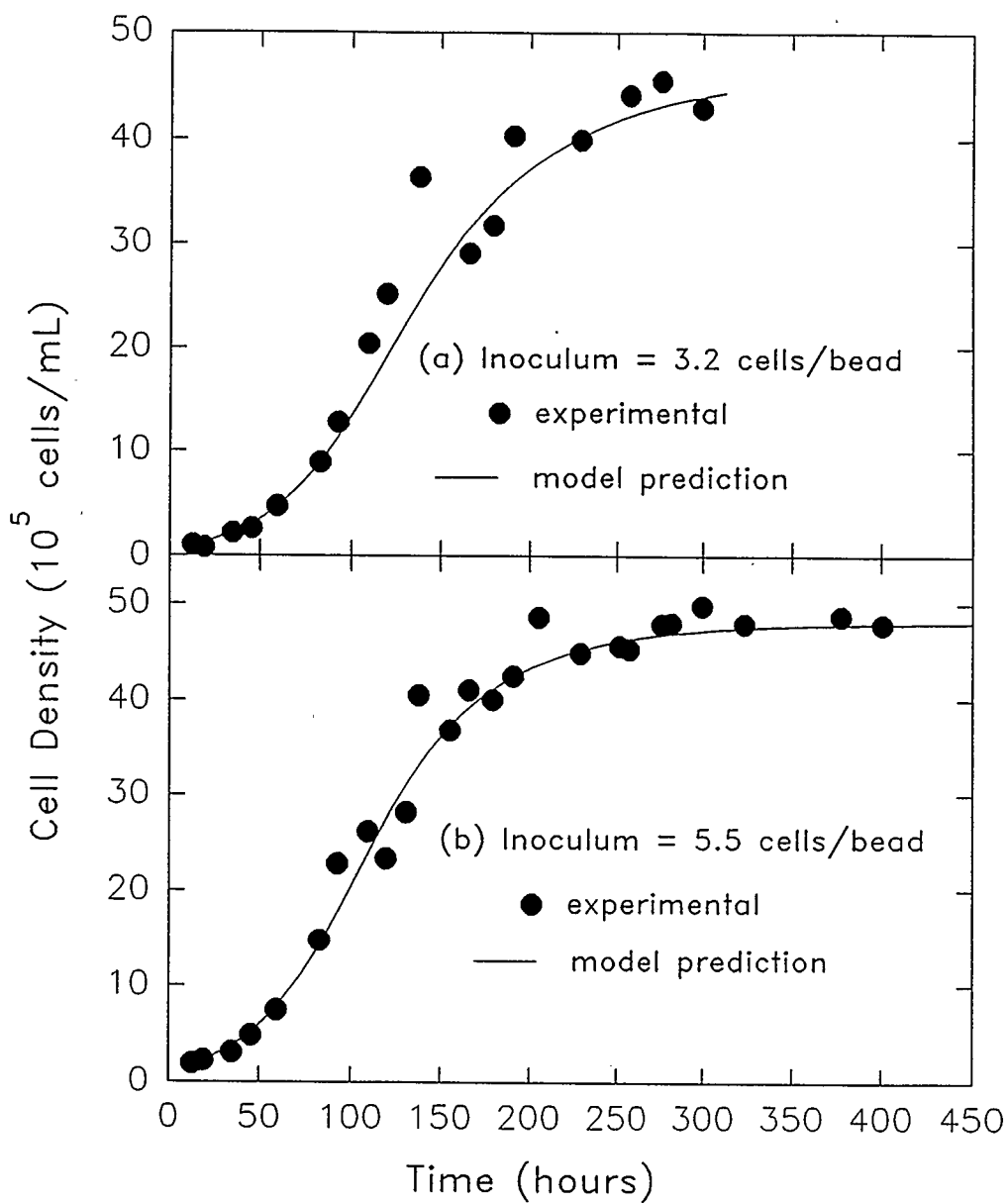


Figure 6.3. Growth curves of the two Vero microcarrier cultures ( $\lambda = 3.2$  (a) and 5.5 (b) cells/bead) used in the flow cytometry experiments. The data points are represented by symbols ( $\bullet$ ) and the cellular automaton model predictions are represented as lines ( $\text{—}$ ).

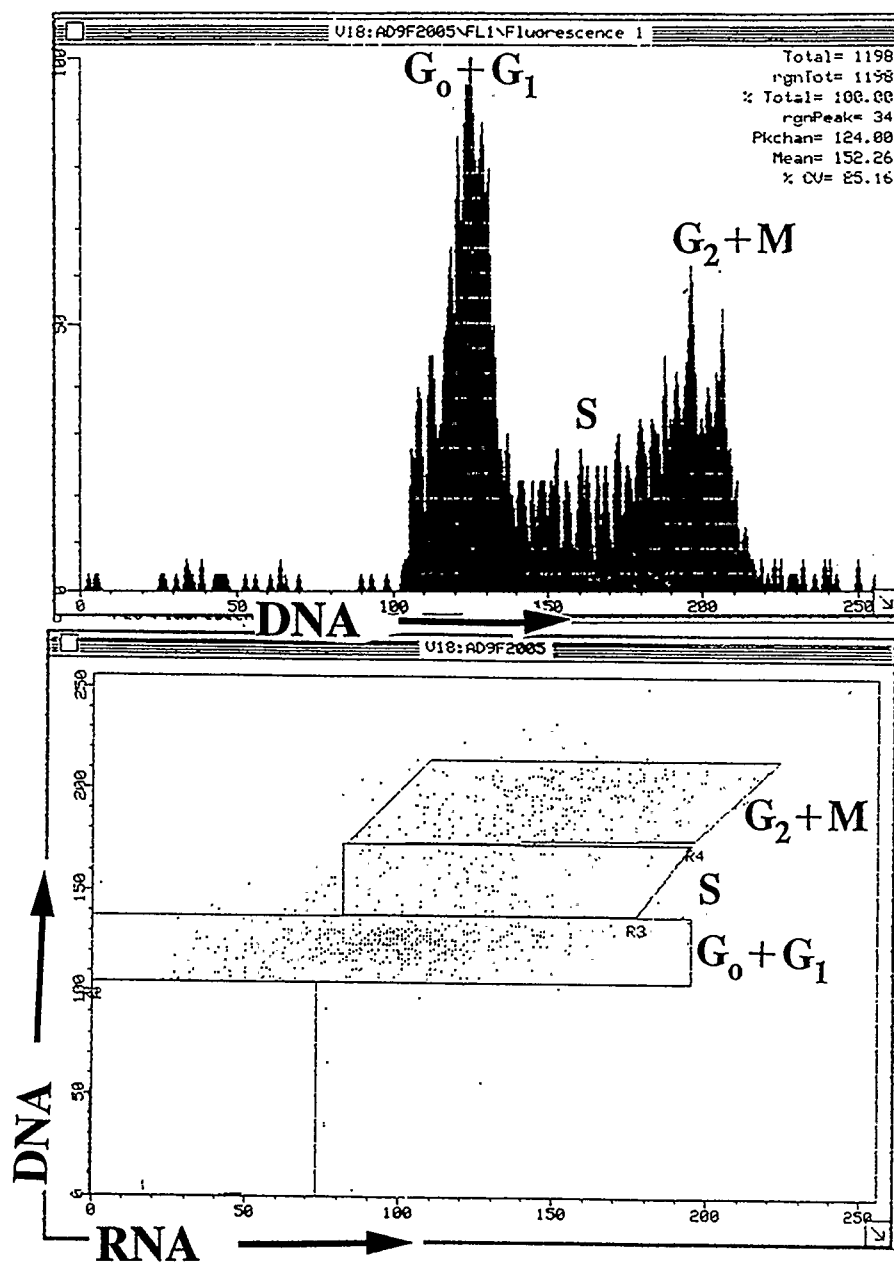


Figure 6.4. (a). DNA histogram of a sample from MRC-5 culture of figure 6.2(b), at a time of 25 hours. the different phases are differentiated by DNA content.  
 (b). Dot plot of DNA (FL1) versus RNA (FL3), of same MRC-5 sample of figure 6.4(a), illustrating the different phases of the cell cycle.

definition between the different phases is difficult to determine strictly from the DNA histogram and therefore the process is somewhat subjective. It was for this reason that instead of using DNA histograms, diagrams of RNA versus DNA content were used.

When DNA is plotted against RNA, Figure 6.4 (b), the symmetry of the peaks can be distinguished more easily. Figure 6.4 (b) is a dot plot, each dot representing one event or cell. From this figure  $G_0+G_1$  are distinguished by the unit DNA levels and gradual increase in the RNA. The S phase is characterized by the onset in the increase in the DNA levels and the  $G_2+M$  phases are denoted by the constant but high level of DNA. The shape of the curve in this figure is the typical S shape of an exponentially growing culture. The cut-off between cycling cells, in  $G_1$ , and noncycling cells,  $G_0$ , is difficult to ascertain strictly by DNA and RNA content.

To further distinguish the dot plot of Figure 6.4 (b) contour plots are often used. The contour plots are simply another method of representing the distribution of cells in the cycle. Each contour in a plot represents a percentage of the total number of events. The area between each pair of contour lines represent an equal percentage of events. The contour plots were used when observing the dynamics of the cell cycle in the microcarrier cultures.

### **V.2.1 The cell cycle in microcarrier cultures**

The progression through the cell cycle by the Vero and MRC-5 microcarrier cultures was observed by differentiating the phases as described in the previous paragraph. Two sets of experiments were run for each cell line. Figures 6.5 and 6.6 illustrate the sequence of cell growth for one of the MRC-5 (Figure 6.2 (b)) and one of

the Vero (Figure 6.3 (b)) cultures. The two cultures (Figures 6.2 (a) and 6.3 (a)) not shown in these figures show the same sort of progression. The figures are a series of contour plots of DNA versus RNA. Each contour represents a percentage of the total number of events with the area between each pair of lines representing an equal percentage of events. The outermost contour is 10% of the total number of cells, the next is 30% then 50%, 70% and 90%.

Plot (a) of both Figures 6.5 and 6.6 shows the state of the initial inoculum. The cells were inoculated into the microcarrier cultures from T-flasks at approximately 80% confluence and therefore the majority of cells are in the  $G_0+G_1$  stages. However, by 25 and 19 hours, 6.5 (b) and 6.6 (b) respectively, the cells are moving out of  $G_1$  towards the S phase, this is illustrated by the upward shift in DNA content. By the second day, plot (c), the fraction of cells in the S and  $G_2+M$  phases has increased. This plot is similar to a typical S shape curve of a culture in the exponential growth phase where the degree of contact inhibition is small. In plots (d) and (e), at 72 and 120 hours respectively, both cultures show a left and downward shift in the distribution of cells indicating that the cells are slowly moving back into the  $G_0+G_1$  phases. Finally, in plot (f), at 265 and 275 hours for Figures 6.4 and 6.5 respectively, the microcarriers are confluent and the bulk of the culture is in the  $G_0+G_1$  phase.

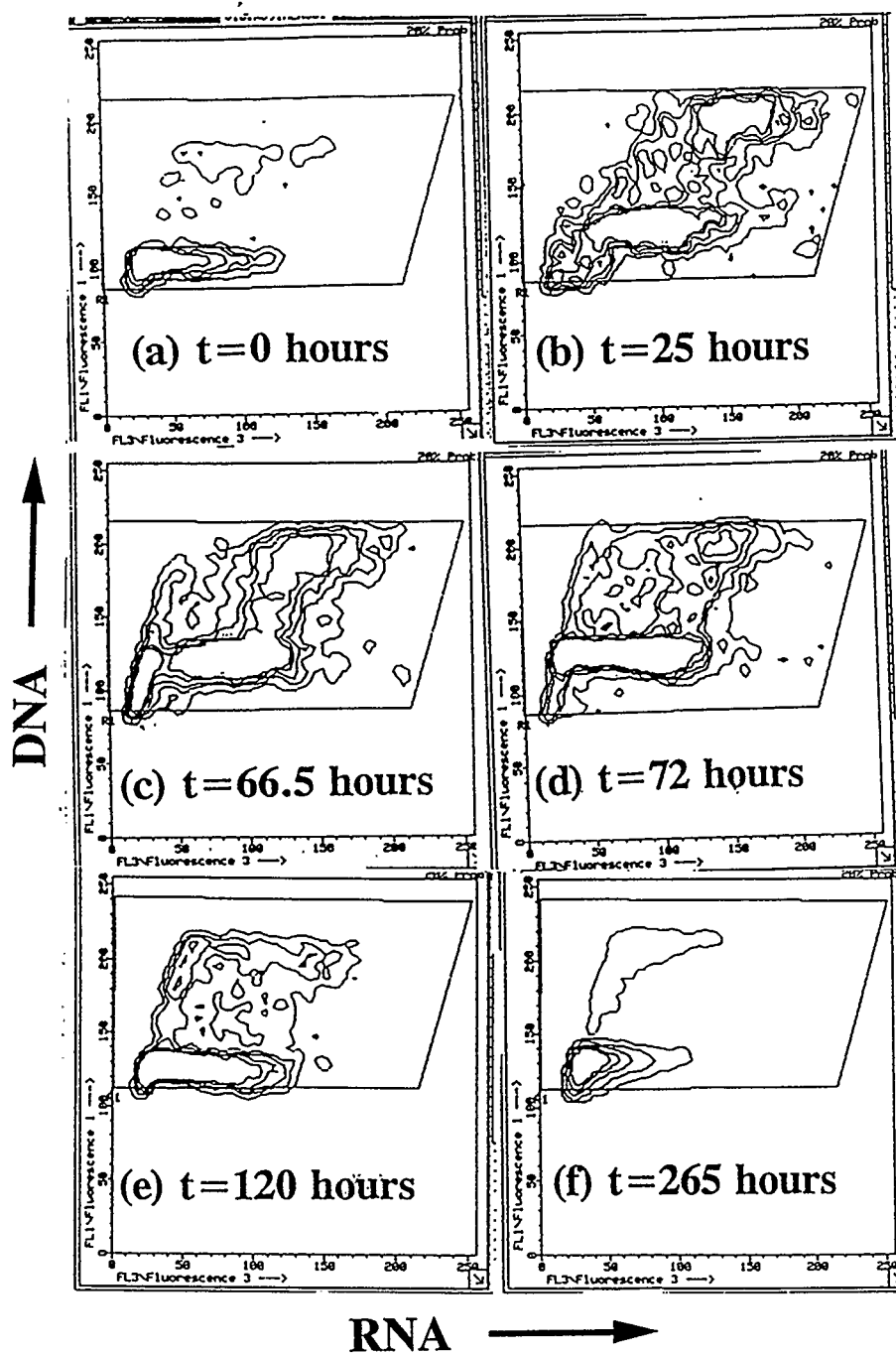


Figure 6.5. Contour plots of DNA (FL1) versus RNA (FL3), of MRC-5 microcarrier culture of figure 6.2(b), illustrating the progression of culture cell cycle from inoculation to confluence. The outermost lines represent 10% of the total cell sample, the next 30%, then 50%, 70% and the innermost contour is 90%.

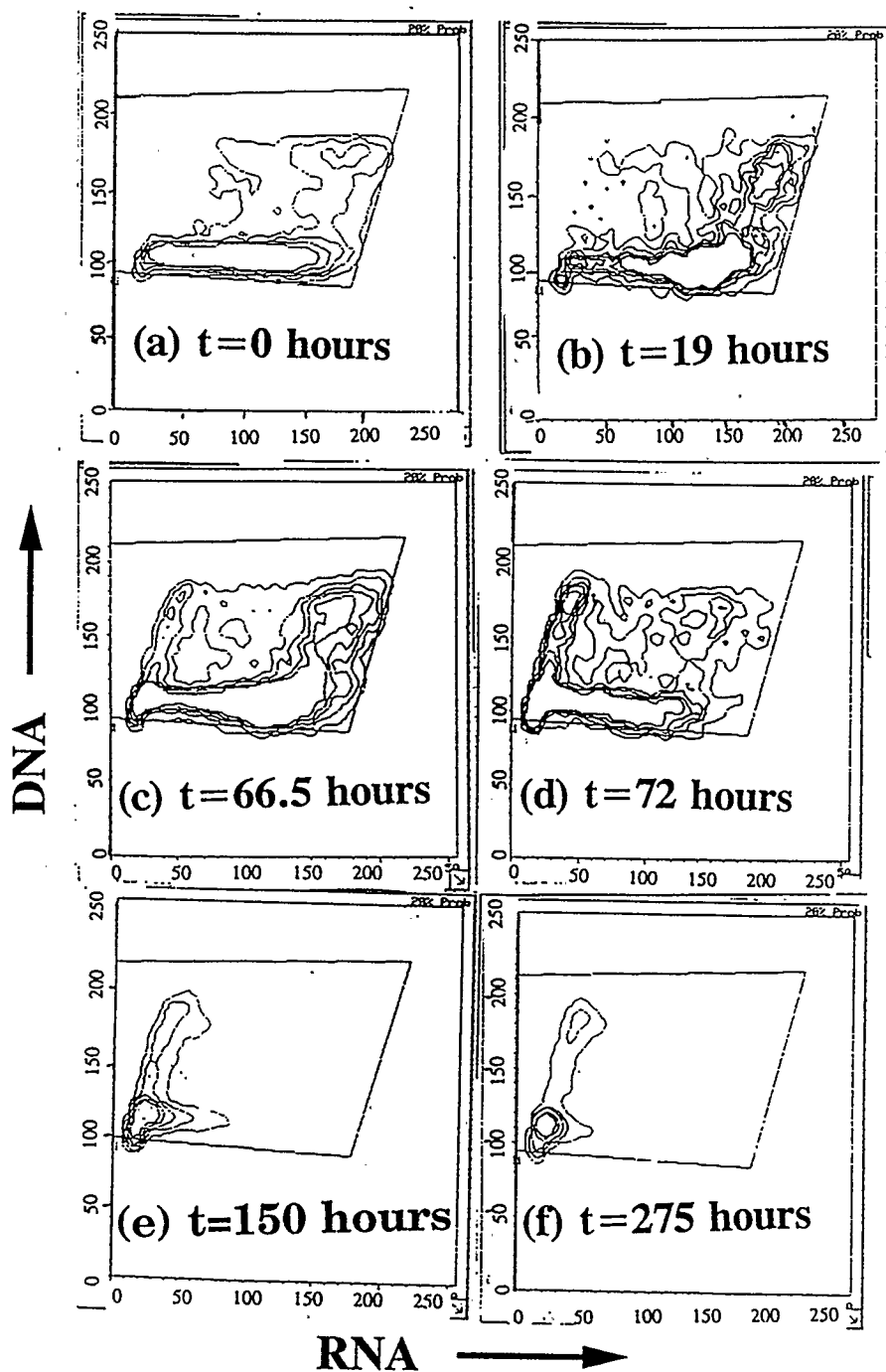


Figure 6.6. Contour plots of DNA (FL1) versus RNA (FL3), of Vero microcarrier culture of figure 6.3(b), illustrating the progression of culture cell cycle from inoculation to confluence. The outermost lines represent 10% of the total cell sample, the next 30%, then 50%, 70% and the innermost contour is 90%.

### VI.3 PROPORTION OF CULTURE IN A GIVEN PHASE

A qualitative representation of Figures 6.5 and 6.6 is depicted in Figures 6.7 (MRC-5) and 6.8 (Vero). From these figures the variation in the fraction of cells in the phases becomes more obvious. The fractions were determined by LYSYS, a software package supplied by Becton and Dickinson. All four plots exhibit the same trend in the three defined phases,  $G_0+G_1$ , S and  $G_2+M$ . The initial spike in the  $G_0+G_1$  and corresponding low fractions of S and  $G_2+M$  may be explained by considering that this point is the initial cell inoculum. The cells were inoculated onto the microcarriers at 80 to 100% confluence and therefore the majority of cells are in  $G_0+G_1$  states. By the second sampling interval the fraction has decreased indicating the attached cells are beginning to grow and divide. This is validated by the increase of the fraction of cells in the S and  $G_2+M$  phases. After the initial rapid growth, between 25 and 50 hours, contact inhibition effects begin to emerge. The effects are characterized by the steady increase in the  $G_0+G_1$  cell fraction and the corresponding the cycling cell fractions. The lower proportion of dividing cells is not unexpected, as time progresses the microcarrier surface area available for growth is decreasing and cells are being surrounded by neighbouring cells. Cells surrounded can no longer grow or divide and therefore the fraction of cycling cells decreases with time. Eventually both  $G_0+G_1$ , S and  $G_2+M$  fractions become relatively constant, this is the stationary or confluent stage of the culture. The fact that the fraction of cells in S and  $G_2+M$  never reaches 0 indicates that even at confluence there is still some cell growth.

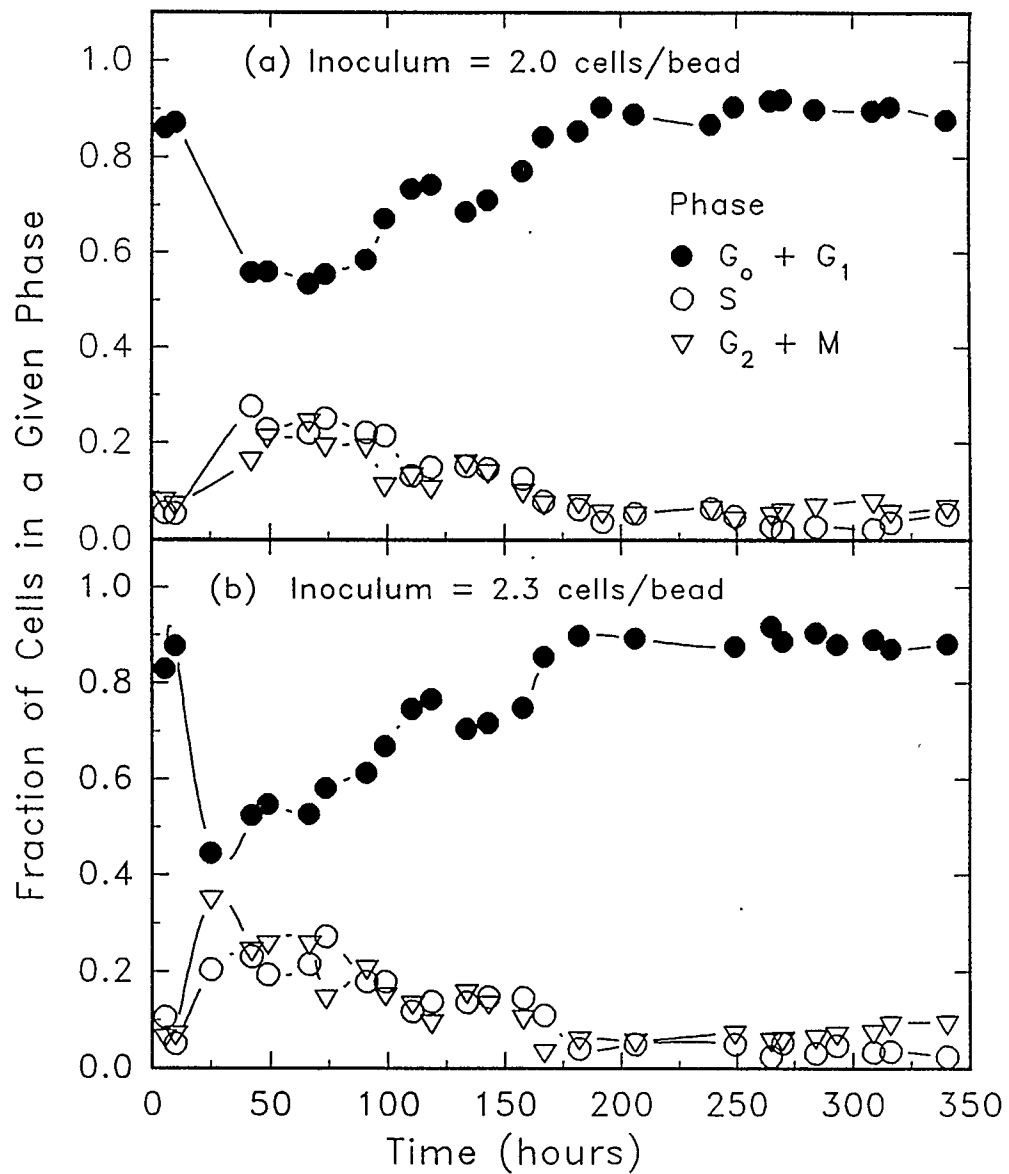


Figure 6.7. Variation of the fraction of cells in each defined phase of the cell cycle, of the two MRC-5 cultures, as time progresses ( $G_0 + G_1$  (●), S (○) and  $G_2 + M$  (▽)).

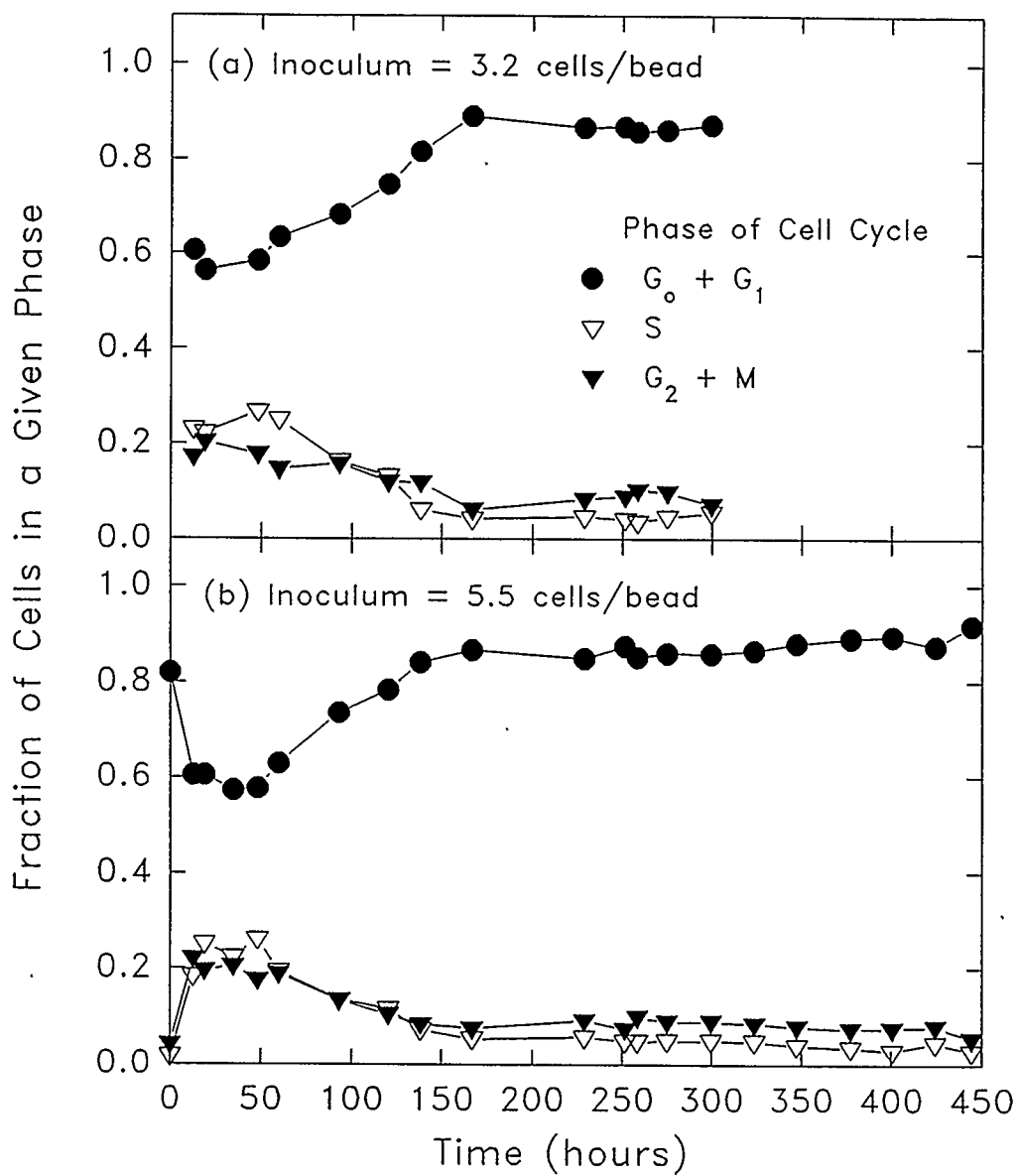


Figure 6.8. Variation of the fraction of cells in each defined phase of the cell cycle, of the two Vero cultures, as time progresses ( $G_0 + G_1$  (●), S (▽),  $G_2 + M$  (▼)).

## **VI.4 CONTACT INHIBITED REGION IN CELL CYCLE**

It would be intuitive to assume cells in the quiescent  $G_0$  phase of the cell cycle represent the contact inhibited region of the cell cycle. However a number of factors may arrest cell growth in different phases. For instance, fibroblast division requires three physiological mediators in order for cell division to occur; growth factors, nutrients and attachment to a surface (Benecke et al., 1978; Delarco and Todaro, 1978; Moses et al., 1980; Pardee, 1989). The removal of any one of these factors will arrest the cell in a specific part of the cell cycle. If growth factors are removed cells will enter the quiescent state,  $G_0$  (Pardee, 1989). The absence of nutrients arrests the cell cycle progression in early  $G_1$  and prevents  $G_1$  associated increases in cell size (Stiles et al., 1979). Guadagno and Assoian (1991) suggested that loss of anchorage arrests cell growth in late  $G_1$ . It follows that contact inhibited cells may not be limited to the  $G_0$  phase of the cell cycle. The determination of a contact inhibited state should take this into account. In this section flow cytometry is used to determine the percentage of contact inhibited cells.

### **VI.4.1 Determination of contact inhibited region**

One approach for the identification of the contact inhibited region in the cell cycle is to perform the flow cytometry analysis when the culture is completely confluent. It would be intuitive to assume that the region in the cell cycle of complete confluence the cells should be contact inhibited. If this region corresponds to the  $G_0$  region then the problem of quantifying the fraction of contact inhibited cells becomes the same definition of the  $G_0$  region in the flow cytometry plots.

As previously mentioned Darzynkiewicz et al. (1980) suggested that the

distinguishing factor between cycling (growing cells) and noncycling (quiescent) cells was the RNA content. A cell needs a critical RNA content in order to continue cycling, therefore cells unable to attain this RNA are contact inhibited or arrested. However, basing the degree of contact inhibition solely on RNA content is limited when applied to anchorage dependent cultures. The determination of this threshold RNA is rather difficult. Examination of the flow cytometry plots illustrates the difficulty. There is no point or region in the RNA fluorescence which would indicate a transition from  $G_0$  to  $G_1$ . A possible solution to this problem would be to run an already confluent population through the flow cytometer. As confluence would indicate a contact inhibited cell culture the maximum RNA fluorescence (content) measured would be the threshold or transition RNA. However, as previously illustrated the cell cycle of the microcarrier cultures never seems to enter a completely contact inhibited state, that is no cell growth or division. This coupled with the difficulty in ascertaining the exact point in the RNA, where the  $G_0$  to  $G_1$  transition occurs, makes the identification of this critical RNA level difficult. It was for these reasons that it was concluded the contact inhibited regions must be defined from a standard sample in which the region of contact inhibited cells could be more accurately defined.

The standard sample should represent cells in the culture which can no longer divide or grow. As there are no nutrient limitations in these experiments the suppression of cell growth should only be due to contact inhibition. If it is assumed that cells present in the medium which have detached or lysed from the microcarrier surface have done so due to contact inhibition effects then the supernatant becomes the contact inhibited

standard. It follows attached cells with similar DNA/RNA contents as the detached/lysed cells then the cells are contact inhibited. As the experiments were done under optimal growth conditions the assumption of contact inhibition resulting in detachment/lysing is valid.

Figure 6.9 is a flow cytometry analysis, in the form of a dot plots, of the DNA versus RNA content from the Vero culture of Figure 6.2 (a), at a time of 92.75 hours. Figure 6.9 (a) is the attached cell sample while 6.9 (b) is the supernatant sample. The cycling cell region is first defined by the attached cell sample (Figure 6.9 (a)). Events which have DNA and RNA content below this region are usually considered debris and are not considered in the determination of contact inhibited cells. Any other cells in the supernatant sample (Figure 6.9 (b)) are assumed to be detached or lysed due to contact inhibition effects. This region is gated and used to define the contact inhibited area in the attached cell sample. With this method the percentage of contact inhibited cells may be determined and compared to the cellular automaton predictions.

#### **VI.4.2 Comparison of flow cytometry data with automaton model predictions**

Figures 6.10 (MRC-5 cultures) and 6.11 (Vero cultures) illustrate the match between the experimental flow cytometry data and the automaton model predictions. In these figures the percentage of contact inhibited cells has been plotted versus time. The trend in the degree of contact inhibition follows the expected trend, that is the experimental data show an increase in the percentage of contact inhibited cells in the microcarrier cultures.

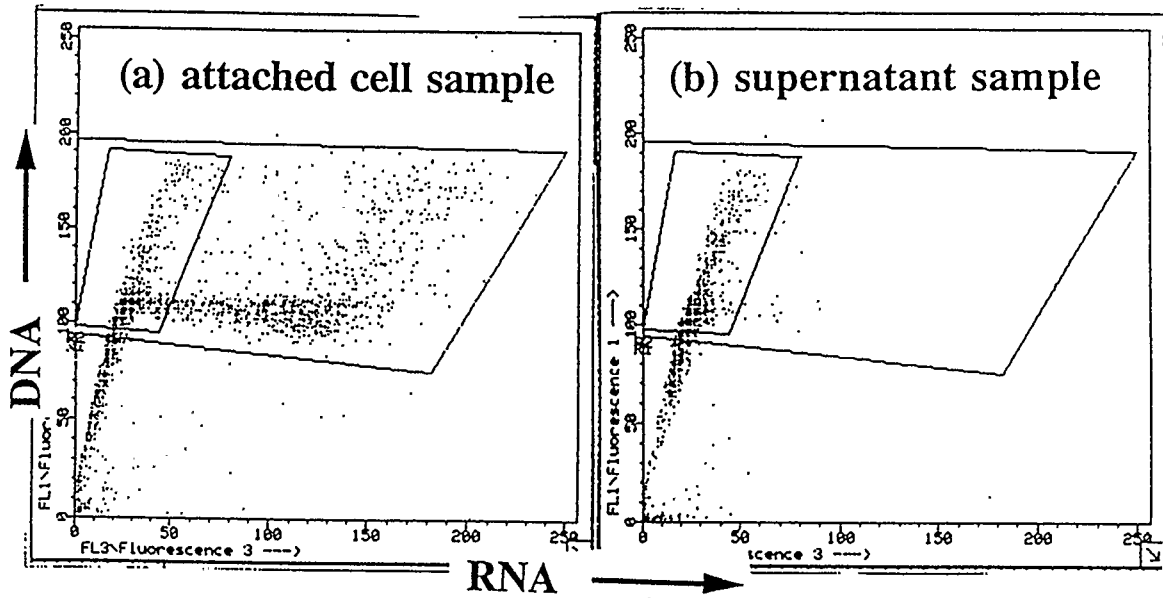


Figure 6.9. (a). Dot plot of DNA (FL1) versus RNA (FL3) of the attached cell sample from the Vero culture of figure 6.3 (b) at a time of 92.75 hours.

(b). Dot plot of DNA (FL1) versus RNA (FL3) of the supernatant sample from the Vero culture of figure 6.3 (b) at a time of 92.75 hours.

These two figures illustrate the technique used to define the contact inhibited region of the attached cell samples. The cycling cells are defined in the attached cell sample (a) and then the contact inhibited region is defined in the supernatant sample (b).

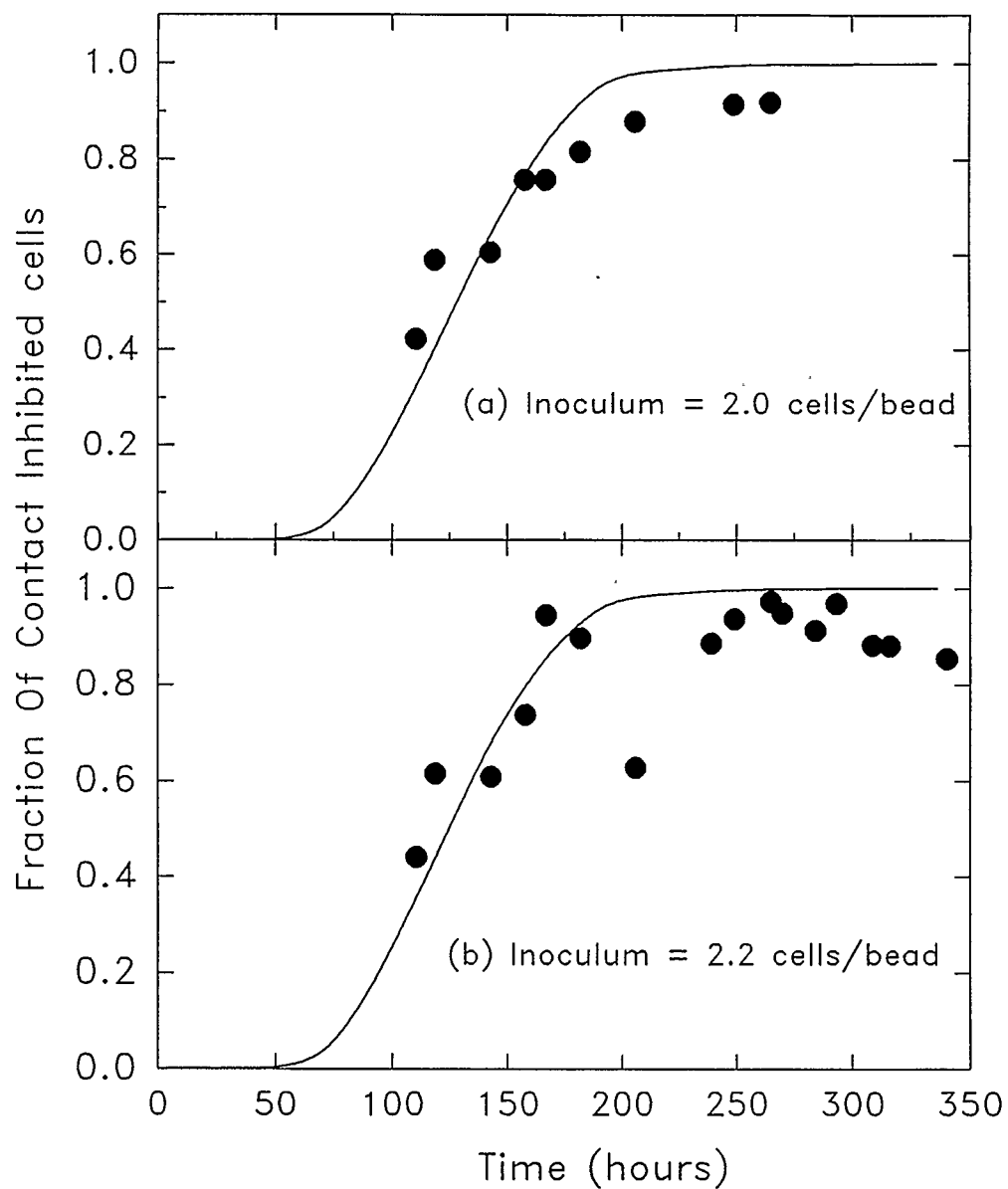


Figure 6.10. Comparison of the fraction of contact inhibited cells predicted by the cellular automaton model (—) and the flow cytometry determined from the experiments (●) for the two MRC-5 cultures ((a)  $\lambda=2.0$  cells/bead, (b)  $\lambda=2.3$  cells/bead).

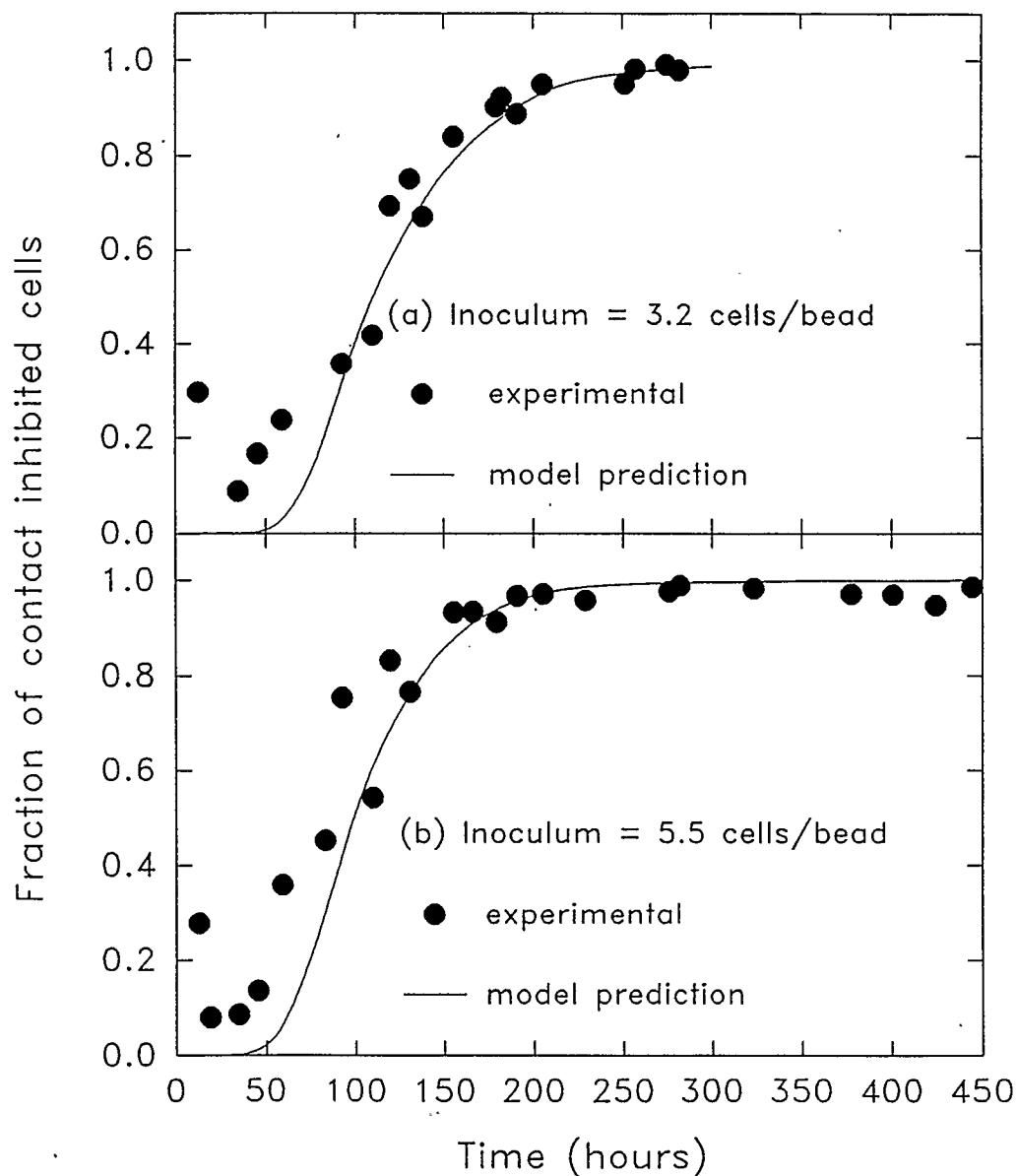


Figure 6.11. Comparison of the fraction of contact inhibited cells predicted by the cellular automaton model (—) and the flow cytometry determined from the experiments (●) for the two Vero cultures ((a)  $\lambda = 3.2$  cells/bead, (b)  $\lambda = 5.5$  cells/bead).

In the Vero cultures, shown in Figure 6.11, supernatant samples were taken at the onset of the experiment. In the Vero cultures for the first 50 hours the model predictions are significantly different from the experimental data. This discrepancy can be accounted for by the previously mentioned initial experimental conditions. Not all cells will attach to the microcarriers upon inoculation and therefore a portion will be present in the supernatant sample. These unattached cells will be measured by the flow cytometry and artificially increase the contact inhibited region. This explanation is further validated by the decreasing trend in the percentage of contact inhibited cells in the first two experimental points. After the first data point a media change was performed, thereby removing a portion of the suspended unattached inoculum and there is a corresponding decrease in the percentage of contact inhibited cells. By the fourth data point three media changes have been performed and therefore the majority of the unattached inoculum has been removed. Beyond 50 hours the agreement between the experimental data and automaton model is quite good. It is worth noting the percentage of contact inhibited cells determined by the flow cytometry never reaches 100 %. Even in the culture's stationary phase there is always a fraction in the  $G_1$ , S or  $G_2+M$  phases. The probable explanation for this continual cell cycling is cell death.

#### VI.4 DEATH RATE

To analyze the presence of a death rate the Vero culture of Figure 6.2 (b) is used. From this figure it is obvious by approximately 240 hours the culture is in the stationary phase of growth. Figure 6.12 illustrates the flow cytometry analyses of the cell cycle dynamics of the stationary phase. The sequence of plots begins at 275 hours, from Figure 6.2 (b) by this point the culture is well into the stationary phase of growth. As the fraction of cycling cells will be very low the contours have been reduced to 5% for better resolution. The area outside the outermost contour represent 2.5% of the total cell population and the innermost 97.5% of the culture. Plot (a) shows the population at 275 hours. Approximately 97% of the cells are in the defined contact inhibited region. In plot (b), at a time of 299.5 hours, the contour lines have shifted slightly to the right, there is also a larger fraction of cells in the S and  $G_2+M$  phases. The contact inhibited region has correspondingly decreased to 96%. However, by 323.5 hours, plot (c), the contour lines have shifted back to the left indicating a smaller fractions are cycling. This is validated by the increase in the contact inhibited region which is now 98.25% of the culture. This pattern is repeated in plots (d) through to (f), or 400.5 to 444.5 hours. In plot (d) the cells are again shifting to the right, towards the growth and division phases. The contact inhibited region is at 97%. The trend continues at 424.5 hours where the percentage of contact inhibited cells has dropped to 95%. By 444.5 hours, shown in plot (f), the cells have shifted back to the arrested state and the contact inhibited cells has increased to 98.6%.

The continual shift in the cell cycle may be an indication of continued cell cycling

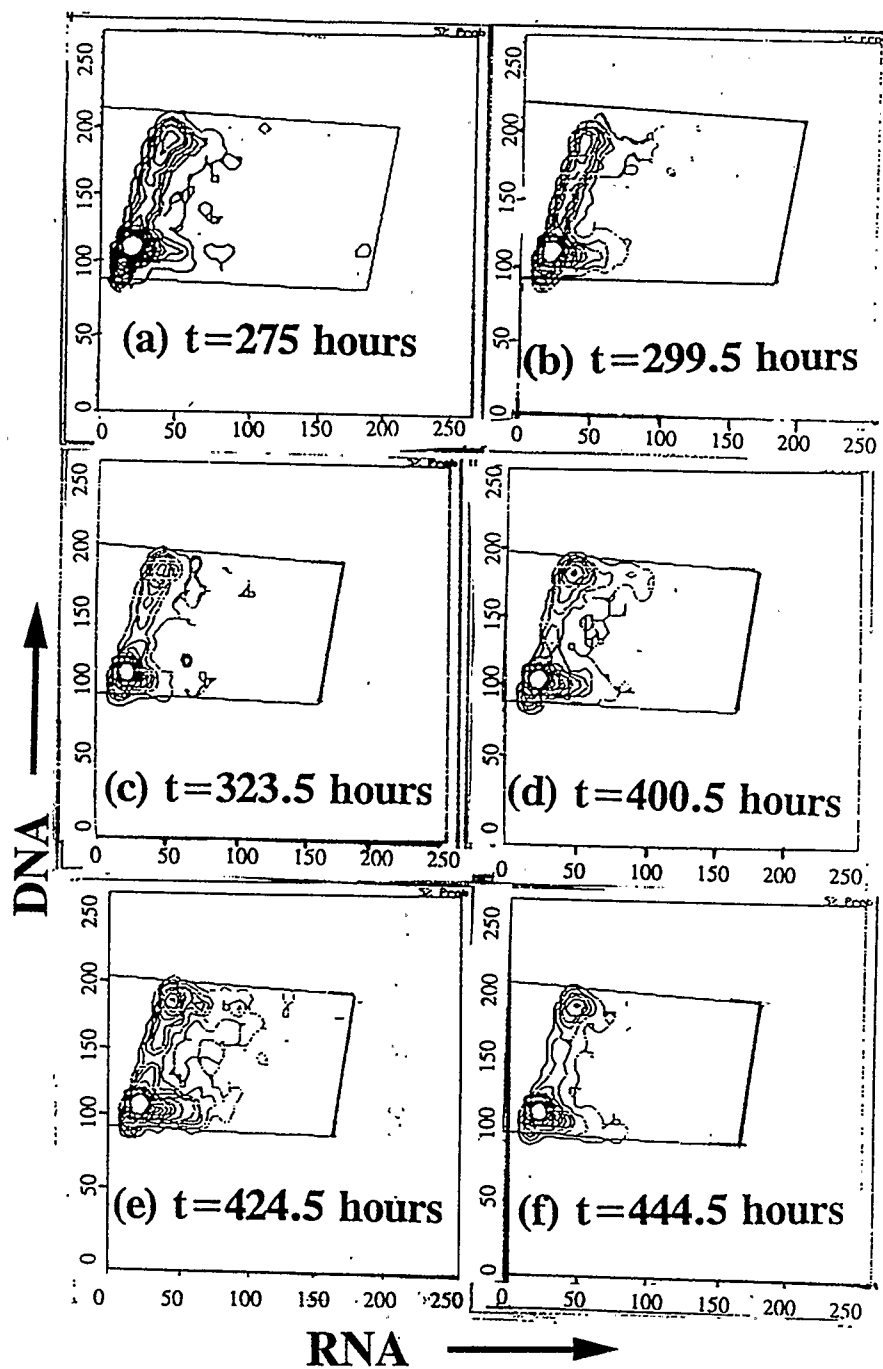


Figure 6.12. Contour plots of DNA (FL1) versus RNA (FL3) of the stationary phase of the Vero culture from figure 6.3 (b). The plots represent samples from 275 to 444.5 hours. The outermost contour represent 2.5% of the total cell sample while the innermost represents 97.5% of the cell sample.

in the stationary phase. From microscopic analysis of the supernatant it became evident that cells do detach/lyse from the microcarrier surface. As time progresses the debris in the supernatant between media changes slowly increases. The continual cycling in and out of the contact inhibited state indicates a small fraction of cells are still growing and dividing. The presence of cycling cell has a number of explanations. The most probable is the presence of a cell death rate. As the cell growth is not a function of nutrient and/or growth factors, the cycling of cells must be due to openings in the spatial environment. Cells detaching or lysing from the microcarrier surface area would provide surface area for growth and division. The reasons for detachment are speculative at this point. One possible explanation is an attached cell divides to form an unstable secondary layer, that is cells grow on top of each other. However, MRC-5 and Vero do not seem to form a stable secondary layer on microcarriers, therefore daughter cells would detach into the medium. As cells require attachment for  $G_1/S$  transition (Guadagno and Assoian, 1991) cells in the supernatant would be in the  $G_0+G_1$  phases. Another possibility is cells may detach due to the inefficiency of the arrested cell to uptake nutrients and as there is no space for growth the cell detaches or lyses ( de la Broise et al., 1991). This would also explain the cells in  $G_0+G_1$  present in the supernatant. However this does not explain the detachment/lysing of cells with higher than normal DNA but no corresponding high RNA present in the supernatant. A possible explanation is upon cell detachment neighbouring cells may begin to grow and divide and thereby compete for the available surface area. As there is limited area available for growth the parent and/or daughter cell may detach or lyse in the growth or division phases. As RNA quickly denatures it would not be

present in the flow cytometry measurements, however the DNA would be measured (Darzynkiewicz et al., 1980). The end result of these hypotheses is that cell death is occurring.

The death of cells is probably present throughout the culture's life, however, in the initial and middle stages its presence is probably masked by the much greater growth rate. In the stationary phase where the growth rate is much lower, due to contact inhibition, the death rate becomes more evident. Wagner et al. (1991) came to a similar conclusion. In their work lactate dehydrogenase (LDH) was used to determine the cell growth and death rate of a microcarrier perfusion culture. Their data suggested the death rate was low and approximately constant throughout the experiment. The apparent stationary phase was actually a result of similar growth and death rates in the latter portion of the experiment. The results from this work suggest the same conclusion. Further, the physiological state of the detached or lysed cells has been shown.

## VI.6 SUMMARY

Through the use of flow cytometry the progression through the cell cycle of microcarrier cultures has been followed from inoculation to confluence. By differential staining of both the RNA and DNA of the cells the different phases of the cycle,  $G_0+G_1$ , S and  $G_2+M$ , were differentiated. The variation in the distribution of cells in each phase was determined by DNA content. Both MRC-5 and Vero microcarrier showed the same trends in cell distributions in each phase. The cultures began in the  $G_0+G_1$  phases and showed an initial rapid progression to the S and  $G_2+M$  phases. After the initial rapid growth the culture showed a gradual movement back to the  $G_0+G_1$  phases. In the final confluent state the majority of the cells were in the  $G_0+G_1$  phases. However, there were a portion of the culture in the growth and division phases of the cycle.

Flow cytometry analyses of the MRC-5 and Vero microcarrier cultures supernatant was combined with the analyses of the cells samples to define a contact inhibited region of the cell cycle. The supernatant contains cells which have probably lysed or detached due to contact inhibition, therefore the DNA/RNA region defined by these cells may be used to define contact inhibited cells attached to the microcarriers. Contrary to original expectations contact inhibited cells were not limited to the  $G_0+G_1$  phases of the cells cycle. The flow cytometry determinations were found to be in good agreement with the percentage of contact inhibited cells predicted by the cellular automaton growth model.

Additional examination of the supernatant by flow cytometry indicated cells were detaching/lysing from the microcarrier surface. As there were no nutrient limitations to growth the cell death was probably a result of contact inhibition effects. The rate of death

was found to be relatively small in the early phases of growth by the small amount of cell matter in the supernatant. However, a flow cytometry analysis of the stationary phase showed a continuous cycling of a small fraction of cells, indicating a possible growth rate. For a cell growth to occur cells must be detaching/lysing from the surface of the microcarrier to provide an area for growth. As the cell density remains approximately constant in the stationary phase the death rate is probably very similar to the growth rate.

## CHAPTER VII

### CONCLUSIONS AND RECOMMENDATIONS

#### VII.1 CONCLUSIONS

This study focused on two subjects. First the development a model to represent the growth of anchorage dependent cells on microcarriers and second the investigation of the cell cycle dynamics of microcarrier cultures using flow cytometry.

The primary objective of the first study was to decouple the effect of contact inhibition from the microcarrier culture growth kinetics. As microcarriers are used extensively in the biopharmaceutical field for large scale cultivation of anchorage dependent cells the accurate determination of the growth kinetics is essential for process optimization. Contact inhibition complicates the determination of kinetic parameters and mask the effects of other environmental factors. A cellular automaton model was developed to model the contact inhibited growth of cells on microcarriers. The advantages to using the cellular automaton theory include; the analogy between the cellular automaton theory and contact inhibited cell growth, the model accurately replicates the transient nature of the growth rate particular to contact inhibited cell growth, the cellular automaton is relatively uncomplicated to program and the cellular automaton is computationally efficient.

When applied to anchorage dependent cell growth on microcarriers the cellular automaton model is particularly effective. Unlike previous models, the cellular automaton

model is inherently capable of accounting for the factors which are unique to microcarrier cultures. Factors include the inoculation density and the microcarrier size distribution. Furthermore, the model developed accounts for the distribution of neighbouring cells a cell may have in a microcarrier culture. The cellular automaton predictions were an accurate representation both quantitatively and qualitatively of experimental microcarrier culture. The model may also be used to decouple the effects of contact inhibition from the growth kinetics.

In the second part of the study an extensive examination of the cell cycle dynamics of microcarrier cultures was performed. The purpose of this analysis was threefold; to observe the cell cycle of a microcarrier culture through all stages of the culture growth, to determine a physiological state in the cell cycle corresponding to contact inhibited cells and to investigate the presence of a cell death rate in microcarrier cultures. Through the use of a flow cytometer the progression of the cell cycle of microcarrier cultures was followed from inoculation, exponential growth and confluence. By differential staining of both DNA and RNA of the attached cells the different phases of the cycle,  $G_0+G_1$ , S and  $G_2+M$  were discriminated. Both the MRC-5 and Vero showed the same trend in phase transition. Combined flow cytometry analyses of the cultures supernatant and attached cells was used to define the contact inhibited region of the cell cycle. The flow cytometry predictions were found to be in good agreement with the fraction of contact inhibited cells predicted by the cellular automaton. A detailed analysis of the stationary cell cycle dynamics indicated there may be a small fraction of cells were still growing and dividing. The conclusion is there is a death rate in microcarrier cultures. In the stationary

phase of the culture when the growth rate is very low, the death rate is closer in value to the growth rate and therefore acts to maintain a constant cells density.

## **VII.2 RECOMMENDATIONS**

The next step, with respect to the application of the automaton model, is in bioreactor operation. One such application is to couple the automaton to current nutrient/toxin growth models to accurately determine; optimal dilution rates, the nutrient uptake rates and maintenance coefficients. Three such reactor experiments were attempted in this study however problems in maintaining cell growth were encountered. Further experiments are required to optimize the use of the PPRF92 supplement in perfusion reactors.

Although the application of macroporous microcarriers is still developing, the possibility of much higher cell densities than conventional microcarriers makes their use very attractive. It would be therefore useful to attempt to apply the cellular automaton model to macroporous microcarrier cultures.

**REFERENCES**

1. Bailey, J.E., Ollis, D.F. 1986. Biochemical Engineering Fundamentals. 2<sup>ND</sup> edition, Mcgraw-Hill, New York.
2. Benecke, B.J., Ben-Ze'ev, A., Penman, S. 1978. The control of mRNA production, translation and turnover in suspended and reattached anchorage dependent fibroblasts. *Cell*. **14**:931-939.
3. Buckley, S.M., Casalls, J. 1970. Lassa Fever, A new virus disease of man from West Africa. *The American Journal of Tropical Medicine and Hygiene*, vol 19, No. 4.
4. Celer, V., Belay, G., Celer, V.Jr. 1991. Kinetics of rabies virus replication in cell cultures. *ACTA Veterinaria BRNO*, **60**(2): 161-164.
5. Cherry, R.S., Papoutsakis, E.T. 1989. Modelling of Contact Inhibited Animal Cell Growth on Flat Surfaces and Spheres. *Biotechnology and Bioengineering* **33**:300-305.
7. Darzynkiewicz, Z., Traganos, F., Sharpless, T., Melamed, M.R. 1975. Conformation of RNA in situ as studied by acridine orange staining and automated flow cytometry. *Exp. Cell Res.* **95**:143-153.
8. Darzynkiewicz, Z., Traganos, F., Sharpless, T., Melamed, M.R. 1976. Lymphocyte simulation: A rapid multiparameter analysis. *Proc. Natl. Acad. Sci. (USA)*, **73**:2881-2884.
9. Darzynkiewicz, Z., Sharpless, T., Staiano-Coico, L., Melamed, M.R. 1980. Subcompartments of the G<sub>1</sub> phase of the cell cycle detected by flow

- cytometry. Proc. Natl. Acad. Sci. USA, **77**(11):6696-6699.
10. Darzynkiewicz, Z., Crissman, H., Traganos, F., Steinkamp, J. 1982. Cell Heterogeneity During the Cell Cycle. *Journal of Cellular Physiology*, **113**:465-474.
  11. de la Broise, D., Noiseux, M., Lemieux, R., Massie, B. 1991. Long-Term Perfusion Culture of Hybridoma: A "Grow or Die" Cell Cycle System. *Biotechnology and Bioengineering*, **38**:781-787.
  12. DeLarco, J.E., Todaro, G. 1978. Growth factors from murine virus transformed cells. Proc. Natl. Sci. USA, **75**:4001-4005.
  13. Forestell, S.P., Milne, B., J., Kalogerakis, N., Behie, L.A. 1992c. A cellular automaton model for the Growth of anchorage-dependent mammalian cells on microcarriers and flat surfaces, *Chem. Eng. Sci.*, **47** (9-11):2381-2386.
  14. Forestell, S., Kalogerakis, N., Behie, L.A., Gerson, D. 1992b. Development of the optimal conditions for microcarrier cultures., *Biotechnology and Bioengineering* **39**:305-313.
  15. Forestell, S.P. 1992. Optimization of Microcarrier Cultures Used in Human Viral Vaccine Production.
  16. Frame, K.K., Hu, W.S. 1988, A model for density-dependent growth of anchorage dependent mammalian cells. *Biotechnology and Bioengineering*, **32**:1061-1066.
  17. Goldberg, A.M., Frazier, J.M. 1989. Alternatives to Animal in Toxicity

- Testing. *Scientific America*, **261**(2):24-30.
18. Griffiths, J.B. 1992b. Animal cell culture processes - batch or continuous. *J.Biotech.*, **22**:21-30.
  19. Griffiths, J.B, Thorton, B., McEntee, I. 1982. The Development and use of microcarrier and glass sphere culture techniques for the propagation of herpes simplex virus. *Develop. Biol. Stand.*, **50**:103-110.
  20. Guadagno, T.M., Assoian, R.K. 1991. G<sub>1</sub>/S Control of Anchorage-independent Growth in the Fibroblast Cell-Cycle. *The Journal of Cell Biology*, **115**:1419-1425.
  21. Hawboldt, K.A., Forestell, S.P., Kalogerakis, N., Behie, L.A. 1992, Growth of Human Fibroblasts on Microcarriers, *Proceedings of the 42<sup>nd</sup> Canadian Chemical Engineering Conference*, Toronto, Canada.
  22. Hawboldt, K.A., Kalogerakis, N., Behie, L.A. 1993. Growth of Anchorage Dependent Human Fibroblasts. *Proceedings of 42<sup>nd</sup> Canadian Chemical Engineering Conference*, Toronto, Canada.
  23. Hawboldt, K.A., Linardos, T., Kalogerakis, N., Behie, L.A. 1993. Cellular automaton model to represent the proliferation of anchorage dependent cells on microcarriers. Submitted to *Biotechnology and Bioengineering*.
  24. Horodniceanu, F. 1982. A critical review of cell substrates with regard to transformation and cancer. *Develop. Biol. Stand.*, **50**:47-57.
  25. Horodniceanu, F., Crainic, R., Barne, M. 1981. Cell substrate and risk in poliomyelitis vaccine. *Develop. Biol. Stand.*, **47**:35-39.

26. Jacobs, J.P. 1970. *Nature*, **227**:168-170.
27. Johnson, K.M., Lange, J.V., Webb, P.A., Murphy, F.A. 1977, Isolation and Partial Characteristics of a new virus causing acute haemorrhagic fever in Zaire. *The Lancet*.
28. Kieff, E.D., Bachenheimer, S.L., Roizman, B. 1971, Size, Composition, and Structure of the Deoxyribonucleic Acid of Herpes Simplex Virus Subtypes 1 and 2. *Journal of Virology.*, **8**(2):125-132.
29. Kuwert, E.K., Marcus, I., Werner, J., Schiereremann, N., Höher, P.G., Thraenhart, O., Hierholzer, E., Wiktor, T.J., Koprowski, H. 1977. Post-exposure use of human diploid cell culture rabies vaccine. *Develop. Biol. Stand.*, **37**:273-286.
30. Lanks, K.W., Kasambalides, E.J. 1980. Factors that regulate proliferation of normal and transformed cells in culture. *Pathibiol. Ann.*, **10**:35-50.
31. Leist, C.L., Meyer, H-P., Fiechter, A. 1990. Potential and problems of animal cells in suspension culture. *Journal of Biotechnology*, **15**:1-46.
32. Lim, J.H.F., Davies, G.A. 1990. A Stochastic Model to Simulate the Growth of Anchorage Dependent Cells on Flat Surfaces. *Biotechnology and Bioengineering* **36**: 547-562.
33. Majer, M., Hilfenhaus, R., Mauler, R., Hennessen, W. 1977. Zonal-centrifuged human diploid cell rabies vaccine. *Develop. Biol. Stand.*, **37**:267-271.
34. Makino, S., Sasaki, K., Kasahara, S. 1964. Studies of measles virus II.

- Propagation in two established simian renal cell lines and development of a plaque assay. *Kitstat<sup>o</sup> Arch. of Exp. Med.*, **XXXVII**(1-4):27-42.
35. Mirchamsy, H., Shafyi, A., Bahrami, S., Kamali, M., Nazari, P. 1977. Use of human diploid cell MRC-5 for production of measles and rubella virus vaccines. *Develop. Biol. Stand.*, **37**:297-300.
  36. Montagnon, B., J., Fanget, B., Nicolas, A.,J. 1981. The large-scale cultivation of Vero cells in micro-carrier culture for virus vaccine production preliminary results for killed poliovirus vaccine. *Develop. Biol. Stand.*, **47**:55-64.
  37. Montagnon, B., J., Fanget, B., Vincent-Falquet, J., C. 1984. Industrial-scale production of inactivated poliovirus vaccine prepared by culture of Vero cells on microcarrier. *Rev. Infect. Dis.*, **6**(2):s341-s344.
  38. Nilsson, K. 1989. Microcarrier Cell Culture. *Biotech. Genet. Eng. Rev.*, **6**:403-429.
  39. Oker-Blom, C., Kalkkinen, N., Kääriäinen, L., Ralf, F. 1983. Rubella virus contains one capsid protein and three envelope glycoproteins, E1, E2a and E2b. *Journal of Virology*, **46**(3):964-973.
  40. Ozturk, S.S. 1990. Kinetic characterization of hybridoma growth, metabolism and monoclonal antibody production rates. PhD Thesis. The University of Michigan.
  41. Pardee, A., B. 1989. G<sub>1</sub> events and regulation of cell proliferation. *Science*, **246**:603-608.

42. Pirt, S.J., 1985. Principles of Microbe and Cell Cultivation, Blackwell Science Publications, Cambridge.
43. Pharmacia Technical publication. 1981. Microcarrier cell culture, principles and methods.
44. Shapiro, H., M. 1988. Practical Flow Cytometry. Alan R. Liss, Inc., New York, N.Y.
45. Simizu, B., Rhim, J., S., Wiebenga, N., H. 1967. Characterization of the Tacaribe group of arboviruses. I. Propagation and plaque assay of Tacaribe virus in a line of African green monkey kidney cells (Vero). Proc. Soc. Exp. Bio. and Med., **125**:119-123.
46. Stiles, C., D., Isberg, W., Pledger, W., J., Antoniades, H., N., Scher, C., D. 1979. Control of the Balb/c-3T3 cell cycle by nutrients and serum factors: analysis using platelet-derived growth factor and platelet-poor plasma. Cell Physiol., **99**:395-406.
47. v.Seefried, A., Chun, J., H. 1981. Serially subcultivated cells as substrates for poliovirus production for vaccine. Develop. Biol. Stand., **47**:25-33.
48. v.Seefried, A., Chun, J., H., Grant, J., A., Letvenuk, L., Pearson, E., W. 1984. Inactivated poliovirus vaccine and test development at Connaught Laboratories Ltd., Rev. Infect. Dis., **6**:s345-s349.
49. Wagner, A., Marc, A., Engasser, J., M. 1992. The use of lactate dehydrogenase (LDH) release kinetics for the evaluation of the death and growth of mammalian cells in perfusion reactors. Biotechnolgy and

- Bioengineering, **39**:320-326.
50. Wolfram, S. 1983. Statistical mechanics of cellular automata. *Rev. Mod. Phys.*, **55**(3):601-644.
  51. Yasumura, Y., Kawakita, Y. 1963. Studies on SV40 in tissue culture—preliminary step for cancer research in vitro. *Nihon Rinsho*, **21**:1201-1215.
  52. Zygourakis, K., Bizios, R., Markenscoff, P. 1991a. Proliferation of Anchorage-Dependent Contact Inhibited Cells: I. Development of Theoretical Models Based on Cellular Automata. *Biotechnology and Bioengineering* **36**: 459-470.
  53. Zygourakis, K., Bizios, R., Markenscoff, P. 1991b. Proliferation of Anchorage-Dependent Contact Inhibited Cells: II. Experimental Results and Validation of the Theoretical Models. *Biotechnology and Bioengineering* **36**: 471-479.

## **APPENDIX A**

**Table A.1. Components of DMEM/F12 cell culture medium.**

Inorganic Salts	mg/L	Amino acids	mg/L	Vitamins	mg/L	other comp.	mg/L
CaCl <sub>2</sub>	116.6	l-alanine	4.45	Biotin	.0035	d-glucose	3151
CuSO <sub>4</sub> (5H <sub>2</sub> O)	.0013	l-arginine	147.5	D-Ca pan tothenate	2.24	Na hy- poxanine	2.39
FeSO <sub>4</sub> (7H <sub>2</sub> O)	0.417	l-asparagine	7.50	Choline Chloride	8.98	linoleic acid	0.042
KCl	311.8	l-aspartic acid	6.65	Folic acid	2.65	lipoic acid	0.105
MgCl <sub>2</sub>	28.64	l-cysteine	17.56	i-Inositol	12.6	phenol red	8.1
MgSO <sub>4</sub>	48.84	l-cystine	31.29	niacinamide	2.02		
NaCl	6999	l-glutamine	365	pyridoxal	2.0	Napyruvate	55.00
NaH <sub>2</sub> PO <sub>4</sub> *H <sub>2</sub> O	65.5	l-glutamic acid	7.35	pyridoxine* HCl	0.031	putrescine* 2HCl	0.081
Na <sub>2</sub> HPO <sub>4</sub>	71.02	glycine	18.75	riboflavin	0.219		
ZnSO <sub>4</sub>	0.432	l-histidine	31.48	thiamine	2.17		
Fe(NO <sub>3</sub> ) <sub>3</sub>	.05	l-isoleucine	54.47	thymidine	0.365		
		l-leucine	59.05	B <sub>12</sub>	0.68		
		l-lysine	91.25				
		l-methionine	17.24				
		l-phenylalani	35.48				
		l-proline	17.25				
		l-serine	26.25				
		l-threonine	53.45				
		l-tryptophan	9.02				
		l-tyrosine	55.79				
		l-valine	52.85				

**Table A.2. Physical characteristics of cytodex 1 microcarriers.**

Composition	cross-linked dextran matrix substituted with positively charged DEAE groups
Degree of DEAE <sup>1</sup> substitution	3.5 meq/g
Density <sup>2</sup>	1.03 g/mL
Size <sup>2</sup> d <sub>50</sub> d <sub>5-95</sub>	180 $\mu\text{m}$ 131-220 $\mu\text{m}$
Approximate surface area <sup>2</sup>	6000 cm <sup>2</sup> /g(dry weight)
Approximate no. of microcarriers/g(dry weight)	6.8 x 10 <sup>6</sup>
Swelling <sup>2</sup>	18 mL/g(dry weight)

<sup>1</sup> refers to N,N-diethylaminoethyl (DEAE) substitution of Sephadex A-50.

<sup>2</sup> size is based on the diameter at 50% of the volume of a sample of microcarriers (d<sub>50</sub>), or the range between the diameter at 5% and 95% of the volume of a sample of microcarriers (d<sub>5-95</sub>). Consequently, size is calculated from cumulative volume distributions.

**Table A.3. Composition of Ca<sup>++</sup> and Mg<sup>++</sup> free PBS**

Composition	Concentration (for 10X stock solution, diluted to 1x) (g/L)
KCl	0.2
KH <sub>2</sub> PO <sub>4</sub>	0.2
NaCl	8.0
Na <sub>2</sub> HPO <sub>4</sub> ·7H <sub>2</sub> O	2.16